Stony Brook University

The role of DNA polymerase lambda in the repair of oxidative DNA damage

A Dissertation Presented

by

Matthew J. Burak

to

The Graduate School

in Partial Fulfillment of the

Requirements

for the Degree of

Doctor of Philosophy

in

Molecular and Cellular Pharmacology

Stony Brook University

May 2016

Stony Brook University
The Graduate School

Matthew J. Burak

We, the dissertation committee for the above candidate for the
Doctor of Philosophy degree, hereby recommend
acceptance of this dissertation.

Miguel Garcia-Diaz, Ph.D. – Dissertation Advisor
Associate Professor, Department of Pharmacological Sciences

Carlos de los Santos, Ph.D. – Chairperson of Defense
Professor, Department of Pharmacological Sciences

Bruce Demple, Ph.D.
Professor, Department of Pharmacological Sciences

Nancy Hollingsworth, Ph.D.
Professor, Department of Biochemistry and Cell Biology

This dissertation is accepted by the Graduate School

Charles Taber
Dean of the Graduate School

Abstract of the Dissertation

The role of DNA polymerase lambda in the repair of oxidative DNA damage

by

Matthew J. Burak

Doctor of Philosophy

in

Molecular and Cellular Pharmacology

Stony Brook University

2015

8-oxo-7,8-dihydro-2′-deoxyguanosine is a major oxidative product present in cells and can arise in either DNA (8-oxo-dG) or the nucleotide pool (8-oxo-dGTP). Both 8-oxo-dG and 8-oxo-dGTP exhibit dual-coding potential and can pair with cytosine or adenine. Accordingly, these lesions interfere with replication by DNA polymerases, lead to mutation and ultimately drive diseases such as cancer. Interestingly, DNA polymerase lambda (Pol λ) is uniquely capable of facilitating the error-free bypass of 8-oxo-dG-containing DNA and has thus been implicated in its repair. As such, I have utilized structural techniques (X-ray crystallography), complemented with biochemical experiments (steady-state kinetics), to gain insight into the mechanism of 8-oxo-dG bypass in Pol λ. Moreover, considering that Pol λ operates under conditions where oxidative damage is prevalent, it is also expected to frequently encounter 8-oxo-dGTP. Thus, I have characterized Pol λ in the context of 8-oxo-dGTP to further understand the mechanisms governing nucleotide selectivity. Together, my results provide a framework for understanding how DNA polymerases cope with oxidative DNA damage.

Dedication Page

To my family – thank you for your unwavering love and support.

Frontispiece

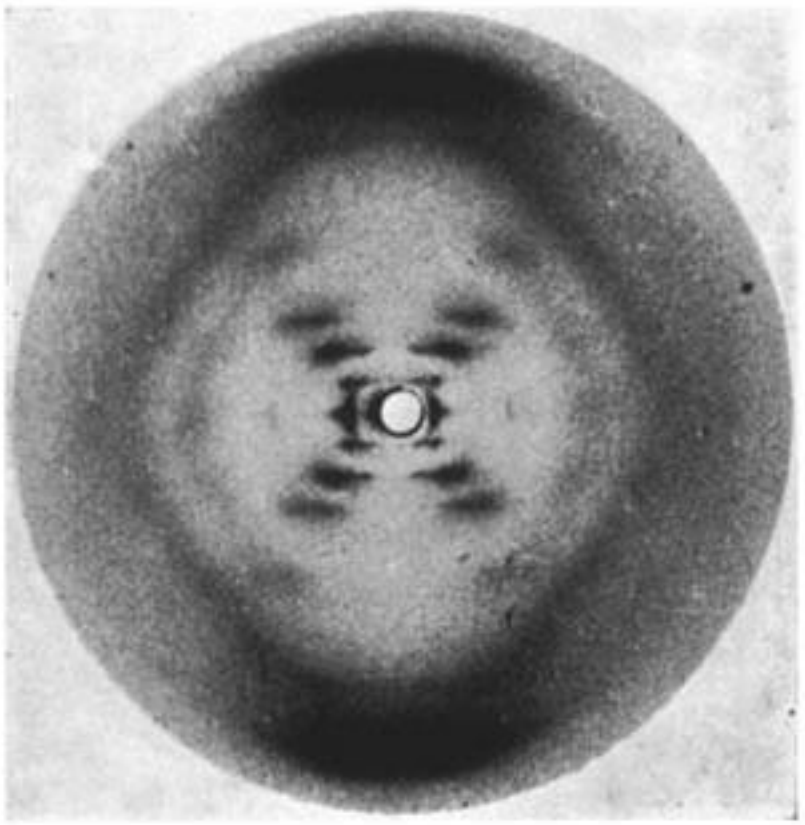

Structure begets function – Photo 51, Rosalind Franklin (1951)

Table of Contents

List of Figures

List of Tables

List of Abbreviations

8-OH-dG	8-hydroxy-deoxyguanosine
8-oxo-dG	8-oxo-7,8-dihydro-2′-deoxyguanosine
8-oxo-dGTP	8-oxo-7,8-dihydro-2′-deoxyguanosine triphosphate
A	Adenine
APE1	Apurinic/apurimidinic endonuclease 1
BER	Base excision repair
C	Cytosine
Cg	Cytosine glycol
dA	2′-deoxyadenosine
dAMP	2′-deoxyadenosine-5′-monophosphate
dATP	2′-deoxyadenosine-5′-triphosphate
dC	2′-deoxycytidine
dCMP	2′-deoxycytidine-5′-monophosphate
dCTP	2′-deoxycytidine-5′-triphosphate
ddCTP	2′,3′-dideoxycytidine-5′-triphosphate
dG	2′,-deoxyguanosine
dGMP	2′-deoxyguanosine-5′-monophosphate
dGTP	2′-deoxyguanosine-5′-triphosphate
DNA	Deoxyribonucleic acid
dNTP	2′-deoxynucleotide-5′-triphosphate
dRP	2′-deoxyribose-5-phosphate
dT	2′-deoxythymidine
dTMP	2′-deoxythymidine-5′-monophosphate
dTTP	2′-deoxythymidine-5′-triphosphate
dUMPNPP	2′-deoxyuridine-5′-[(α,β)-imido]triphosphate
FEN1	Flap endonuclease 1
G	Guanine
MMR	Mismatch repair
MUTYH	MUTY homolog
NHEJ	Nonhomologous end-joining
OGG1	Oxoguanine glycosylase
OH	Hydroxyl
PCNA	Proliferating cell nuclear antigen
Pol β	DNA polymerase beta
Pol λ	DNA polymerase lambda
PPi	Pyrophosphate
ROS	Reactive oxygen species
RPA	Replication protein A
T	Thymine
Tg	Thymine glycol
UNG	Uracil-DNA glycosylase

Acknowledgments

The work presented here would not be possible without the patience and guidance from my research advisor, Dr. Miguel Garcia-Diaz. I am truly thankful for the opportunity to have trained under one of the most intelligent people that I know, and could not have imagined having a better mentor during my time at Stony Brook. I would like to thank my committee of Dr. Carlos de los Santos, Dr. Bruce Demple, and Dr. Nancy Hollingsworth for their helpful discussions regarding my projects. Furthermore, I thank the Bogenhagen lab, Seeliger lab, and all my friends for their continuous support. I would also like to recognize the many scientists whose work paved the way for the studies reported here.

Finally, I would like to thank my family. To my mother and father, thank you for all of the sacrifices that you have made for Mary and me. Thank you for driving us all over the place (and to Kentucky), helping us with homework, and most importantly for your unconditional love. I would also like to thank the love of my life, Michelle Krawczynski, for sticking by my side during my time at Stony Brook, pushing me to be the best that I can be, and supporting me during my greatest triumphs and in my times of need. I hope that upon graduation I have made all of you proud.

Chapter 1: Introduction to oxidative DNA damage and repair

1.1 Reactive oxygen species (ROS) and their formation

A paradox in cellular metabolism is that all aerobic life requires oxygen to survive; yet, oxygen is highly reactive and thus inherently damaging to cells. Mitochondria are the main sites of oxidative metabolism in eukaryotes (85-90% of all oxygen consumption). Accordingly, these unique cellular organelles generate energy by reducing oxygen to water. However, reactive oxygen species (ROS) are constantly generated as the byproducts of oxidative metabolism (1-3% of all mitochondrial oxygen consumption) (Murphy 2009).

The primary byproduct of incomplete oxidative metabolism is superoxide ($^{\bullet}O_2^-$). Mitochondrial superoxide is formed by the one-electron reduction of oxygen, caused by electron leakage from the respiratory chain. This side-reaction occurs at complex I (NADH dehydrogenase) (Hinkle, Butow et al. 1967, Cadenas, Boveris et al. 1977) and complex III (coenzyme Q) (Loschen, Azzi et al. 1974, Dionisi, Galeotti et al. 1975, Boveris, Cadenas et al. 1976, Grigolava, Ksenzenko et al. 1980, Turrens and Boveris 1980). Superoxide is subsequently dismutated to hydrogen peroxide (H_2O_2) (Forman and Kennedy 1974, Loschen, Azzi et al. 1974). Interestingly, hydrogen peroxide is the only ROS that is not a free radical, and is therefore far less reactive than superoxide. However, hydrogen peroxide is integral in forming hydroxyl radicals ($^{\bullet}OH$) via the Fenton reaction (Halliwell 1978, McCord and Day 1978). Additionally, hydroxyl radicals can also be formed from water radiolysis by ultraviolet (UV) light and ionizing radiation (LaVerne 1989). The hydroxyl radical has the highest reduction potential (+2.31V) among all ROS (superoxide: +0.94V, hydrogen

peroxide: +0.32V), and is therefore the most reactive and damaging (Korycka-Dahl and Richardson 1978).

1.2 ROS in cell signaling

Interestingly, low levels of ROS are beneficial, and function as signaling molecules. In particular, hydrogen peroxide is recognized as a ubiquitous intracellular messenger that reversibly oxidizes the thiol groups of many proteins. Accordingly, these redox changes alter the activity of these proteins, and ultimately affect various cellular processes. Thus, ROS are integrated into many signaling pathways including, but not limited to, proliferation and survival (MAP kinases, PI3K and PTEN), ROS homeostasis and antioxidant gene regulation (Ref-1, Nrf-2 and thioredoxin), aging (p66Shc), DNA damage response (ATM), and iron homeostasis (various iron-regulatory proteins and iron-responsive elements). Together, ROS such as hydrogen peroxide mediate many signaling pathways collectively termed redox signaling (Ray, Huang et al. 2012).

1.3 Antioxidant defense systems

ROS homeostasis is essential for redox signaling. Accordingly, a number of cellular mechanisms have evolved to counterbalance ROS production. Antioxidants are the first line of defense against ROS. They can be divided into two categories: enzymatic and non-enzymatic. Enzymatic antioxidants include superoxide dismutase (SOD), catalase, and glutathione peroxidase (GSH-Px). SOD catalyzes the conversion of superoxide into hydrogen peroxide and oxygen, while catalase subsequently converts hydrogen peroxide to

water and oxygen. Additionally, GSH-Px can also catalyze the degradation of hydrogen peroxide. Interestingly, no enzymatic antioxidants exist to detoxify hydroxyl radicals, likely due to the short half-life (nanoseconds) of the chemical species (Birben, Sahiner et al. 2012).

Alternatively, non-enzymatic small molecule antioxidants also play a role in the cellular detoxification of ROS including hydroxyl radicals. Among them, glutathione (GSH) may be the most important intra-cellular defense against the deleterious effects of ROS. Moreover, vitamin C (ascorbic acid) and vitamin E (α-tocopherol) are water-soluble and lipid-soluble antioxidants, respectively (Birben, Sahiner et al. 2012).

1.4 Cellular consequences of oxidative stress

A delicate balance exists between ROS production and cellular antioxidant defenses. Oxidative stress occurs when ROS exceed the antioxidant-scavenging ability of a cell. High levels of ROS are extremely damaging to proteins, lipids, and nucleic acids. Accordingly, ROS are a major source of DNA damage (10^4 lesion per cell per day) (Lindahl 1993) and can result in single- or double-strand breaks, base modifications, deoxyribose modifications, and DNA cross-linking. The most frequent type being the chemical modification of DNA bases induced by hydroxyl radicals (Cooke, Evans et al. 2003).

Hydroxyl radicals preferentially react with DNA by addition to the electron-rich double-bonds of bases. Accordingly, hydroxyl radicals can add to the C5 and C6 positions of a pyrimidine, leading to the formation of either cytosine glycol (Cg) or thymine glycol (Tg). Conversely, hydroxyl radicals can add to the C4, C5, and C8 double bonds of purines. In particular, hydroxyl-radical attack at the C8 position of guanine leads to the formation of 8-

hydroxy-deoxyguanine (8-OH-dG), which can be further oxidized to 8-oxo-7,8-dihydroxy-2'-deoxy-guanosine (8-oxo-dG) (Figure 1-1) (Cooke, Evans et al. 2003). 8-oxo-dG is an abundant type of oxidative base damage (~1000 lesions per cell per day), and as a result, is frequently used as a biomarker for oxidative stress (van Loon, Markkanen et al. 2010).

1.4.1 The dual-coding potential and deleterious nature of 8-oxo-dG

The specific hydrogen-bonding pattern between complementary DNA bases — A with T and G with C — is crucial for preserving the information content of the genome. However, the base pairing properties of DNA are often modified by ROS. The resulting oxidative lesions interfere with replication by DNA polymerases, lead to mutation and ultimately drive diseases such as cancer.

In comparison to guanine, 8-oxo-dG contains a C8-carbonyl and protonated N7. These chemical modifications alter the biochemical properties and modulate the coding potential of the DNA lesion. Similar to other undamaged nucleotides, 8-oxo-dG can adopt both the *anti*- and *syn*-conformation by rotating about its N-glycosidic bond. However, an electrostatic clash between the C8-carbonyl and the 5′-phosphate causes the lesion to preferentially adopt the *syn*-conformation (Figure 1-2A).

Interestingly, the base-pairing potential of 8-oxo-dG is closely tied to the conformation of the base. In the *anti*-conformation, the oxidized base is capable of forming a Watson–Crick base pair with cytosine (Figure 1-2B, left panel). Conversely, the *syn*-conformation exposes the Hoogsteen edge of 8-oxo-dG, and thus modifies its base pairing properties. Accordingly, 8-oxo-dG is particularly deleterious because of its ability to functionally mimic thymine in the *syn*-conformation, and form an 8-oxo-dG(*syn*):dA mispair

(Figure 1-2B, right panel). This is in part due to the protonated N7, which functions as a hydrogen bond donor to the N1-group of adenine. (Kouchakdjian, Bodepudi et al. 1991, Oda, Uesugi et al. 1991, Mcauleyhecht, Leonard et al. 1994, Lipscomb, Peek et al. 1995).

In contrast to many other types of DNA damage, these features allow efficient, although inaccurate, bypass of 8-oxo-dG by replicative DNA polymerases (Shibutani, Takeshita et al. 1991, Zhang, Yuan et al. 2000, Einolf and Guengerich 2001, Haracska, Prakash et al. 2002, Haracska, Prakash et al. 2003). Thus, failure to remove 8-oxo-dG prior to replication will ultimately result in a dG:dC to dT:dA (G–T) transversion mutation (Klungland, Rosewell et al. 1999, Hirano, Tominaga et al. 2003, Russo, De Luca et al. 2004). In order to counteract the deleterious effects of 8-oxo-dG, all cells have evolved a number of DNA repair mechanisms aimed at removing the oxidized DNA lesion.

1.5 The base-excision repair (BER) pathway

The identification of the *Escherichia coli* (*E. coli*) uracil-DNA glycosylase (UNG) in 1974 by Tomas Lindahl marked the discovery of the base excision repair (BER) pathway (Lindahl 1974). BER is the most important mechanism that responds to alkylated, deaminated, and oxidized DNA base damage. BER is also regarded as the simplest repair mechanism, next to direct reversal. The main reason for this perception is that the function and structure of each core component has been extensively resolved (Parikh, Mol et al. 1997, Mol, Parikh et al. 1999, Bruner, Norman et al. 2000). Moreover, BER machinery is well conserved (Demple and Harrison 1994, Wood 1996, Krokan, Standal et al. 1997, Lindahl and Wood 1999, Denver, Swenson et al. 2003), underscoring the vital role that this pathway plays in maintaining genomic integrity in all cells.

BER proceeds through multiple concerted steps involving a DNA glycosylase, apurinic/apyrimidinic (AP) endonuclease 1 (APE1), DNA polymerase, and DNA ligase. Importantly, each reaction step generates a new intermediate lesion recognized by the next enzyme in the pathway (Kubota, Nash et al. 1996). Thus, BER is a highly coordinated process consisting of consecutive cooperative enzymatic reactions.

BER is initiated by a DNA glycosylase that recognizes and cleaves the N-glycosylic bond of the damaged base. The resulting AP site is both an intermediate of BER and a highly prevalent DNA lesion produced by spontaneous base loss (Lindahl 1993). In either case, AP sites are incised by APE1. APE1 hydrolyzes the 5′-phosphodiester bond at the AP site, resulting in a 3′-hydroxyl (OH) and a 5′-deoxyribose phosphate (dRP) group (Demple, Herman et al. 1991, Robson, Milne et al. 1991). Alternatively, some DNA glycosylases are bifunctional and also possess AP lyase activity. These enzymes are capable of cleaving AP sites through β-elimination. This results in the formation of a 3′-phospho-α,β-unsaturated aldehyde and 5′-phosphate (Jacobs and Schar 2012). Interestingly, APE1 also has 3′-phosphodiesterase activity, thereby restoring the 3′-OH required for the subsequent DNA polymerase reaction (Suh, Wilson et al. 1997).

The next steps in the BER process involve repair of the DNA strand break through DNA synthesis and ligation. However, depending on the nature of the AP site and lesion encountered, repair may then advance through either a short-patch or long-patch mechanism (Frosina, Fortini et al. 1996). SP-BER requires DNA polymerase beta (Pol β) to extend the 3′-OH terminus (Singhal and Wilson 1993, Sobol, Horton et al. 1996) and remove the 5′-terminal dRP group (Matsumoto and Kim 1995). Finally, the resulting nick is sealed by DNA ligase III in complex with the X-ray repair cross-complementing protein 1

(XRCC1) (Wei, Robins et al. 1995). Conversely, long-patch BER results in the strand-displacement synthesis of 2–12 nucleotides past the lesion site. However, the identity of the DNA polymerase involved remains unclear. DNA synthesis and strand displacement are stimulated by the presence of proliferating cell nuclear antigen (PCNA) (Matsumoto, Kim et al. 1994) and replication protein A (RPA) (DeMott, Zigman et al. 1998). The resulting flap generated by this process is then removed by flap endonuclease 1 (FEN1) (Klungland and Lindahl 1997, Kim, Biade et al. 1998), and the nick is sealed by DNA ligase I (Pascucci, Stucki et al. 1999).

As with most DNA-repair processes, BER is mediated through a series of transient protein complexes that assemble at the damaged site. These complexes vary slightly as a function of the initial lesion encountered. Moreover, lesion specificity is usually dictated during the first step of the repair reaction. To date, at least twelve DNA glycosylases have been identified in mammalian cells, each with unique substrate specificity (Jacobs and Schar 2012). In particular, repair of 8-oxo-dG is initiated by 8-oxo-dG glycosylase (OGG1) and MutY homolog (MUTYH) (van Loon, Markkanen et al. 2010).

1.5.1 OGG1 mediates the removal of genomic 8-oxo-dG

The majority of knowledge regarding the repair of 8-oxo-dG has been derived from genetic studies involving *E. coli*. Bacteria possess extensive error-avoidance mechanisms to mitigate oxidative damage. This system is comprised of several components including the bifunctional DNA glycosylase/AP lyase, MutM, which recognizes and excises 8-oxo-dG opposite cytosine (Boiteux, O'Connor et al. 1987, Tchou, Kasai et al. 1991). *mutM*-deficient

bacteria exhibit an increased G–T transversion frequency (15-fold), consistent with a role in the repair of 8-oxo-dG (Cabrera, Nghiem et al. 1988, Michaels, Pham et al. 1991).

However, in eukaryotes, 8-oxo-dG is processed by a structurally unrelated enzyme, OGG1. *OGG1* was identified in the yeast *Saccharomyces cerevisiae* (*S. cerevisiae*) through the functional complementation of *mutM*-deficient *E. coli* (van der Kemp, Thomas et al. 1996). OGG1 belongs to a superfamily of bifunctional DNA glycosylases that contain a two-domain fold consisting of a helix-hairpin-helix DNA binding motif, followed by a Gly/Pro-rich stretch and an invariant Asp (HhH-GPD) (Lu, Li et al. 2001). HhH-GPD glycosylases employ a conserved mechanism to facilitate catalysis. A catalytic lysine initiates nucleophilic attack at C1′ of the deoxyribose, ultimately resulting in cleavage of the N-glycosylic bond. DNA strand scission subsequently occurs through a β-elimination of the 5′-phosphate (Dodson, Schrock et al. 1993, Dodson, Michaels et al. 1994, Sun, Latham et al. 1995, Tchou and Grollman 1995, Nash, Bruner et al. 1996).

Similar to MutM, OGG1 also displays a clear preference for 8-oxo-dG. Accordingly, ablation of *OGG1* in yeast also results in an increased G–T transversion frequency (11-fold) (Thomas, Scot et al. 1997). While MutM and OGG1 play important cellular roles in bacteria and yeast, the effect is less pronounced in higher eukaryotes. *Ogg1*-knockout mice are viable, and show no marked pathological changes including increased tumor incidence (Klungland, Rosewell et al. 1999, Minowa, Arai et al. 2000, Arai, Kelly et al. 2002, Arai, Kelly et al. 2003). This suggests that alternative pathways operate to control the mutational potential of 8-oxo-dG in higher eukaryotes.

1.5.2 MUTYH provides a backup function to OGG1

While MutM/OGG1 excise 8-oxo-dG opposite cytosine, both glycosylases fail to do so if it is already mispaired with an adenine (Hamm, Gill et al. 2007). In this case, direct removal of 8-oxo-dG would result in a G–T transversion. Instead, excision of the misincorporated dA is performed by the *E. coli* monofunctional DNA N-glycosylase, MutY (Bulychev, Varaprasad et al. 1996). The functional homolog to MutY, MUTYH, was later characterized in humans (Slupska, Baikalov et al. 1996). Interestingly, no homolog has been found in *S. cerevisiae*.

The MUTYH protein has several functional domains: a helix-hairpin-helix (HhH) motif, a pseudo HhH motif, an iron-sulfur cluster loop motif, a NUDIX hydrolase domain, and binding sites for RPA, MSH6, APE1, the Rad9-Rad1-Hus1 (9-1-1) complex, and PCNA. Similar to OGG1, the HhH motif is critical for DNA N-glycosylase activity. However, other motifs are also indispensable for MUTYH to properly function in cells. Accordingly, MUTYH binds to several long-patch factors including RPA and PCNA, suggesting that MUTYH repair is involved in long-patch mediated BER (Markkanen, Dorn et al. 2013).

Similar to the other 8-oxo-dG DNA glycosylases, *mutY* and *Mutyh* have the ability to suppress G–T transversions *in vivo*. *mutY*-deficient *E. coli* display an increased mutation frequency (21-fold) (Au, Cabrera et al. 1988, Nghiem, Cabrera et al. 1988, Michaels, Cruz et al. 1992). Interestingly, *mutM*/*mutY* double mutants result in a greater mutation frequency (633-fold) than each single mutant alone (Michaels, Cruz et al. 1992). Interestingly, M*utyh*-deficient mice do not exhibit an increase in age-related tumorigenesis. However, *Ogg1*/*Mutyh* double-knockout mice show a marked increase in tumor predisposition, most notably in the lung, ovaries, and small intestine (Xie, Yang et al. 2004). Thus, the lack of

both DNA glycosylases in mice parallels the synergistic effects of *mutM* and *mutY* in E. coli. As a result, OGG1 and MUTYH have distinct, but overlapping roles in mediating the repair of 8-oxo-dG.

1.6 MTH1 scavenges for 8-oxo-dGTP

In addition to genomic DNA, nucleotide pools are also vulnerable to oxidative damage. In particular, oxidation of dGTP results in the formation of 8-oxo-7,8,dihyro-2'-deoxyguanosine triphosphate (8-oxo-dGTP) (up to 10% of the total dGTP pool) (Pursell, McDonald et al. 2008). 8-oxo-dGTP is capable of mispairing with a templating dA, thus driving A–C transversions. Accordingly, bacteria encode MutT, which sanitizes the deoxynucleotide triphosphate (dNTP) pool. This enzyme is a pyrophosphohydrolase that hydrolyzes 8-oxo-dGTP to 8-oxo-dGMP and pyrophosphate. The biological importance of this function is revealed by the strong dA:dT to dC:dG (A–C) mutator phenotype of *mutT*-deficient *E. coli* (1000-fold) (Maki and Sekiguchi 1992).

Ortholog searches have revealed the presence of the MutT homologue, MTH1, in higher eukaryotes. MTH1 belongs to the NUDIX hydrolase superfamily and catalyzes the hydrolysis of 8-oxo-dGTP and 8-oxo-dATP (Cai, Kakuma et al. 1995, Kakuma, Nishida et al. 1995). Accordingly, *Mth1*-knockout mice or cells depleted for MTH1 accumulate 8-oxo-dG in their DNA and display a slight increase in mutation and cancer rates (Tsuzuki, Egashira et al. 2001).

1.7 OGG1, MUTYH, and MTH1 constitute the GO repair pathway

The deleterious nature of 8-oxo-dG/8-oxo-dGTP is demonstrated by the concerted

cellular defense mechanisms employed in all cells to mitigate mutagenesis. Accordingly, MutM/OGG1, MutY/MUTYH, and MutT/MTH1 constitute the canonical GO repair pathway (Figure 1-3). MutM/OGG1 initiate the excision and minimize the cellular accumulation of 8-oxo-dG. However, if this does not occur, and replication takes place, then MutY/MUTYH can intercept the resulting 8-oxo-dG:dA mispair. Accordingly, MutY/MUTYH and MutM/OGG1 provide unique, synergistic roles in the repair of 8-oxo-dG. Alternatively, MTH1 hydrolyzes 8-oxo-dGTP, thus sanitizing the dNTP pool (Michaels and Miller 1992, Barnes and Lindahl 2004).

1.8 Redundancy of oxidative DNA damage repair of 8-oxo-dG

Despite the importance of *Ogg1*, *Mutyh*, and *Mth1* in mitigating the mutagenic effects of 8-oxo-dG, disruption of these genes in mice does not cause embryonic lethality (Klungland, Rosewell et al. 1999, Minowa, Arai et al. 2000, Tsuzuki, Egashira et al. 2001, Arai, Kelly et al. 2002, Arai, Kelly et al. 2003, Xie, Yang et al. 2004). This is likely due to the fact that all cells contain redundant oxidative DNA damage recognition systems. A striking example of this reciprocity involves the repair of 8-oxo-dG:dA in *E. coli*. Interestingly, mismatch repair (MMR) shares functional overlap with MutY-initiated BER. Accordingly, overexpression of the MMR protein, MutS, decreases the G–T transversion rate in *mutY*-deficient cells (3-fold) (Zhao and Winkler 2000). Moreover, MMR is particularly important in *S. cerevisiae*, as this organism lacks a functional MutY homolog. Accordingly, MMR has a synergistic effect with OGG1-initiated BER in yeast (Ni, Marsischky et al. 1999). Conversely, MMR appears to play a slightly different role in humans, and is suggested to function as a backup to MTH1 (DeWeese, Shipman et al. 1998, Colussi, Parlanti et al. 2002).

1.9 DNA polymerases are the last line of defense against DNA damage

Despite the presence of several overlapping DNA repair systems, DNA polymerases frequently encounter 8-oxo-dG during replication, trans-lesion synthesis (TLS), and gap-filling associated with MUTYH-initiated BER. Accordingly, the mutagenic effects of 8-oxo-dG are ultimately mediated by the action of these enzymes. Thus, discrimination against dAMP misincorporation outright is an important factor in the prevention of mutagenesis.

1.9.1 DNA polymerases can be subdivided into several distinct families

The replication of DNA is likely one of the earliest enzymatic activities to appear in the evolution of life. In 1958, Arthur Kornberg discovered DNA polymerase I (Pol I) in *E. coli*, and described the process by which these enzymes replicate DNA (Lehman, Bessman et al. 1958). Since then, a plethora of DNA polymerases have been identified and characterized. The human genome alone encodes at least 14 DNA polymerases, which have been grouped into several families based on sequence similarity: A, B, X, Y, and reverse transcriptase (RT).

Pol γ (gamma) and Pol θ (theta) are both family A DNA polymerases. Pol γ is the only mitochondrial DNA polymerase, and contains both replicative and repair activity (Graziewicz, Longley et al. 2006). Pol θ is less understood, and has been suggested to participate in somatic recombination, TLS, and DNA repair (Yousefzadeh and Wood 2013).

Family B DNA polymerases are the major replicative enzymes in humans. This group of proteins includes Pol α (alpha), Pol δ (delta), Pol ε (epsilon), and Pol ζ (zeta). Pol α is responsible for initiating replication and is composed of four subunits including P180,

P70, P49 and P58. The P49 subunit initiates replication by synthesizing an RNA primer, which is subsequently extended by the DNA polymerase subunit P180. Pol δ and Pol ε continue replication by catalyzing lagging and leading strand synthesis, respectively (Garg and Burgers 2005).

Interestingly, Pol δ and Pol ε are also involved in other non-replicative processes as well. Pol δ participates in DNA repair pathways including nucleotide-excision repair (NER) (Jessberger, Podust et al. 1993) and MMR (Longley, Pierce et al. 1997). Pol ε has also been implicated in NER, and appears to play a role in homologous recombination (HR) (Jessberger, Podust et al. 1993). Pol ζ is the only family B member that does not inherently have a replicative function, and has been suggested to play a role in TLS (Gan, Wittschieben et al. 2008).

Family X polymerases appear to perform gap-filling synthesis during DNA repair. Accordingly, these enzymes contain an N-terminal 8 kDa DNA binding domain, which facilitates binding to gapped substrates. This group of proteins consist of Pol β (beta), Pol λ (lambda), Pol μ (mu), and terminal deoxynucleotidyl transferase (TdT). Pol β is exclusively involved in short-patch BER. Pol λ has also been suggested to play a role in BER. Additionally, Pol λ, Pol μ, and TdT are implicated in non-homologous end joining (NHEJ) (Ramadan, Shevelev et al. 2004).

Pol η (eta), Pol ι (iota), and Pol κ (kappa) are specialized family Y DNA polymerases that appear to play a role in TLS. Specifically, Pol η appears to be specialized in mediating bypass of cyclobutane pyrimidine dimers (CPD) (Sale, Lehmann et al. 2012). Finally, telomerase belongs to the RT family. Telomerase is a ribonucleoprotein consisting of telomerase reverse transcriptase (TERT), telomerase RNA (TR), and dyskerin (DKC1).

Telomerase extends the 3′-ends of telomeres using TR as a template (Autexier and Lue 2006).

1.9.2 DNA polymerases share a conserved fold and catalytic mechanism

Despite the functional diversity among all DNA polymerases, most of these enzymes share common features (Steitz 1999). The Klenow fragment of *E. coli* Pol I was the first DNA polymerase structurally characterized (Ollis, Brick et al. 1985). Since then, the structures of a number of DNA polymerases have been solved, with at least one representative member from each DNA polymerase family (Sawaya, Prasad et al. 1997, Wang, Sattar et al. 1997, Huang, Chopra et al. 1998, Ling, Boudsocq et al. 2001). In all cases, the catalytic domain of a DNA polymerase resembles a hand consisting of thumb, finger, and palm subdomains (Figure 1-4A). The fingers and thumb subdomains facilitate DNA and dNTP binding, while the palm contains two to three conserved aspartic acid residues. These residues coordinate two divalent metal ions, which ultimately facilitate a nucleotidyl transferase reaction using an existing DNA strand as a template. Additionally, polymerases also require a primer. The primer is generally a fragment of DNA/RNA that contains a free 3′-OH, which functions as the starting point for the replication reaction (Steitz 1999).

A general model for the nucleotidyl transferase reaction is known as the two-metal ion mechanism (Figure 1-4B) (Beese and Steitz 1991, Steitz and Steitz 1993). Metal A (catalytic) lowers the pK_a of the 3′-OH on the primer strand, thereby enhancing nucleophilic attack of the α-phosphate of the incoming dNTP. This leads to a penta-coordinated transition state. The transition state is resolved by the release of pyro-phosphate (PP_i), and stereochemical inversion about the α-phosphate of the newly

incorporated nucleotide. Conversely, metal B (nucleotide binding) facilitates binding of the incoming dNTP, and subsequently stabilizes the negative charge on the pyrophosphate.

1.9.3 General DNA polymerase fidelity mechanisms

In order to maintain genomic stability, DNA must be replicated with high fidelity. DNA polymerases ensure that each nucleotide added to the growing chain is the Watson–Crick complement of the corresponding templating base. Accordingly, the fidelity of human DNA replication by DNA polymerases is exceptionally high (error rate of $\sim 10^{-6}$) (Loeb and Kunkel 1982). The hydrogen-bond interactions between an incoming nucleotide and a templating base provide the basis for this discrimination (Petruska, Sowers et al. 1986). However, DNA polymerases are more faithful than these interactions alone. Instead, fidelity is the result of a sequential multi-step proofreading process.

Importantly, the geometry of the nascent base pair is a crucial fidelity checkpoint. In the minor groove, hydrogen-bond acceptors are present in the same positions for all canonical Watson–Crick base pairs (Figure 1-5A) (Seeman, Rosenberg et al. 1976). DNA polymerases form sequence-independent interactions with the minor groove of the nascent base pair in order to probe for correct geometry (Morales and Kool 1999, Kunkel and Bebenek 2000). The importance of these residues is demonstrated by the reduced fidelity (10-100-fold) exhibited by polymerases with altered minor groove interactions (Beard, Osheroff et al. 1996, Werneburg, Ahn et al. 1996, Ahn, Werneburg et al. 1997).

Moreover, comparison of several DNA polymerase structures has revealed that conformational changes occur during dNTP binding. These include, but are not limited to, repositioning of the fingers (right-handed DNA polymerases) or thumb (left-handed DNA

polymerases) subdomains (Sawaya, Prasad et al. 1997, Doublie, Tabor et al. 1998, Huang, Chopra et al. 1998, Li, Korolev et al. 1998). Together, these observations have led to a generalized conformational description of a polymerase being in either an open (binary: polymerase–DNA) or a closed (ternary: polymerase–DNA–dNTP) state (Doublie, Sawaya et al. 1999, Kunkel and Bebenek 2000). Interestingly, all Watson-Crick base pairs are nearly identical in size and shape (Figure 1-5A) (Seeman, Rosenberg et al. 1976). Binding of the correct dNTP causes the active site to close around the nascent base pair (Figure 1-5B), facilitating the nucleotidyl transferase reaction. Accordingly, this open-to-closed transition (Kunkel 2004) has been identified as key rate-limiting step in many DNA polymerases (Wong, Patel et al. 1991, Esnouf, Ren et al. 1995). Conversely, binding of the incorrect dNTP inhibits closure and catalysis, thus providing additional selectivity during polymerization (Doublie, Sawaya et al. 1999, Kunkel and Bebenek 2000).

Furthermore, many replicative polymerases contain an auxiliary 3′–5′ exonuclease domain, which removes terminal mispairs by hydrolysis (Figure 1-5C). In addition to the nascent base pair in the active site, polymerases are also sensitive to distortions at the primer terminus. In either case, a mispair will cause polymerization to stall, allowing the exonuclease site to excise the incorrect nucleotide (Kunkel and Bebenek 2000). The importance of this proofreading function is demonstrated by the reduced fidelity (~100-fold) observed in proofreading-defective DNA polymerases (Kunkel 2004).

1.9.4 8-oxo-dG is capable of evading various fidelity checkpoints

An 8-oxo-dG(*syn*):dA mispair is particularly mutagenic as it is treated as a Watson–Crick base pair by many DNA polymerases. In particular, the minor groove geometry of the

mispair is identical to a canonical base pair (Figure 1-2B, right panel), and is thus able to bypass various fidelity checkpoints. Importantly, 8-oxo-dG(*syn*) is capable of utilizing the minor groove interactions used to probe for correct geometry in many DNA polymerases (Brieba, Eichman et al. 2004, Hsu, Ober et al. 2004, Batra, Beard et al. 2010, Batra, Shock et al. 2012, Freudenthal, Beard et al. 2013, Patra, Nagy et al. 2014).

Moreover, the dual-coding potential of 8-oxo-dG is contingent on the N-glycosylic *anti–syn* equilibrium. Depending on the flexibility of the polymerase active site, 8-oxo-dG can adopt either the *anti*- or *syn*-conformation, and thus drive either error-free (dCMP) or error-prone (dAMP) insertion, respectively. Replicative DNA polymerases have a compact active site intolerant of the electrostatic distortions imposed by the C8-carbonyl of 8-oxo-dG(*anti*) (Figure 1-2A, left panel). Accordingly, these enzymes preferentially accommodate 8-oxo-dG in the *syn*-conformation, and thus promote dAMP misincorporation (Hsu, Ober et al. 2004).

Additionally, an 8-oxo-dG(*syn*):dA mispair does not distort the polymerase active site at the primer terminus. Structural distortions induced by terminal mispairs represent the final opportunity for replicative DNA polymerases to recognize a mismatch. Therefore, by mimicking a Watson–Crick base pair, an 8-oxo-dG(*syn*):dA mispair is capable of evading proofreading (Brieba, Eichman et al. 2004, Hsu, Ober et al. 2004, Patra, Nagy et al. 2014).

1.10 Specialized DNA polymerases permit the error-free bypass of 8-oxo-dG

Most replicative DNA polymerases cannot discriminate against an 8-oxo-dG(*syn*):dA mispair or tolerate an 8-oxo-dG(*anti*):dC base pair in their active site. Consequently, these enzymes bypass the lesion with both low fidelity and efficiency (Table 1-1) (Shibutani,

Takeshita et al. 1991, Einolf and Guengerich 2001). Alternatively, polymerases involved in MUTYH-initiated BER must facilitate error-free bypass of 8-oxo-dG in order to prevent a futile round of repair. Pol β and Pol λ incorporate dCMP opposite 8-oxo-dG with both high fidelity and efficiency (Table 1-1) (Miller, Prasad et al. 2000, Brown, Duym et al. 2007, Picher and Blanco 2007), and are thus implicated in this repair pathway.

1.11 DNA polymerase beta (Pol β)

Pol β is a 39 kDa (335 amino acids) family X DNA polymerase encoded by the *POLB* gene (SenGupta, Zmudzka et al. 1986, Abbotts, SenGupta et al. 1988). This polymerase contains distinct N- (8 kDa) and C-terminal (31 kDa) domains (Figure 1-6A). The 31 kDa domain contains nucleotidyl transferase activity (Kumar, Abbotts et al. 1990). Conversely, the 8 kDa domain harbors dRP lyase activity (Matsumoto and Kim 1995) and allows the polymerase to interact with gapped DNA (Sawaya, Prasad et al. 1997). Accordingly, Pol β prefers nicked or small gapped DNA substrates containing a 3′-OH and a 5′-phosphate (Chagovetz, Sweasy et al. 1997, Ahn, Kraynov et al. 1998), consistent with its role in BER (Singhal, Prasad et al. 1995, Sobol, Horton et al. 1996).

Due to its compact size, Pol β has been used extensively as a model to study DNA polymerase activity and fidelity (Beard and Wilson 2014). Pol β is a left-handed DNA polymerase consisting of fingers, palm, and thumb subdomains (Figure 1-6B). The palm contains three conserved catalytic aspartic acid residues, which include Asp^{190}, Asp^{192}, and Asp^{256} (Figure 1-6B). Similar to other DNA polymerases, Pol β undergoes dNTP-induced conformational changes. Specifically, formation of a catalytically active complex requires the closure of the thumb subdomain in order to form a tight pocket around the

nascent base pair. This pocket consists of Asp^{276}, Asn^{279}, Lys^{280}, and Arg^{283} (Figure 1-6B). Asp^{276} and Lys^{280} form Van der Waals stacking interactions with the nascent base pair. Moreover, Asn^{279} and Arg^{283} interact with the minor groove of the incoming nucleotide and templating base, respectively (Sawaya, Prasad et al. 1997). Together, these residues are critical for fidelity (Beard, Osheroff et al. 1996, Beard, Shock et al. 2002).

1.11.1 Pol β promotes error-free incorporation of dCMP opposite 8-oxo-dG

Pol β facilitates the error-free bypass of 8-oxo-dG *in vitro* (Miller, Prasad et al. 2000, Brown, Duym et al. 2007), and has been extensively structurally characterized in the context of this lesion (Krahn, Beard et al. 2003, Batra, Beard et al. 2010, Batra, Shock et al. 2012, Freudenthal, Beard et al. 2013, Freudenthal, Beard et al. 2015, Vyas, Reed et al. 2015). Absent the constraints of a DNA polymerase active site, 8-oxo-dG-containing DNA preferentially adopts the pro-mutagenic *syn*-conformation (Kouchakdjian, Bodepudi et al. 1991, Oda, Uesugi et al. 1991). However, prior to initial dNTP binding, Pol β accommodates the lesion in both the *anti*- and *syn*-conformation (Batra, Shock et al. 2012), thus mitigating the aforementioned miscoding-bias.

Pol β is also capable of tolerating an 8-oxo-dG(*anti*):dCTP base pair in its active site with only minor structural distortions. Specifically, dCTP binding results in repositioning of the DNA backbone (Figure 1-7A, red arrow). This backbone rearrangement alleviates the electrostatic clash between the C8-carbonyl and 5′-phosphate of 8-oxo-dG. Additionally, binding of an 8-oxo-dG(*anti*):dCTP base pair also results in a repositioning of the active site

residue Lys^{280}. In the undamaged structure, Lys^{280} provides a Van der Waals stacking interaction with the templating base and forms a hydrogen bond with the 5′-phosphate. However, upon repositioning of the 5′-phosphate, this interaction can no longer be established. Instead, the ε-amino group of Lys^{280} establishes a weak hydrogen bond with the C6-amino group of 8-oxo-dG. This interaction may stabilize the anti-conformation and facilitate error-free incorporation of dCMP (Figure 1-7A, black arrow) (Krahn, Beard et al. 2003).

1.11.2 Pol β fails to discriminate against the *syn*-conformation of 8-oxo-dG

Although Pol β preferentially inserts dCMP opposite 8-oxo-dG, it is still capable of misincorporating dAMP (2:1 preference – dCMP/dAMP incorporation opposite 8-oxo-dG) (Miller, Prasad et al. 2000, Brown, Duym et al. 2007). Surprisingly, the active site of Pol β can accommodate an 8-oxo-dG(*syn*):dATP mispair. Moreover, the mispair mimics the canonical minor groove geometry of a Watson-Crick base pair. Accordingly, Asn^{279} and Arg^{283} are capable of interacting with the N3 group on the incoming dATP and C8-carbonyl of the templating 8-oxo-dG (Figure 1-7B). Similar to what is observed in replicative DNA polymerases, 8-oxo-dG(*syn*) is also capable of utilizing these minor groove interactions (Freudenthal, Beard et al. 2013), thus evading mismatch detection in Pol β. Together, these structural features further demonstrate the challenge of discriminating against the pro-mutagenic *syn*-conformation of 8-oxo-dG.

1.11.3 Pol β preferentially misincorporates 8-oxo-dGTP opposite dA

Pol β has also been characterized in the context of the 8-oxo-dGTP. 8-oxo-dGTP(*syn*) is stabilized through hydrogen bonding with the Asn^{279} (Batra, Beard et al. 2010). While the polymerase can modify the DNA backbone to accommodate 8-oxo-dG in the *anti*-conformation, repositioning of the α-phosphate of an incoming 8-oxo-dGTP would likely result in a loss of insertion efficiency. In agreement with this idea, Pol β preferentially incorporates 8-oxo-dGMP opposite dA rather than dC (25:1 preference) (Miller, Prasad et al. 2000, Brown, Duym et al. 2007).

1.12 Functional overlap between Pol β and Pol λ during oxidative stress

Pol β contains dRP lyase and nucleotidyl transferase activity, both of which are critical for BER (Dianov and Hubscher 2013). Accordingly, Pol β is widely considered to be the main DNA polymerase involved in this repair pathway and thus functions as a tumor suppressor. Consistent with this idea is the observation that a high percentage of human tumors contain Pol β variants (Wang, Patel et al. 1992, Dobashi, Shuin et al. 1994, Bhattacharyya, Chen et al. 1999, Miyamoto, Miyagi et al. 1999, Starcevic, Dalal et al. 2004). The importance of this protein is further demonstrated by the fact that deletion of the *Polb* gene in mice is embryonic lethal (Sugo, Aratani et al. 2000). Additionally, *Polb*-deficient mouse embryonic fibroblasts (MEFs) are sensitive to methyl methanesulfonate (alkylating agent) (Ochs, Sobol et al. 1999, Sobol and Wilson 2001) and hydrogen peroxide (oxidizing agent) (Horton, Baker et al. 2002), suggesting a universal role in BER. However, hydrogen peroxide sensitivity can be partially complemented by overexpression of Pol λ (Tano,

Nakamura et al. 2007, Braithwaite, Kedar et al. 2010). Thus, Pol λ is also suggested to be involved in the repair of oxidative DNA damage.

1.13 DNA polymerase lambda (Pol λ)

Pol λ is a 68 kDa (576 amino acids) family X DNA polymerase encoded by the *POLL* gene (Garcia-Diaz, Dominguez et al. 2000). This polymerase contains a BRCT, Ser/Pro-rich, 8kDa (dRP lyase), and 31 kDa (nucleotidyl transferase) domain (Figure 1-8A). The BRCT domain is important in mediating protein-protein interactions during NHEJ (Mahajan, Nick McElhinny et al. 2002, Fan and Wu 2004). Conversely, the Ser/Pro-rich domain is the target of post-translational modifications. Specifically, this region is phosphorylated by Cdk2/A, which protects Pol λ from degradation (Markkanen, van Loon et al. 2012). Interestingly, the catalytic core (8 kDa and 31 kDa domains) remains closely related to Pol β (32% amino acid identity) (Garcia-Diaz, Bebenek et al. 2004). Accordingly, Pol λ shares several biochemical features with Pol β, and is thus capable of utilizing short gapped BER intermediates (Garcia-Diaz, Bebenek et al. 2002). Pol λ can also utilize longer gapped substrates, which frequently occur during double-strand break repair (Fan and Wu 2004, Lee, Blanco et al. 2004, Ma, Lu et al. 2004, Nick McElhinny, Havener et al. 2005). Because of these properties, Pol λ was originally suggested to play a role in both BER and NHEJ.

Similar to Pol β (Sawaya, Prasad et al. 1997, Beard and Wilson 2014), Pol λ is a left-handed DNA polymerase consisting of finger, palm, and thumb subdomains (Figure 1-8B). Moreover, the palm subdomain contains three aspartic acids (Asp^{427}, Asp^{429}, and Asp^{490}), which are essential for catalysis (Figure 1-8B). However, unlike Pol β, an open-to-closed

conformational change does not seem to be essential to the Pol λ catalytic cycle (Garcia-Diaz, Bebenek et al. 2005, Liu, Tsai et al. 2016).

Instead, dNTP binding results in the subtle repositioning of both the templating strand and several residues in the thumb subdomain. Tyr^{505}, which initially obstructs dNTP binding, repositions and forms a minor groove interaction with the primer-terminal base. Another significant movement involves Arg^{517}, which initially stacks with the templating base. Upon dNTP binding, this residue relocates to a position similar to that of Arg^{283} in the Pol β closed conformation. Arg^{517} forms part of the nascent base pair binding pocket and establishes minor groove interactions with the templating base in the active site and at the primer terminus. The pocket also consists of Ala^{510}, Asn^{513}, and Arg^{514}, which are analogous to Asp^{276}, Asn^{279}, and Lys^{280} in Pol β, respectively. In Pol λ, Asn^{513} establishes minor groove interactions with the incoming nucleotide. Conversely, Ala^{510} and Arg^{514} form Van der Waals interactions with the nascent base pair (Garcia-Diaz, Bebenek et al. 2005, Bebenek, Pedersen et al. 2014). Together, these residues surround the nascent base pair (Figure 1-8B) and are critical for fidelity (Brown, Pack et al. 2010).

1.13.1 Pol λ may mediate MUTYH-initiated BER

While Pol β is thought to be the main DNA polymerase involved in BER, it is clear that other DNA polymerases also participate in this pathway (Dianov and Hubscher 2013). Multiple lines of evidence have demonstrated the involvement of Pol λ in MUTYH-initiated BER. In contrast to *Polb*, *Poll* is not required for survival in mice (Bertocci, De Smet et al. 2002), which is consistent with the backup role of MUTYH-mediated repair. However, *Poll*-deficient cells are sensitive to hydrogen peroxide (Braithwaite, Kedar et al. 2005, Tano,

Nakamura et al. 2007, Vermeulen, Bertocci et al. 2007), indicating the importance of the polymerase in the cellular tolerance of oxidative stress. Additionally, Pol λ and MUTYH colocalize to cellular sites of oxidative DNA damage (van Loon and Hubscher 2009), suggesting activation of repair upon induction of oxidative stress.

Similar to Pol β (Miller, Prasad et al. 2000, Brown, Duym et al. 2007), Pol λ also preferentially incorporates dCMP opposite 8-oxo-dG (Brown, Duym et al. 2007, Picher and Blanco 2007), an essential feature required for MUTYH-mediated repair. Interestingly, MUTYH-initiated BER appears to proceed through the long-patch route (van Loon and Hubscher 2009). Accordingly, Pol λ bypasses 8-oxo-dG(*anti*):dC base pairs at the primer terminus with a higher propensity than an undamaged base pair, thus promoting long-patch extension (Picher and Blanco 2007). Moreover, error-free bypass of 8-oxo-dG by Pol λ is promoted by the long-patch auxiliary factors PCNA and RPA (Maga, Villani et al. 2007). Together, these properties make Pol λ well suited in facilitating the error-free bypass of 8-oxo-dG during MUTYH-mediated long-patch BER.

1.13.2 Pol λ, oxidative DNA damage, and NHEJ

In addition to base-modifications, ROS are also a major cause of double-strand DNA breaks (Cooke, Evans et al. 2003). NHEJ is one of two pathways that respond to this type of damage, and is initiated by the binding of the Ku70/80 heterodimer to the broken ends. Ku70/80 functions as a scaffold for the recruitment of other protein factors including the DNA ligase IV/XRCC4 complex. This complex can directly ligate aligned, compatible termini that possess a 3′-OH and a 5′-phosphate, but not complex ends, such as those produced by ROS. Alternatively, NHEJ employs additional nucleases, DNA polymerases, polynucleotide

kinases, and other enzymes to render these ends ligatable (van Gent and van der Burg 2007). Moreover, gap-filling synthesis is likely restricted to a DNA polymerase that can tolerate lesions associated with ROS-mediated double strand breaks.

In addition to its role in the repair of 8-oxo-dG, Pol λ can also perform gap-filling synthesis on certain NHEJ-intermediates (Fan and Wu 2004, Lee, Blanco et al. 2004, Ma, Lu et al. 2004, Nick McElhinny, Havener et al. 2005). Additionally, this reaction is stimulated in the presence of ligase IV and XRCC4 (Fan and Wu 2004). Pol λ is also capable of interacting with the Ku70/80 heterodimer through its BRCT domain (Mahajan, Nick McElhinny et al. 2002, Fan and Wu 2004, Lee, Blanco et al. 2004). Thus, the polymerase appears to play a role in NHEJ. In agreement with this idea, *POLL*-defective cells are deficient in NHEJ (Capp, Boudsocq et al. 2006, Terrados, Capp et al. 2009).

1.14 Concluding remarks

Pol λ is implicated in several repair pathways related to oxidative DNA damage (BER and NHEJ), and is thus expected to frequently encounter 8-oxo-dG. Accordingly, the active site of this DNA polymerase must be adapted to cope with the mutagenic nature of the lesion. Interestingly, Pol λ is uniquely capable of mediating error-free bypass of 8-oxo-dG *in vitro*. However, the mechanistic basis for this process is unknown. Therefore, it is important to structurally characterize Pol λ in the context of 8-oxo-dG in order to further understand its cellular role.

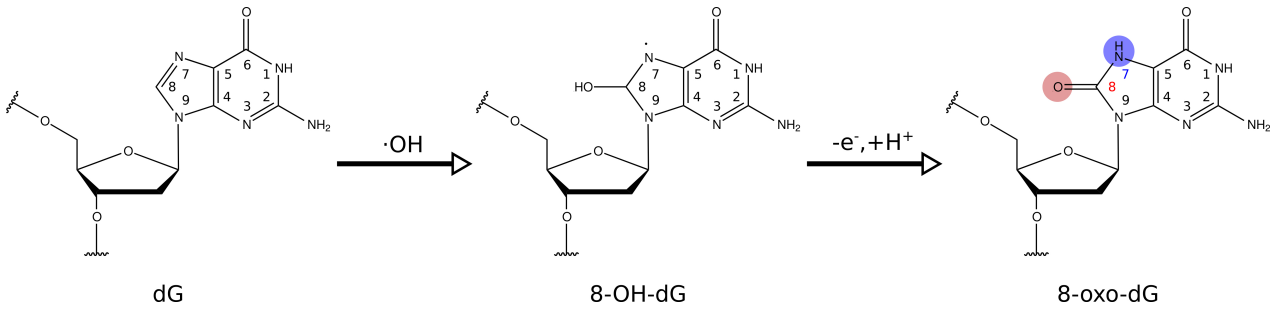

Figure 1-1. Guanine oxidation products
Hydroxyl radical attack of the C8-position of dG and subsequent oxidation results in the formation of 8-OH-dG and 8-oxo-dG, respectively. In comparison to an undamaged guanine, 8-oxo-dG contains an additional carbonyl and proton at the C8 (red circle) and N7 (blue circle) positions.

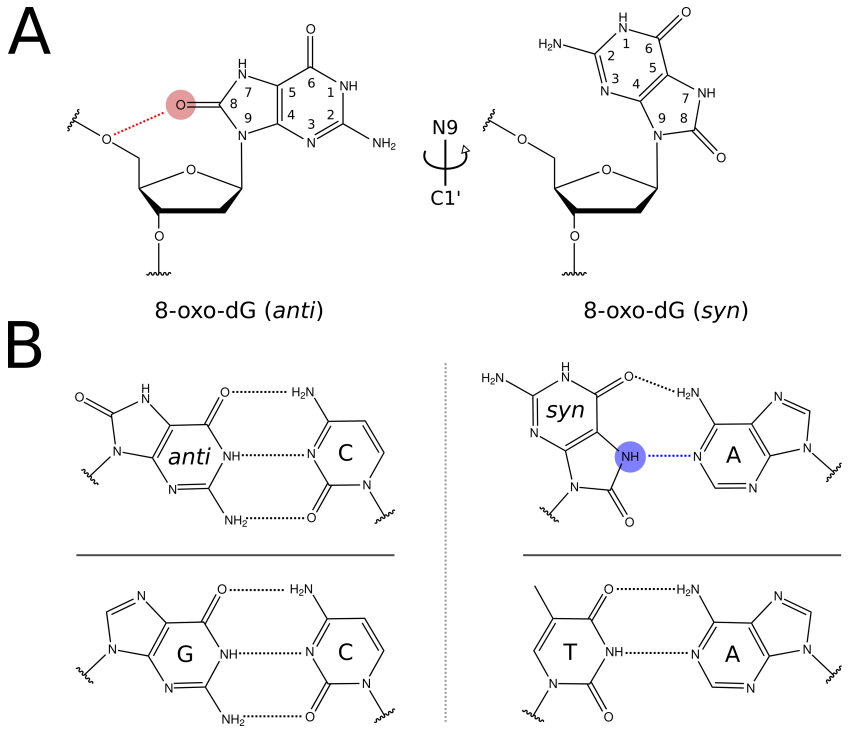

Figure 1-2. Alternate base conformations and dual-coding potential of 8-oxo-dG
(A) 8-oxo-dG can adopt either *anti*- (left panel) or *syn*-conformation (right panel) through rotation about the N9-C1′ glycosidic bond. However, an electrostatic clash between the C8-carbonyl and 5′-phosphate (red-dotted line) causes the damaged base to preferentially adopt the *syn*-conformation. (B) In an *anti*-conformation, 8-oxo-dG forms a Watson-Crick base pair with dC (left panel). For comparison, a canonical dG:dC base pair is shown for reference. Conversely, in the *syn*-conformation, 8-oxo-dG forms a Hoogsteen mispair with dA (right panel). Protonation of N7 contributes to this structure by donating a hydrogen bond (blue-dotted line) to N1-group of adenine. A canonical dT:dA base pair is shown for reference.

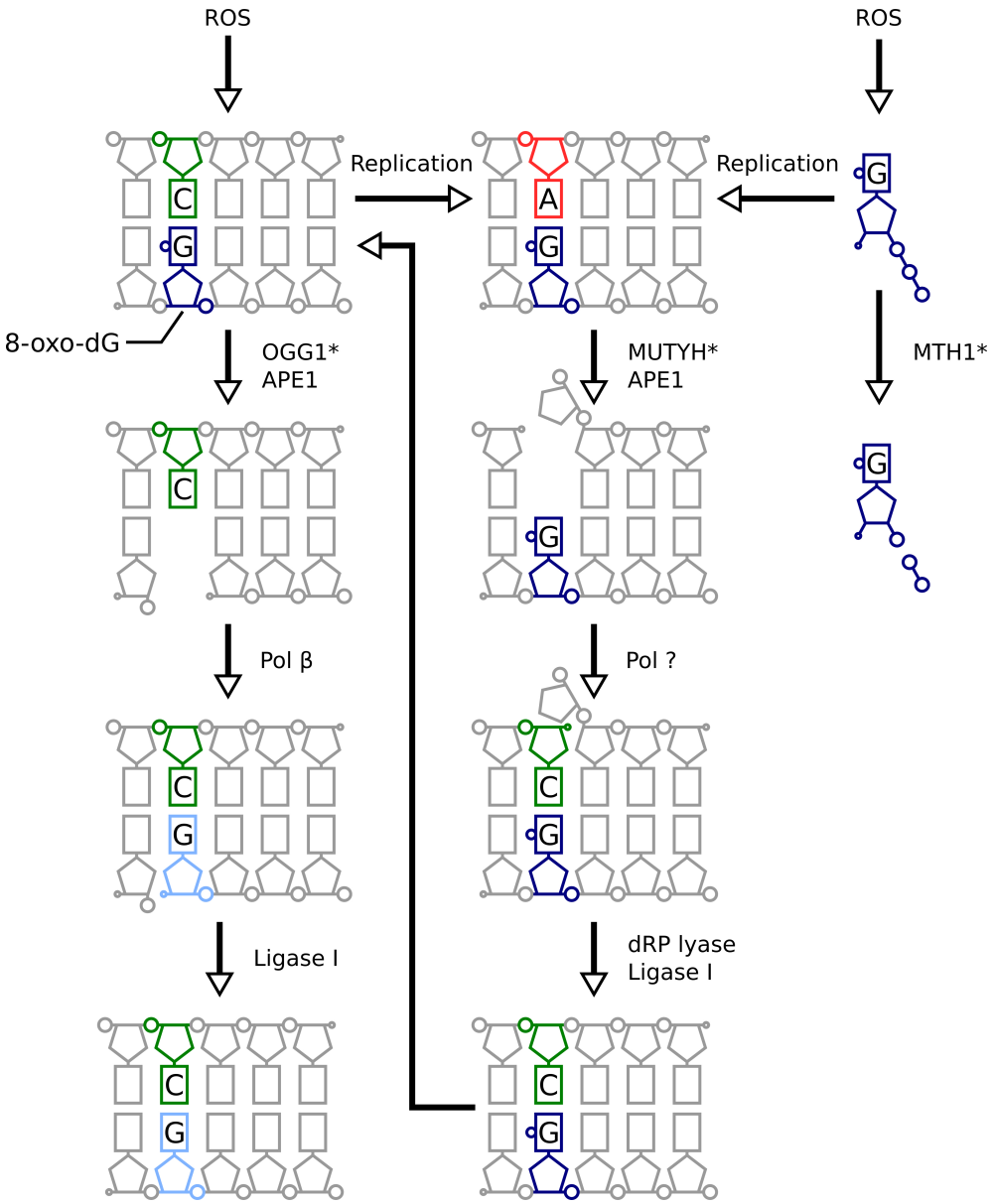

Figure 1-3. The GO repair pathway
Oxidation of DNA and free nucleotides can result in the formation of 8-oxo-dG and 8-oxo-dGTP, respectively. OGG1 initiates the excision of genomic 8-oxo-dG. The resulting 1-nt gap is subsequently filled by the specialized DNA polymerase, Pol β, creating a nick. The nick is then sealed by ligase I to complete repair. If 8-oxo-dG escapes repair and replication occurs, dA will be misincorporated opposite the lesion. In this case, MUTYH recognizes the 8-oxo-dG:dA mispair and excises the misincorporated dA. The resulting 1-nt gap is subsequently filled by specialized DNA polymerases in an error-free manner. Additionally, 8-oxo-dGTP is degraded by the pyrophosphohydrolase, MTH1.

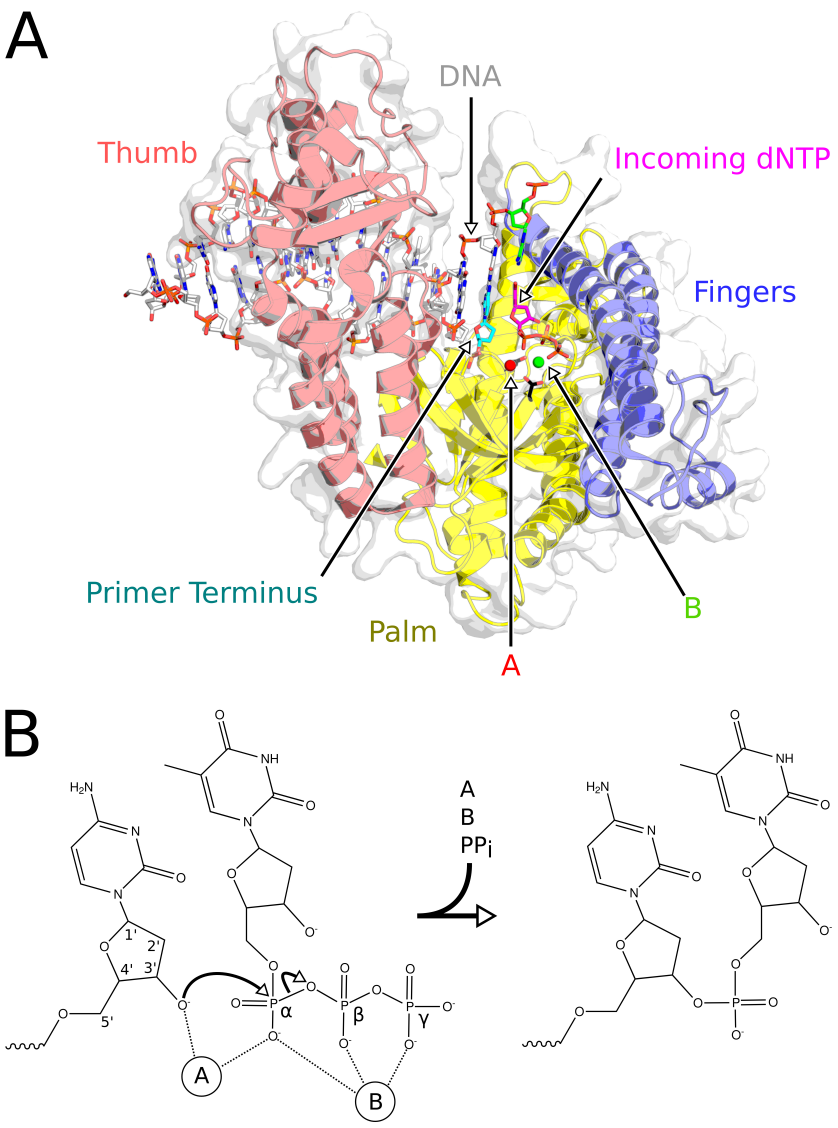

Figure 1-4. Overall fold and mechanism of DNA polymerases
(A) DNA polymerases resemble a right hand consisting of fingers (purple), palm (yellow), and thumb (salmon) subdomains. The fingers and thumb wrap around the DNA (grey) and position it into the active site, which consists of several conserved aspartic acids (black) residues within the palm. These residues coordinate two divalent metal ions, A (red) and B (neon), which are required for the dNTP (magenta) incorporation on the primer terminal strand (cyan). Structure shown – PDB: 1IG9. (B) All DNA polymerases catalyze the same reaction, which is dependent on two metal ions. Metal A stabilizes the deprotonated state of the 3′-OH, thereby facilitating the nucleophile attack of the α-phosphate of the incoming nucleotide. Conversely, Metal B enhances the leaving ability of the β- and γ- pyrophosphate (PP_i) group by counterbalancing the negative charge.

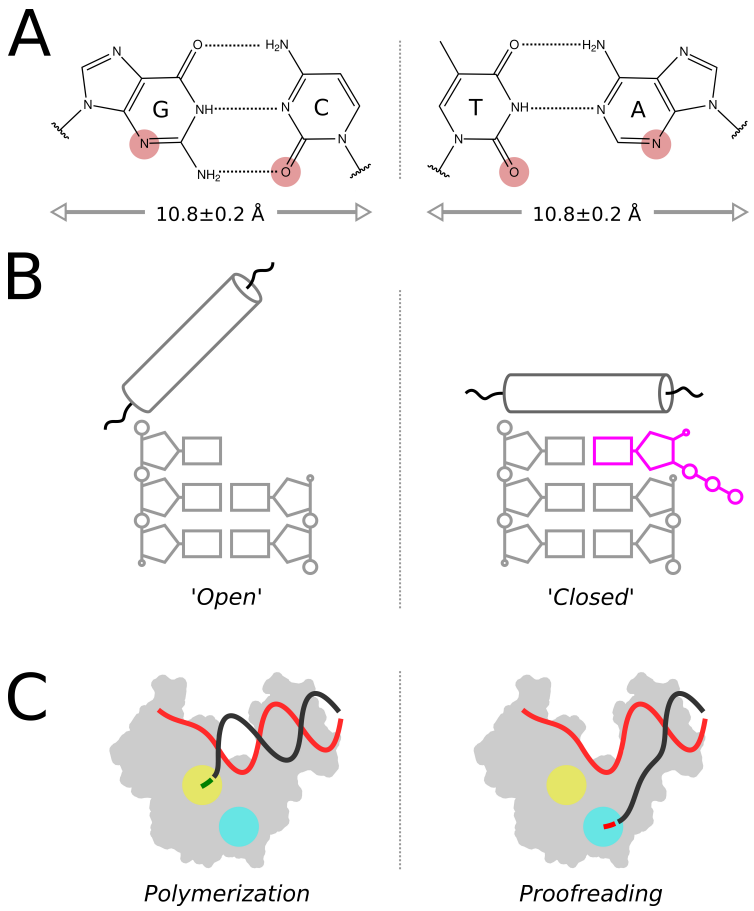

Figure 1-5. General DNA polymerase fidelity mechanisms
(A) Watson-Crick base pairs are the same size and contain minor groove hydrogen-bond acceptor groups (red circle) in the same positions. DNA polymerases utilize these molecular patterns in order to ensure that a proper base pair is formed. (B) Prior to dNTP binding, DNA polymerases adopt an open conformation (left panel). However, binding of the correct dNTP (magenta) induces an open-to-closed conformational change in the DNA polymerase active site into which only Watson-Crick base pairs can fit (right panel). (C) Terminal mispairs halt polymerization (yellow, left panel) and are removed in an alternate proofreading site (teal, right panel).

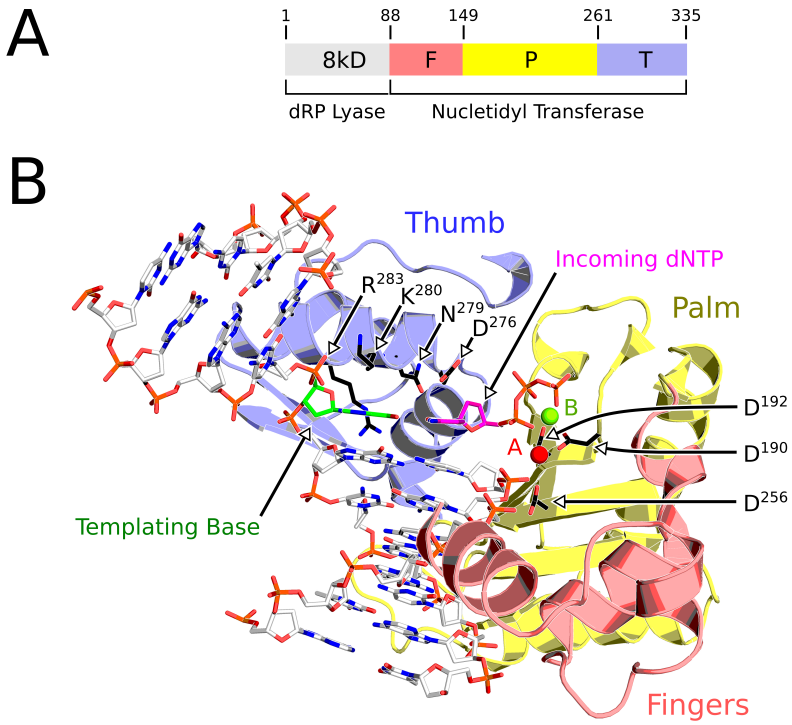

Figure 1-6. Overall structure of DNA polymerase beta
(A) Domain organization of Pol β. (B) Overview of the Pol β structure. The catalytic domain (8-kDa subdomain not shown for clarity) is colored by subdomain: fingers (salmon), palm (yellow), and thumb (purple). The polymerase is in complex with a 1-nt gapped oligonucleotide (grey). The incoming dNTP and corresponding templating base are shown in magenta and green, respectively. Key residues that contribute to the nascent base pair binding pocket (D^{276}, N^{279}, K^{280} and R^{283}) and are involved in catalysis (D^{190}, D^{192} and D^{256}) are shown in black. The metal A and metal B sites are shown in red and neon, respectively. Structure shown – PDB: 1BPY.

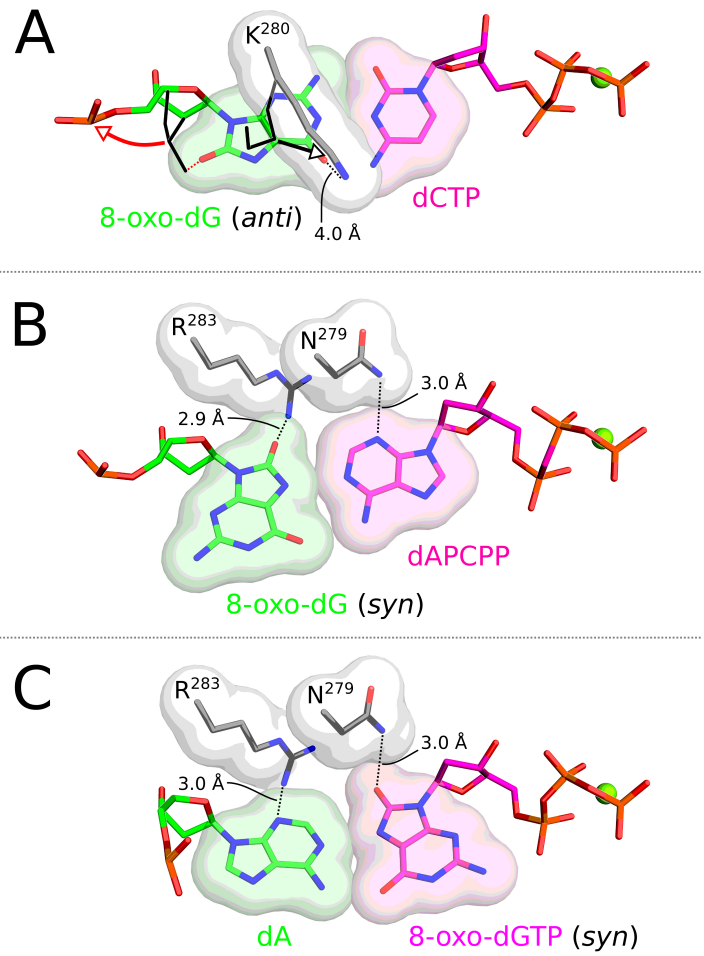

Figure 1-7. Structures of Pol β in complex with 8-oxo-dG-containing DNA/8-oxo-dGTP (A) Overlay of a structure containing a nascent 8-oxo-dG(*anti*):dCTP base pair (PDB: 1MQ3, colored) with an undamaged structure (PDB: 1BPY, black). Binding of 8-oxo-dG in the *anti*-conformation involves a repositioning of the 5′-phosphate (red arrow). Furthermore, the Lys^{280} that normally stacks with the templating base also repositions (black arrow) and forms a weak hydrogen bond with the C6-carbonyl of 8-oxo-dG. (B and C) Structures containing either a nascent 8-oxo-dG(*syn*):dAPCPP (B, PDB: 3RJF) or dA:8-oxo-dGTP(*syn*) mispair (C, PDB: 3MBY). Both mispairs mimic the minor-groove geometry of a canonical Watson-Crick base pair and are capable of interacting with Arg^{283} and Asn^{279}.

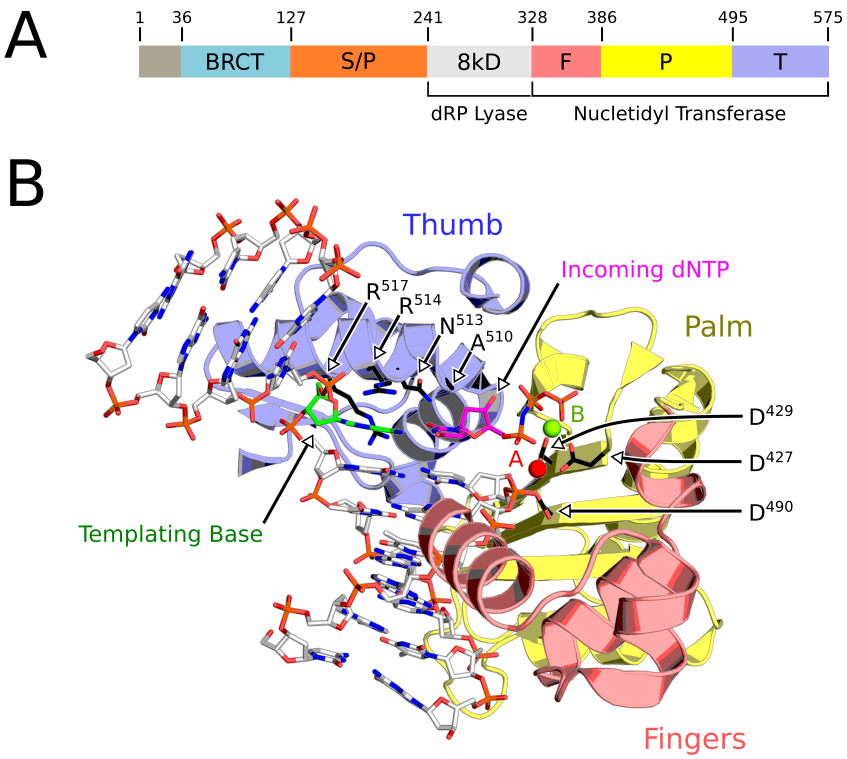

Figure 1-8. Overall structure of DNA polymerase lambda
(A) Domain organization of Pol λ. (B) Overview of the Pol λ structure. The catalytic domain (8-kDa subdomain not shown for clarity) is colored by subdomain: fingers (salmon), palm (yellow), and thumb (purple). The polymerase is in complex with a 1-nt gapped oligonucleotide (grey). The incoming dNTP and corresponding templating base are shown in magenta and green, respectively. Key residues that contribute to the nascent base pair binding pocket (A^{510}, N^{513}, R^{514} and R^{517}) and are involved in catalysis (D^{427}, D^{429} and D^{490}) are shown in black. The metal A and metal B sites are shown in red and neon, respectively. Structure shown – PDB: 2PFO.

Table 1-1. Fidelity/efficiency of insertion opposite 8-oxo-dG by various DNA polymerases

DNA polymerase	Family	Function	Fidelity*	Efficiency**	Reference
Pol α	B	Replication	1:10	50:1	Shibutani et al. 1991
Pol δ			1:2	200:1	Einolf et al. 2001
Pol β	X	Repair	2:1	2:1	Miller et al. 2000
Pol λ			1:1	3:1	Brown et al. 2007

*Fidelity is measured as the ratio of $(k_{cat}/K_M)_{dCTP}$:$(k_{cat}/K_M)_{dATP}$ opposite 8-oxo-dG
**Efficiency is measured as the ratio of $(k_{cat}/K_M)_{dCTP}$:$(k_{cat}/K_M)_{dCTP}$ opposite dG and 8-oxo-dG, respectively

Chapter 2: A novel fidelity mechanism in DNA polymerase lambda promotes error-free bypass of 8-oxo-dG

This chapter contains a description of results that will be incorporated in a manuscript currently in preparation: Burak MJ, Guja KE, Hambardjieva E, Derkunt B, Garcia-Diaz M.

Author contributions: MJB and MGD conceived the project. MJB, EH and BD performed experiments. MJB, KEG and MGD analyzed data. MJB, KEG and MGD wrote the manuscript.

2.1 Abstract

8-oxo-dG has high mutagenic potential as it is prone to mispair with deoxyadenine (dA). In order to maintain genomic integrity, post-replicative 8-oxo-dG:dA mispairs are removed through DNA polymerase lambda (Pol λ) dependent MUTYH-initiated base excision repair (BER). Here, we describe seven novel crystal structures and kinetic data that fully characterize 8-oxo-dG bypass by Pol λ. We demonstrate that Pol λ has a flexible active site that can tolerate 8-oxo-dG in either the *anti*- or *syn*-conformation. Importantly, we show that discrimination against the pro-mutagenic *syn*-conformation occurs at the extension step, and identify the residue responsible for this selectivity. This residue acts as a kinetic switch, shunting repair towards long-path BER upon correct dCMP incorporation, thus enhancing repair efficiency. Moreover, this switch also provides a potential mechanism to increase repair fidelity of MUTYH-initiated BER.

2.2 Introduction

DNA is susceptible to damage by reactive oxygen species (ROS) such as hydroxyl radicals. In particular, hydroxyl radical addition to the C8 position of guanine leads to the formation of 8-oxo-7,8-dihydroxy-2′-deoxyguanosine (8-oxo-dG). 8-oxo-dG is one of the most prevalent types of oxidative DNA damage (Beckman and Ames 1997, Helbock, Beckman et al. 1998). The damaged base is capable of adopting either an *anti*- or *syn*-conformation and can thus base pair with deoxycytosine (dC) or deoxyadenosine (dA), respectively (Kouchakdjian, Bodepudi et al. 1991, Oda, Uesugi et al. 1991, Mcauleyhecht, Leonard et al. 1994, Lipscomb, Peek et al. 1995). As a consequence of this dual coding potential, dAMP is misincorporated opposite 8-oxo-dG by several DNA polymerases (Shibutani, Takeshita et al. 1991, Zhang, Yuan et al. 2000, Einolf and Guengerich 2001, Haracska, Prakash et al. 2002, Haracska, Prakash et al. 2003). Accordingly, failure to remove the DNA lesion prior to replication leads to the accumulation of guanine to thymine (G–T) transversions (Klungland, Rosewell et al. 1999, Hirano, Tominaga et al. 2003, Russo, De Luca et al. 2004). The deleterious nature of 8-oxo-dG is further demonstrated by the concerted cellular defense mechanisms employed in all cells to reduce this particular mutagenic burden (Boiteux, O'Connor et al. 1987, van der Kemp, Thomas et al. 1996).

The base excision repair (BER) pathway is the main mechanism for purging the genome of oxidative lesions such as 8-oxo-dG (Michaels and Miller 1992). Two DNA glycosylases initiate repair of 8-oxo-dG lesions. In humans, OGG1 excises 8-oxo-dG adducts from double stranded DNA, but fails to remove the lesion when mispaired to dA (Aburatani, Hippo et al. 1997, Arai, Morishita et al. 1997, Bjoras, Luna et al. 1997), as direct removal and subsequent repair would also result in a G–T transversion mutation. Instead, another

glycosylase, MUTYH, specifically recognizes the 8-oxo-dG:dA mispair and excises the misincorporated dA (Slupska, Baikalov et al. 1996). The MUTYH-initiated BER pathway ultimately results in the formation of a single nucleotide gap that is subsequently filled by a specialized DNA polymerase. While DNA polymerase beta (Pol β) is involved in OGG1-initiated BER (Dianov, Bischoff et al. 1998, Fortini, Parlanti et al. 1999), DNA polymerase lambda (Pol λ) has been implicated in the MUTYH-dependent BER (Braithwaite, Kedar et al. 2005, Maga, Villani et al. 2007, Tano, Nakamura et al. 2007, Vermeulen, Bertocci et al. 2007, Maga, Crespan et al. 2008, van Loon and Hubscher 2009, Markkanen, Castrec et al. 2012, Pande, Haraguchi et al. 2015).

The success of the repair *in vivo* is contingent on the incorporation of dCMP opposite 8-oxo-dG. In agreement with this idea, Pol λ is capable of mediating error-free bypass of 8-oxo-dG (Brown, Duym et al. 2007, Picher and Blanco 2007). Interestingly, MUTYH-initiated repair appears to preferentially proceed through the alternative long-patch BER pathway (van Loon and Hubscher 2009). Long-patch results in the additional incorporation of several nucleotides, and thus relies on the ability of a polymerase to extend from the original lesion (Frosina, Fortini et al. 1996). Accordingly, Pol λ extends past an 8-oxo-dG:dC base pair with a higher propensity than an undamaged base pair. Moreover, Pol λ is also capable of discriminating against extension of an 8-oxo-dG:dA mispair at the primer terminus (Picher and Blanco 2007). Together, these properties make Pol λ well suited in facilitating the error-free bypass of 8-oxo-dG during MUTYH-mediated BER. However, the mechanistic basis for these unique properties has not yet been elucidated.

Here, we describe seven novel crystal structures that fully characterize the 8-oxo-dG bypass reaction in Pol λ. Each structure corresponds to one of the three key steps during

long-patch bypass – initial binding of the DNA (DNA binding), binding of the dNTP (insertion) and polymerization past the lesion site (extension). Curiously, our structures revealed that Pol λ is incapable of discriminating against the pro-mutagenic *syn*-conformation of 8-oxo-dG during initial DNA binding. We have also demonstrated that the high efficiency of incorporation is attributable to the uniquely malleable active site of Pol λ. During insertion, Pol λ can bind 8-oxo-dG in either the *anti*- or *syn*-conformation with minimal structural distortion.

Importantly, we provide structural and kinetic evidence demonstrating that discrimination against the pro-mutagenic *syn*-conformation occurs during the extension step. This bias depends on a conserved active site residue in the thumb subdomain that enhances nucleotide selectivity and fidelity during 8-oxo-dG bypass. Taken together, our results reveal that Pol λ promotes long-patch BER in order to facilitate the error-free bypass of 8-oxo-dG.

2.3 Results and Discussion

In order to elucidate the mechanism of 8-oxo-dG bypass by Pol λ, we structurally characterized several key steps in the context of long-patch BER – initial binding of 8-oxo-dG-containing DNA (DNA binding), subsequent binding of the incoming dNTP (insertion), and polymerization past the lesion site (extension). Each of these steps can function as a fidelity checkpoint, and present an opportunity for the polymerase to discriminate against dAMP misincorporation opposite 8-oxo-dG.

2.3.1 Pol λ accommodates 8-oxo-dG in the *syn*-conformation during DNA binding

Solution structures demonstrate that an 8-oxo-dG:dA mispair is more stable than an 8-oxo-dG:dC pair (Kouchakdjian, Bodepudi et al. 1991, Oda, Uesugi et al. 1991). Despite this underlying bias, *in vitro* studies with various polymerases indicate that other factors likely influence polymerization fidelity (Miller, Prasad et al. 2000, Brown, Duym et al. 2007). Accordingly, the propensity for either dCMP or dAMP synthesis may be determined by the *anti*/*syn*-conformational equilibrium of 8-oxo-dG in the polymerase active site. We hypothesized that Pol λ may promote dCMP incorporation by preferentially stabilizing the *anti*-conformation of 8-oxo-dG upon initial binding. Therefore, we decided to crystallize Pol λ in complex with a gapped oligonucleotide containing 8-oxo-dG in the templating position Figure 2-1A.

We obtained crystals that diffracted to a resolution of 2.08 Å and contained four molecules of Pol λ in complex with DNA per asymmetric unit (Supplementary Table I, PDB: 5IIO). This structure represents the initial DNA binding step Figure 2-1B. Overall, this structure is very similar to that of the enzyme in a reference structure with unmodified gapped DNA (PDB: 1XSL, RMSD of 0.523 Å over 1258 Cα atoms) (Garcia-Diaz, Bebenek et al. 2005).

Surprisingly, our structure reveals that Pol λ accommodates 8-oxo-dG exclusively in the *syn*-conformation (Figure 2-1C, left panel). In the *anti*-conformation, the C8-carbonyl would clash with the 5′-phosphate (Figure 2-1C, right panel, red-dotted line) in the absence of a substantial rearrangement of the DNA backbone. This rearrangement is likely prohibited as 8-oxo-dG(*syn*) is stabilized by an intramolecular hydrogen bond between its

N2-amino group and a non-bridging oxygen on its 5′-phosphate (3.2 Å) (Figure 2-1D). Additionally, the oxidized base also forms multiple interactions with Tyr^{505} and Arg^{517}. Consistent with what is observed in 1XSL, Tyr^{505} is obstructing the position of the incoming dNTP and forms a hydrogen bond with the C6-carbonyl of 8-oxo-dG (2.8 Å) (Figure 2-1D). Conversely, Arg^{517} provides a Van der Waals stacking interaction with the templating base. Importantly, this residue also forms a hydrogen bonding interaction with another non-bridging oxygen on the phosphate backbone of 8-oxo-dG (2.9 Å) (Figure 2-1D). Together, these interactions likely stabilize 8-oxo-dG in the *syn*-conformation.

2.3.2 Pol λ indiscriminately accommodates 8-oxo-dG during catalysis

Despite the bias in favor of 8-oxo-dG(*syn*) upon initial binding, Pol λ is capable of incorporating dCMP opposite 8-oxo-dG with an efficiency similar to that of an undamaged base (Brown, Duym et al. 2007, Picher and Blanco 2007). In order to identify the structural features that promote error-free incorporation, we crystallized Pol λ in a complex with an 8-oxo-dG:ddCTP base pair in the active site (Figure 2-2A). Our crystallization attempts yielded crystals of a pre-catalytic insertion complex that diffracted to a resolution of 1.72 Å (Table 2-1, PDB: 5IIJ). This structure depicts a polymerase poised for catalysis after undergoing a dNTP-induced conformational change (Figure 2-2B).

The structure reveals that Pol λ can tolerate an 8-oxo-dG:ddCTP base pair in the active site. The damaged base adopts the *anti*-conformation and forms a Watson-Crick base pair with an incoming ddCTP (Figure 2-2C). Moreover, the C8-carbonyl of 8-oxo-dG is far removed from the 5′-phosphate (Figure 2-2C) so as to avoid an electrostatic clash.

Interestingly, the geometry of the pair is similar to other canonical Watson-Crick base pairs. The λ_R angle for the incoming ddCTP is 57.4°, while the λ_γ angle for the templating 8-oxo-dG is 58.1°. Moreover, the C1′–C1′ width of the base pair is 10.6 Å which is similar to other base pairs (10.5 Å – dA:ddTTP, 10.6 Å – dA:dUMPNPP) (Garcia-Diaz, Bebenek et al. 2005, Garcia-Diaz, Bebenek et al. 2007) (Figure 2-2C).

In Pol λ, formation of a catalytically active complex requires a dNTP-induced conformational change that repositions several residues including Asn^{513} and Arg^{517}. These residues form sequence-independent interactions with the minor groove and probe for correct geometry of the nascent base pair in the active site (Garcia-Diaz, Bebenek et al. 2005). Asn^{513} establishes a hydrogen bond with the O2 of the incoming ddCTP while Arg^{517} interacts with the N3 of the templating 8-oxo-dG. These interactions are mostly preserved (Figure 2-2C). However, the hydrogen bonding distance between Arg^{517} and 8-oxo-dG is longer than in a normal Watson-Crick base pair (3.2 Å) (Garcia-Diaz, Bebenek et al. 2005).

Despite this perturbation, an overlay with an undamaged pre-catalytic structure reveals minimal structural distortion around the primer terminus and catalytic active site residues (Figure 2-2D). This is further evidenced by the small RMSD between our structure and a reference structure containing undamaged DNA (PDB: 2PFO, RMSD of 0.241 Å over 233 Cα atoms). Together, these results suggest that Pol λ is capable of accommodating 8-oxo-dG (*anti*) in a catalytically relevant conformation without significant distortion in the active site during catalysis. These results are also consistent with the high efficiency of dCMP insertion opposite 8-oxo-dG observed in Pol λ (Brown, Duym et al. 2007, Picher and Blanco 2007).

In addition to being highly efficient at polymerizing opposite 8-oxo-dG, Pol λ is also capable of discriminating against dAMP misincorporation. However, misincorporation is still a relatively frequent event (2-fold preference for incorporating dCMP over dAMP) (Brown, Duym et al. 2007, Picher and Blanco 2007). In order to obtain insight into the structural basis of this reaction, we crystallized Pol λ in complex with an 8-oxo-dG:dATP mispair in the active site (Figure 2-3A and 3B). Our crystals diffracted to a resolution of 1.80 Å (Table 2-1, PDB: 5III).

As expected, 8-oxo-dG adopts the *syn*-conformation and forms a Hoogsteen mispair with the incoming dATP (Figure 2-3C). In contrast to the 8-oxo-dG(*anti*):dC base pair, which does not substantially alter the DNA conformation, the Watson–Crick base-pairing edge of 8-oxo-dG(*syn*) protrudes into the major groove of the DNA. However, given the absence of protein contacts with the major groove of the DNA in this region (Garcia-Diaz, Bebenek et al. 2005), the Hoogsteen base pair appears to be well tolerated. The λ_R angle for the incoming dATP and the λ_Y angle for the templating 8-oxo-dG are 60.5 and 45.9°, respectively. Interestingly, the C1′–C1′ width of the base pair is 10.6 Å which is also comparable to a Watson-Crick base pair (Garcia-Diaz, Bebenek et al. 2005, Garcia-Diaz, Bebenek et al. 2007). Moreover, an 8-oxo-dG(*syn*):dA mispair mimics the minor groove geometry of a canonical Watson-Crick base pair. Accordingly, Asn^{513} and Arg^{517} are capable of interacting with the N3 group on the incoming dATP and C8-carbonyl of the templating 8-oxo-dG(*syn*) (Figure 2-3C). Similar to what has been observed in other DNA polymerases (Brieba, Eichman et al. 2004, Batra, Shock et al. 2012, Freudenthal, Beard et al. 2013, Vyas, Reed et al. 2015), 8-oxo-dG(*syn*) is also capable of hijacking these interactions in Pol λ, thus circumventing an important fidelity checkpoint mechanism.

An overlay with an undamaged pre-catalytic structure reveals minimal structural distortion around the active site (Figure 2-3C). This is consistent with the small RMSD between our structure and a reference undamaged structure (PDB: 2PFO, RMSD of 0.243 Å over 234 Cα atoms). Together, these results suggest that Pol λ can bind 8-oxo-dG in the *syn*-conformation without significant distortion in the active site. These findings are in agreement with previous kinetic results demonstrating that dCMP/dAMP are incorporated with similar efficiency opposite 8-oxo-dG by Pol λ (Brown, Duym et al. 2007, Picher and Blanco 2007).

2.3.3 Active site rearrangements facilitate incorporation opposite 8-oxo-dG

Close inspection of both structures reveal that the C8-carbonyl of 8-oxo-dG(*anti*) and the N2-group of 8-oxo-dG(*syn*) impose local structural changes in the DNA backbone (Figure 2-4A and 4B, red-dotted lines). Binding of 8-oxo-dG is only possible because Pol λ can tolerate a drastic repositioning of the 5′-phosphate to avoid these clashes (Figure 2-4A and 4B, red arrows). This in turn leads to a notable change in the conformation of active site residue Arg^{514}, which is displaced by 3.1 Å (Figure 2-4A and 4B, black arrows). In an undamaged complex, Arg^{514} forms a Van der Waals stacking interaction with the templating base and a hydrogen bond with the 5′-phosphate (Garcia-Diaz, Bebenek et al. 2005). However, upon repositioning of the 5′-phosphate this hydrogen bond can no longer be established (Figure 2-4A and 4B, blue-dotted lines).

Upon ddCTP binding, the ε guanidinium group of Arg^{514} is in a position to hydrogen bond with the C6-amino group of 8-oxo-dG (Figure 2-4A). This interaction may function as a

conserved mechanism to stabilize the oxidized lesion. Accordingly, Pol λ exhibits a high efficiency of dNTP incorporation opposite 8-oxo-dG (Miller, Prasad et al. 2000, Brown, Duym et al. 2007). This rearrangement is also observed in the presence of an 8-oxo-dG:dATP mispair. In this case, Arg^{514} forms a hydrogen bond with the C6-amino group of the incoming dATP (Figure 2-4B).

Interestingly, Arg^{514} forms a sequence-dependent interaction with the nascent base pair in both 8-oxo-dG-containing structures. We thus hypothesized that these interactions may facilitate oxidative bypass of the lesion. In order to characterize the putative role of Arg^{514}, we generated an R514L active site substitution. The R514L substitution is expected to exhibit a Van der Waals stacking profile similar to the wild-type (WT) Arg^{514}, while abrogating the hydrogen-bonding potential. Steady-state kinetic parameters for both WT and R514L Pol λ were determined (Table 2-2). Accordingly, the R514L substitution had a modest, but consistent, effect on all substrates tested (2-3-fold). Thus, the interactions established in both damaged structures act in a compensatory manner and nonspecifically enhance the efficiency of 8-oxo-dG bypass.

Together, these results highlight the importance of the malleability of the Pol λ active site to efficiently polymerize opposite 8-oxo-dG. The high efficiency of incorporation opposite 8-oxo-dG is a direct consequence of the ability of the active site to tolerate substantial distortion in the DNA backbone and the fact that compensatory interactions with active site residues help overcome the structural perturbations induced by 8-oxo-dG.

2.3.4 Pol λ accommodates 8-oxo-dG at the primer terminus

The inability of Pol λ to discriminate against dAMP misincorporation opposite 8-oxo-dG implies that other factors must explain the high fidelity of MUTYH-dependent repair *in vivo*. Since MUTYH-dependent repair tends to proceed through long-patch, one possibility is that Pol λ may discriminate against dAMP misincorporation during the incorporation of the next nucleotide (extension). Consistent with this idea, biochemical analysis has shown that Pol λ promotes error-free extension of 8-oxo-dG:dC base pairs (Picher and Blanco 2007). In order to better understand this mechanism, we crystallized Pol λ in a pre-catalytic conformation with DNA containing an 8-oxo-dG:dC base pair at the primer terminus (Figure 2-5A). We obtained crystals that diffracted to 2.15 Å (Table 2-1, PDB: 5IIN). This structure represents a complex poised for extension past an 8-oxo-dG:dC base pair (Figure 2-5B).

Unsurprisingly, the structure reveals that 8-oxo-dG adopts the *anti*-conformation and forms a canonical Watson-Crick base pair with the primer terminal cytosine (Figure 2-5C). Strikingly, the base pair forms several minor groove interactions with Tyr^{505}, Arg^{517} and Glu^{529} (Figure 2-5C). Here, Tyr^{505} and Arg^{517} establish sequence-independent hydrogen bonds with the O2/N3 acceptor groups of the base pair to probe for correct geometry. Interestingly, Glu^{529} forms a sequence specific interaction with the N2-amino group of the primer terminal templating 8-oxo-dG in the *anti*-conformation.

Furthermore, an overlay with an undamaged reference structure reveals minimal structural distortion around the primer terminus and the active site (Figure 2-5D). This is evidenced by the small RMSD between both structures (PDB: 2PFO, RMSD of 0.219 Å over 247 Cα atoms). Thus, Pol λ is capable of tolerating an 8-oxo-dG:dC base pair at the primer

terminus without impeding catalysis. Curiously, while Mg^{2+} is occupying the metal B site, metal A is absent, resulting in a non-catalytic position of the 3′-OH (Figure 2-5D).

The use of non-hydrolyzable analogs in crystallography has been associated with subtle structural deviations (Garcia-Diaz, Bebenek et al. 2007). In order to validate whether our pre-catalytic structure is in a catalytically relevant conformation, we decided to obtain a structure of the pot-catalytic complex. Completion of the nucleotidyl transfer reaction and advancement from pre-catalytic to the post-catalytic complex in Pol λ involves no significant conformational changes, other than stereochemical inversion of the α-phosphate (Garcia-Diaz, Bebenek et al. 2005). Therefore, the post-catalytic complex is also representative of a catalytically relevant conformation. Accordingly, we crystallized the post-catalytic complex containing a newly incorporated dTMP in the active site (Table 2-1, PDB: 5IIK). An overlay between the pre- and post-catalytic structure reveals minimal structural distortion around the primer terminus and the active site (Figure 2-7A) as evidenced by the small RMSD between both structures (RMSD of 0.209 Å over 279 Cα atoms). This confirms that our structure is in a catalytically relevant conformation.

We also crystallized Pol λ with DNA containing an 8-oxo-dG:dA mispair at the primer terminus (Figure 2-6A and 6B). These crystals diffracted to a resolution of 1.94 Å (Table 2-1, PDB: 5IIM). The resulting structure reveals that 8-oxo-dG adopts the *syn*-conformation and forms a Hoogsteen mispair with the primer terminal adenine (Figure 2-6C). As expected, the mispair mimicks the minor groove geometry of a Watson-Crick base pair and is thus capable of interacting with Tyr^{505} and Arg^{517} (Figure 2-6C).

Additionally, an 8-oxo-dG:dA base pair at the primer terminus does not distort the active site of Pol λ (Figure 2-6D). This is further demonstrated by the small RMSD between

our structure and an undamaged structure (PDB: 2PFO, RMSD of 0.295 Å over 247 Cα atoms). Similar to the other extension structure, the catalytic metal A was also absent (Figure 2-6D). We again crystalized a corresponding post-catalytic structure (Table 2-1, PDB: 5IIL) further confirming that the presence of an 8-oxo-dG:dA base pair at the primer terminus does not distort the active site (Figure 2-7B). This is demonstrated by the small RMSD between the pre- and post-catalytic structures (RMSD of 0.168 Å over 305 Cα atoms).

Together, our results suggest that Pol λ is capable of accommodating 8-oxo-dG in both the *syn*- and *anti*- conformations without any significant distortion at the primer terminus, explaining the ability of Pol λ to extend past both pairs.

2.3.5 A key conserved residue discriminates against 8-oxo-dG(*syn*)

While Pol λ appears to tolerate both 8-oxo-dG conformations at the primer terminus, biochemical results (Picher and Blanco 2007) that we were able to reproduce (Table 2-3) demonstrate that it strongly discriminates against extension of an 8-oxo-dG:dA mispair. Surprisingly, close inspection of the extension structures revealed a specific interaction with 8-oxo-dG in the *anti*-conformation. A conserved residue in the SD2 region of the thumb subdomain, Glu^{529}, forms a hydrogen bond with the N2-group of the templating 8-oxo-dG in the *anti*-conformation (Figure 2-8A). Strikingly, this interaction is abolished when 8-oxo-dG adopts the pro-mutagenic *syn*-conformation (Figure 2-8B, red-dotted line). This is likely due to an electrostatic clash between the negatively charged carboxyl group of the aspartic acid side chain and the C8-carbonyl of 8-oxo-dG (Figure 2-8B, blue-dotted line). Thus, Glu^{529} may selectively stabilize correct 8-oxo-dG(*anti*):dC base

pairs while destabilizing 8-oxo- dG(*syn*):dA mispairs. Accordingly, this residue may be responsible for the observed extension bias.

To test this hypothesis and characterize the role of Glu^{529} on 8-oxo-dG discrimination at the extension step, we generated an E529A active-site substitution. We determined steady-state kinetic parameters for dGTP incorporation opposite a templating dC containing either an 8-oxo-dG:dC or dA base pair at the primer terminus (Table 2-3). Interestingly, the E529A substitution had a differential effect on the catalytic efficiency of extension past both base pairs (Figure 2-8C, Table 2-3). With respect to the WT protein, the catalytic efficiency for dGMP incorporation decreased by 2.2-fold when an 8-oxo-dG:dC base pair was at the primer terminus. Conversely, the E529A substitution resulted in a 3.0-fold increase in extension activity past an 8-oxo-dG:dA base pair. Furthermore, the E529A substitution eliminated the extension bias, as the catalytic efficiencies for extension of both pairs were nearly identical (Figure 2-8C, Table 2-3). Thus, our results demonstrate that Glu529 is responsible for the inherent discrimination against extension of 8-oxo-dG:dA mispairs and is likely a key element that allows Pol λ to participate in MUTYH-dependent repair. Interestingly, Glu^{529} is conserved among all species in Pol λ (Figure 2-9), highlighting its evolutionary importance and suggesting that the ability to selectively extend an 8-oxo-dG: dC base pair is a unique and essential adaptation to facilitate MUTYH-dependent repair.

2.3.6 Glu^{529} does not affect polymerization on undamaged substrates

The observation that Glu^{529} can interact with 8-oxo-dG(*anti*) prompted us to determine if this residue can also interact with an undamaged guanine. Analysis of an existing Pol λ complex containing a guanine in the templating position at the primer

terminus (PDB: 2PFO) revealed an identical interaction with Glu^{529} (Figure 2-10A). Conversely, this interaction was absent in all the structures containing and adenine in this position (PDB: 1XSN and others) (Figure 2-10B) (Garcia-Diaz, Bebenek et al. 2005). Surprisingly, this observation suggests that Glu^{529} is able to establish a sequence-specific interaction with the DNA template. This is unexpected for a polymerase, where interactions are typically non-specific, so as to avoid inducing sequence context effects. We thus decided to analyze whether Glu^{529} influences polymerization on undamaged substrates in a sequence-context-dependent manner. Interestingly, our kinetic results indicate that the substitution has no effect on undamaged substrates (Figure 2-8C, Table 2-3), which explains why the mutational spectrum of the polymerase does not appear biased towards sites preceded by a guanine residue in the templates (Bebenek, Garcia-Diaz et al. 2003).

2.4 Discussion

Pol λ is an important repair DNA polymerase that has been implicated in MUTYH-dependent BER (Braithwaite, Kedar et al. 2005, Maga, Villani et al. 2007, Tano, Nakamura et al. 2007, Vermeulen, Bertocci et al. 2007, Maga, Crespan et al. 2008, van Loon and Hubscher 2009, Markkanen, Castrec et al. 2012, Pande, Haraguchi et al. 2015). The DNA glycosylase, MUTYH, initiates repair by excising the misincorporated adenine. The resulting gap must then be filled with dCMP. The structural and kinetic studies presented here reveal the unique mechanism by which Pol λ contributes to the error-free bypass of 8-oxo-dG.

2.4.1 Pol λ stabilizes 8-oxo-dG in the *syn*-conformation prior to dNTP binding

Surprisingly, Pol λ initially binds 8-oxo-dG-containing DNA exclusively in the *syn*-conformation, which is stabilized by Tyr^{505} and Arg^{517}. The clear preference for binding 8-oxo-dG(*syn*) is particularly striking, as this would predispose Pol λ to misinsert dAMP. Interestingly, the structurally related DNA polymerase, Pol β, also facilitates the error-free bypass of 8-oxo-dG *in vitro* (Miller, Prasad et al. 2000, Brown, Duym et al. 2007), and has been extensively characterized in the context of this lesion (Krahn, Beard et al. 2003, Batra, Beard et al. 2010, Batra, Shock et al. 2012, Freudenthal, Beard et al. 2013, Freudenthal, Beard et al. 2015, Vyas, Reed et al. 2015). However, in contrast to Pol λ, Pol β can initially accommodate 8-oxo-dG in both the *anti*- and *syn*-conformation with no strong preference (Batra, Shock et al. 2012). The reason for this is largely related to the substantial differences in the dNTP-induced conformational changes that take place in both enzymes. While Pol λ remains in a closed conformation throughout the catalytic cycle, Pol β initially adopts an open conformation where the equivalent residues to Tyr^{505} (Tyr^{272}) and Arg^{517} (Arg^{283}) are far removed from the templating base (Batra, Shock et al. 2012). Thus, in Pol β, the binding pocket for the templating base is only partially formed prior to dNTP binding, likely explaining why 8-oxo-dG freely adopts either conformation.

2.4.2 Pol λ cannot discriminate against 8-oxo-dG(*syn*) during insertion

During dNTP binding, Pol λ is capable of tolerating 8-oxo-dG in either the *anti*- or *syn*-conformation. Correct and incorrect nucleotides are discriminated from each other on

the basis of proper base pairing geometry. Interestingly, the minor groove geometry of an 8-oxo-dG(*syn*):dA mispair is similar to a canonical Watson-Crick base pair. Thus, 8-oxo-dG(*syn*) is capable of interacting with the minor groove probing residues in Pol λ, Asn^{513} and Arg^{517}. This appears to be a common theme among DNA polymerases that rely on this particular type of interaction for fidelity, such as T7 DNA polymerase (Brieba, Eichman et al. 2004) and *Bacillus stearothermophilus* DNA polymerase I (Hsu, Ober et al. 2004). Accordingly, an 8-oxo-dG(*syn*):dA mispair is also capable of hijacking these minor groove interactions in Pol β (Batra, Beard et al. 2010, Batra, Shock et al. 2012, Freudenthal, Beard et al. 2013, Freudenthal, Beard et al. 2015, Vyas, Reed et al. 2015).

Moreover, in Pol β, it has been postulated that a transient third metal ion (metal C) is important for catalysis. The presence metal C was also suggested to play a role in proper base pair discrimination (Freudenthal, Beard et al. 2013). In agreement with the idea that an 8-oxo-dG(*syn*):dA mispair mimics a canonical base pair, metal C binding was observed following dATP binding (Vyas, Reed et al. 2015). This further demonstrates the difficulty in distinguishing between the *anti*- and *syn*-conformations of 8-oxo-dG. Evidence for the presence of metal C was not seen in any of our structures. It is possible that this mechanism is not conserved in Pol λ. However, due to the transient nature of metal C binding, this might also be due to the fact that we were not able to adequately trap the reaction intermediate.

2.4.3 Pol λ allows for efficient bypass of 8-oxo-dG

Interestingly, the active site of Pol λ is extremely malleable during 8-oxo-dG bypass. Binding of 8-oxo-dG in the *anti*-conformation is only possible as Pol λ can tolerate a drastic

repositioning of the 5′-phosphate. This backbone rearrangement alleviates the electrostatic clash between the C8-carbonyl and 5′-phosphate of 8-oxo-dG. Additionally, binding of an 8-oxo-dG(*anti*):ddCTP also results in a repositioning of the active site residue Arg^{514}. Here, the ε-amino group of Arg^{514} establishes a weak hydrogen bond with the C6-amino group of 8-oxo-dG. This interaction may stabilize the *anti*-conformation and facilitate error-free incorporation of dCMP. Similar rearrangements have also been observed in the active site of Pol β (Krahn, Beard et al. 2003).

Curiously, unlike in Pol β (Batra, Shock et al. 2012, Vyas, Reed et al. 2015), these rearrangements were also observed during dATP binding opposite 8-oxo-dG in Pol λ. Thus, our data implies that Pol λ nonspecifically enhances 8-oxo-dG bypass. As a consequence, Pol λ is able to maintain a high efficiency of incorporation opposite 8-oxo-dG. By contrast, DNA polymerase iota (Pol ι) has a restrictive active site that promotes dCMP incorporation opposite 8-oxo-dG(*syn*) (Kirouac and Ling 2011). Consistently, the restrictive nature of the Pol ι active site likely explains its reduced insertion efficiency opposite the lesion (Zhang, Yuan et al. 2001, Kirouac and Ling 2011). Furthermore, most eukaryotic polymerases involved in replication incorporate nucleotides opposite 8-oxo-dG with very low efficiency relative to undamaged DNA (Shibutani, Takeshita et al. 1991, Zhang, Yuan et al. 2000, Einolf and Guengerich 2001, Haracska, Prakash et al. 2002, Haracska, Prakash et al. 2003).

Although Pol λ incorporates dCMP opposite 8-oxo-dG more frequently than many other polymerases (Hashimoto, Tominaga et al. 2004, Brown, Duym et al. 2007, Picher and Blanco 2007), the fidelity of this reaction is modest at best (2:1 preference – dCMP/dAMP incorporation opposite 8-oxo-dG). This reveals that the high efficiency of incorporation is

perhaps achieved at the expense of replication fidelity. Thus, during the insertion step, efficiency may be more important than fidelity.

Failure to complete BER can result in accumulation of BER intermediates that are cytotoxic to cells (Sobol, Prasad et al. 2000, Sobol, Kartalou et al. 2003). Thus, the low fidelity of incorporation opposite 8-oxo-dG might be an acceptable price to pay to avoid the cytotoxic consequences of stalling BER. Moreover, the high efficiency of 8-oxo-dG bypass by Pol λ is also consistent with its role during NHEJ (Fan and Wu 2004, Lee, Blanco et al. 2004, Nick McElhinny, Havener et al. 2005, Capp, Boudsocq et al. 2006), where the polymerase would frequently encounter oxidatively damaged ends.

2.4.4 Pol λ is adapted to discriminate against 8-oxo-dG during extension

A very interesting and yet unexplained observation is that Pol λ is endowed with the extraordinary ability to extend past 8-oxo-dG with both high efficiency and fidelity (Picher and Blanco 2007). Here, we have identified a residue in the SD2 region of the thumb subdomain that forms a unique sequence-specific hydrogen bond with 8-oxo-dG(*anti*). In fact, owing to this interaction, extension of an 8-oxo-dG:dC pair is even more efficient than extension of an undamaged dG:dC pair (Picher and Blanco 2007). Conversely, the same residue results in an unfavorable interaction with an 8-oxo-dG(*syn*):dA mispair, which reduces the catalytic efficiency of extension. Together, these two effects result in a clear bias towards extension of correct 8-oxo-dG:dC pairs.

Interestingly, the analogous residue in Pol β is also a glutamate (Glu^{295}) (Figure 2-9). However, Glu^{295} does not interact with the primer terminus (Sawaya, Prasad et al. 1997). Instead, this residue plays a role in the catalytic transition from the inactive to active

conformation upon dNTP binding (Sawaya, Prasad et al. 1997). Prior to dNTP binding, one of the active site aspartic acids (Asp^{192}) forms a salt bridge with Arg^{258}, sequestering it in an inactive conformation. Binding of the correct nucleotide results in a conformational change that ultimately disrupts this salt bridge. As a result, Asp^{192} moves in position to anchor the catalytic metal B, while Arg^{258} instead establishes an interaction with Glu^{295}.

Taken together, this is striking example of a residue that is conserved in two related enzymes that play completely different functional roles. This functional divergence stresses how subtle differences in the active site can drastically affect both the functional properties and perhaps the cellular role of a DNA polymerase.

2.4.5 Pol λ dependent MUTYH-initiated BER pathway

The structural and kinetic results that we describe here provide a framework for understanding error-free bypass of 8-oxo-dG by Pol λ in the context of MUTYH-initiated BER. Interestingly, MUTYH-initiated BER appears to predominantly proceed through long-patch (van Loon and Hubscher 2009). Consistent with this observation, the short-patch protein, DNA ligase III, is inefficient at ligating the 3′-terminus of a correct 8-oxo-dG:dC base pair (Hashimoto, Tominaga et al. 2004). Thus, short-patch BER is futile and repair must instead proceed through the alternative long-patch route.

Our results lead to a model for MUTYH-dependent repair (Figure 2-11) where Pol λ plays a central role acting as a kinetic switch that drives the reaction towards long-patch. Pol λ and Pol β exhibit a similar efficiency and fidelity with respect to nucleotide insertion opposite 8-oxo-dG (Brown, Duym et al. 2007, Picher and Blanco 2007). Thus, the DNA polymerase involved during the insertion step may be interchangeable. However, Pol λ

appears to have the unique ability to promote error-free bypass during the extension step. Strikingly, Pol λ bypasses an 8-oxo-dG(*anti*):dC pair at the primer terminus with a higher propensity than an undamaged pair, thus promoting long-patch extension (Picher and Blanco 2007). Moreover, error-free bypass of 8-oxo-dG by Pol λ is promoted by the long-patch auxiliary factors PCNA and RPA (Maga, Villani et al. 2007). Together, these properties make Pol λ well suited in facilitating the error-free bypass of 8-oxo-dG during MUTYH-mediated long-patch BER.

Additionally, Pol λ is also capable of discriminating against error-prone extension, thereby preventing error prone long-patch BER. While it is possible that DNA ligase III can seal the 3′-terminus of an 8-oxo-dG:dA mispair (Hashimoto, Tominaga et al. 2004), this would result in a futile cycle of short-patch repair. Instead, failure to extend the mispair may promote removal of the misincorporated dA in an exonuclease-dependent manner. Accordingly, this increased fidelity may be attributed to the high pyrophosphorolytic activity of Pol λ and its ability to preferentially operate on 8-oxo-dG:dA mispairs (Crespan, Maga et al. 2012). Another possibility is that an extrinsic exonuclease is instead recruited. Interestingly, the primary abasic endonuclease involved in BER, APE1, possesses 3′-5′-exonuclease activity. Moreover, the exonuclease activity of APE1 is enhanced at 3′-termini of mismatches (Wong, DeMott et al. 2003), which suggests a possible proofreading role during BER. Together, our results indicate that Pol λ may stall extension past the 8-oxo-dG:dA mispair to promote excision, thus acting as form of proofreading.

In summary, we have shown here how a family X polymerase takes advantage of subtle active site adaptations to carry out a critical repair reaction. Our results highlight the importance of Pol λ as a key enzyme during MUTYH-initiated BER, provide a mechanistic

explanation for its unique behavior during repair, and uncover a potential mechanism to enhance the fidelity of repair.

2.5 Materials and Methods

2.5.1 Protein purification

The sequence corresponding to residues 242–575 of human DNA polymerase lambda (Pol λ) was previously cloned into the bacterial expression vector pET-22b (Garcia-Diaz, Bebenek et al. 2004). Site-directed mutagenesis was performed on the Pol λ expression vector to generate the R514L and E529A mutants. WT, R514L and E529A Pol λ were subsequently expressed in the *E. coli* strain BL21-CodonPlus(DE3)-RIL and purified as described (Garcia-Diaz, Bebenek et al. 2004).

2.5.2 Oligonucleotides for crystallography

Oligonucleotides used for crystallography (Figure 2-12A-D) were synthesized by solid-state synthesis methods using an automated DNA synthesizer and were subsequently purified by HPLC, ethanol precipitated and quantified by UV absorbance (A_{260}).

2.5.3 Crystallization

All crystallization complexes were formed using an upstream primer, downstream primer containing a 5'-phosphate group, and template. Oligonucleotides were mixed (1:1:1) and heated to 80°C for 10 min before slowly cooling to room temperature in 25 mM Tris–HCl

pH 7.5 and 50 mM $MgCl_2$. Oligonucleotides were subsequently mixed with Pol λ. However, due to the low melting temperature of the downstream primer (DP4, 16 °C), a second annealing step in the presence of protein was used to ensure the proper formation of the final substrate. The resulting mixture (100 µl) contained 15 mM Tris–HCl pH 7.5, 75 mM NaCl, 10 mM $MgCl_2$, 1 mM DTT, DNA (0.5 mM) and Pol λ (0.4 mM).

DNA binding complex: Binary complexes were formed with the oligonucleotides shown in Figure 2-12A. Crystals were grown using the hanging drop method at 4°C by mixing 1 µl of a protein-DNA solution with 1 µl of a reservoir solution containing 0.1 M KCl, 0.01 M $CaCl_2$, 0.05 M HEPES pH 7.0, and 10% PEG 400. The crystals were then transferred to a solution containing 0.1 M KCl, 0.01 M $CaCl_2$, 0.05 M HEPES pH 7.0, and 30% PEG 400 and 25 % w/v glycerol and cryo-cooled in liquid nitrogen prior to data collection.

Insertion complex: Pre-catalytic ternary complexes were formed with the oligonucleotides shown in Figure 2-12B. ddCTP (1 mM) and dATP (4 mM) were sequentially added to a prehybridized protein-DNA solution to allow for the proper formation of a dideoxy-terminated oligonucleotide and binding of the incoming dATP. Crystals were then grown as previously described above. Complexes containing a nascent 8-oxo-dG:ddCTP base pair were formed at 4°C in 0.1 M sodium cacodylate pH 7.0 and 1.0 M sodium acetate trihydrate. The resulting crystals were then transferred to a solution containing 0.1 M sodium cacodylate pH 7.0 and 1.1 M sodium acetate trihydrate and 25 % w/v glycerol for cryo-storage in liquid nitrogen prior to data collection. A subset of these crystals were also soaked overnight in a cryo-solution containing 0.1 M sodium cacodylate pH 7.0, 1.5 M

sodium acetate trihydrate, 25 % w/v glycerol, 100 mM $MgCl_2$ and 15 mM dATP in order to fully exchange the residual ddCTP with dATP.

Extension complex: Pre-catalytic ternary complexes were formed with the oligonucleotides shown in Figure 2-12C-D. dUMPNPP (4 mM) was added to a prehybridized protein-DNA solution. Crystals were then grown as previously described above. Complexes containing either an 8-oxo-dG:dC or dA base pair at the primer terminus were formed at 4°C in 0.2 M ammonium acetate, 0.1 M sodium citrate pH 4.8, and 2-7% PEG 4000, and then transferred to a solution containing 0.2 M ammonium acetate, 100 mM sodium citrate pH 4.8, 2-7% PEG 4000, and 25 % w/v glycerol for cryo-storage in liquid nitrogen prior to data collection.

Post-catalytic nick complexes were formed with the oligonucleotides shown in Figure 2-12E-F. Crystals were grown using a prehybridized protein-DNA solution as previously described above. Complexes containing either 8-oxo-dG:dC or dA base pair at the -1 position were formed at 4°C in 0.2 M ammonium acetate, 0.1 M sodium citrate pH 4.8, and 3-5% PEG 4000 and then transferred to a solution containing 0.2 M ammonium acetate, 0.1 M sodium citrate pH 4.8, 3-5% PEG 4000, and 25 % w/v glycerol for cryo-storage in liquid nitrogen prior to data collection.

2.5.4 X-ray data collection and structure determination

Diffraction data were collected on beamlines X6A, X12C, and X29 of the National Synchrotron Light Source at Brookhaven National Laboratory (BNL) and on beamline BL14-1 at the Stanford Synchrotron Radiation Lightsource (SSRL). All datasets were

collected at 100 K using a wavelength of 0.9795, 1.0, or 1.075 Å. All diffraction data were processed using XDS(Kabsch 2010) and Aimless (Evans and Murshudov 2013) as implemented in the autoPROC pipeline(Vonrhein, Flensburg et al. 2011). Phases were obtained by molecular replacement using Phaser (McCoy, Grosse-Kunstleve et al. 2007); search models for the binary, pre- and post-catalytic complexes were created from 1XSL (Garcia-Diaz, Bebenek et al. 2005), 1XSN (Garcia-Diaz, Bebenek et al. 2005) and 1XSP (Garcia-Diaz, Bebenek et al. 2005) respectively. Model building was carried out in Coot (Emsley, Lohkamp et al. 2010), followed by refinement in Phenix (Zwart, Afonine et al. 2008), Refmac(Murshudov, Skubak et al. 2011), and BUSTER(Smart, Womack et al. 2012). The geometric quality of the refined models was assessed with MolProbity (Chen, Arendall et al. 2010) and the structure validation tools in the Phenix suite. Data collection and refinement statistics are shown in Table 2-1,

2.5.5 Oligonucleotides for steady-state primer extension assays

Oligonucleotides used for steady-state primer extension assays were obtained from Invitrogen (Figure 2-13A-E). Oligonucleotides were purified by HPLC and polyacrylamide gel-electrophoresis (PAGE), quantified by UV absorbance (A_{260}), and heated to 80°C for 10 min before slowly cooling to room temperature overnight in 20 mM Tris–HCl pH 7.5 and 150 mM $MgCl_2$.

2.5.6 Steady-state primer extension assays

Oligonucleotides used to evaluate the biochemical role of Arg^{514} and Glu^{529} in Pol λ are

shown in Figure 2-13A-B and C-E respectively. Upstream primers were 5′ labeled with a Cy3 fluorophore and downstream primers contained a 5'-phosphate group. Pre-hybridized gapped DNA (1:1.2:1.2) or an open duplex (1:1.2) were mixed with either WT, R514L or E529A Pol λ. The resulting mixture (18 µl) contained 50 mM Tris–HCl pH 8.5, 10 mM $MgCl_2$, 1 mM DTT, 4% glycerol, 0.1 mg/ml BSA, P/T (200 nM) and either WT, R514L or E529A Pol λ. The protein/DNA mixture was directly added to varying amounts of the appropriate dNTP to start the polymerization reaction. Reaction mixtures (20 µl) were quenched by the addition of 95% v/v formamide, 10 mM EDTA, 0.001% xylene cyanol, 0.001% bromophenol blue (10 µL). Extended primers were separated by denaturing (8 M urea) 18% w/v PAGE. The fluorescence intensity of the bands was quantified using a Typhoon FLA 9000 imager and ImageQuant software.

2.5.7 Kinetic analysis of the primer extension assays

The observed rate of nucleotide incorporation (extended primer) was plotted as a function of nucleotide concentration. Steady-state kinetic parameters, $V_{\max}$ and K_M, were determined by fitting the data to the Michaelis-Menten equation: $V=V_{max}[S]/(K_M+[S])$. k_{cat} was determined with the equation: $k_{cat} = V_{max}/[E]$.

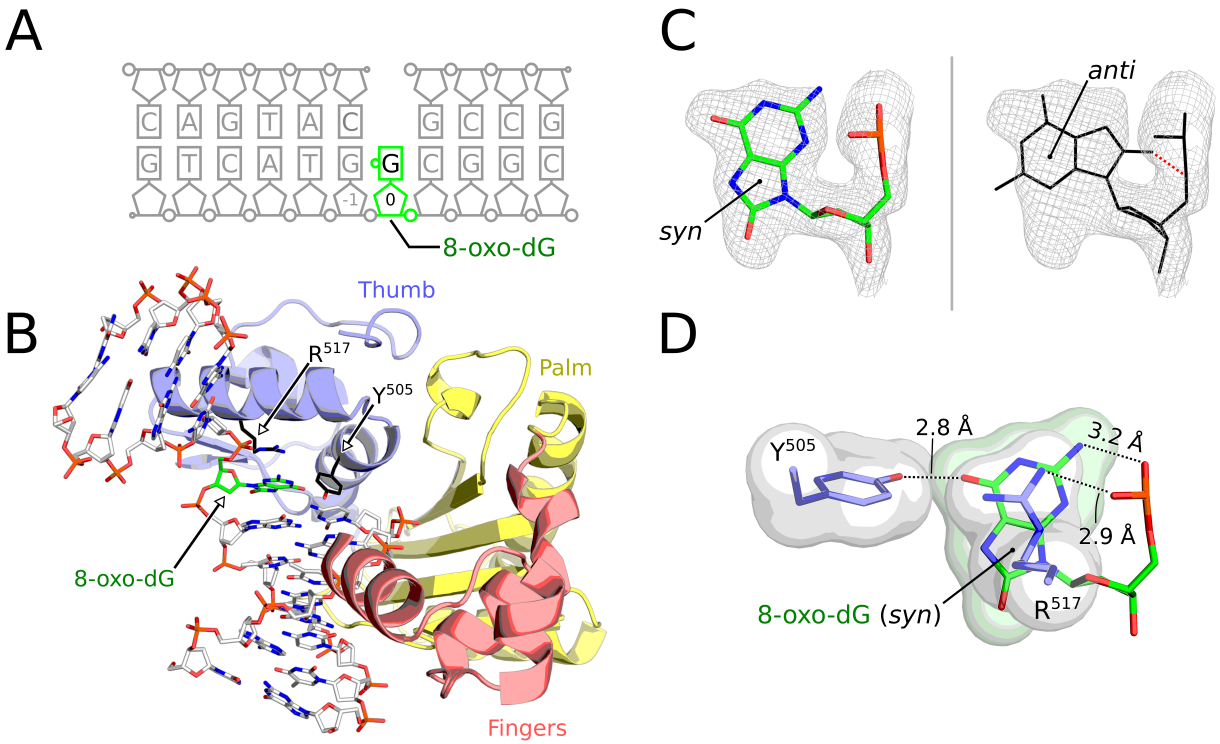

Figure 2-1. Pol λ stablizes 8-oxo-dG in the *syn*-conformation upon initial DNA binding
(A) Substrate used for crystallization of the DNA binding complex. The oligo contains a templating 8-oxo-dG shown in green. (B) The 39-kDa catalytic domain (8-kDa subdomain not shown for clarity) is colored by subdomain: fingers (salmon), palm (yellow) and thumb (purple). The polymerase is in complex with a 1-nt gapped 16-mer oligo (grey) containing a templating 8-oxo-dG (green). Key residues involved in stabilizing the templating base (Y^{505} and R^{517}) are shown in black. (C) (Left panel) 8-oxo-dG (green) preferentially adopts the pro-mutagenic *syn*-conformation. A simulated annealing Fo-Fc omit density map is shown for 8-oxo-dG (contoured at 3σ). (Right panel) 8-oxo-dG(*anti*) (black, modeled using 2PFO)was overlayed with the Fo-Fc omit density map. In the *anti*-conformation, the C8-carbonyl would directly clash with the 5′-phosphate (red-dotted line). (D) 8-oxo-dG(*syn*) (green) is stabilized by multiple interactions, including Tyr^{505} and Arg^{517} (grey).

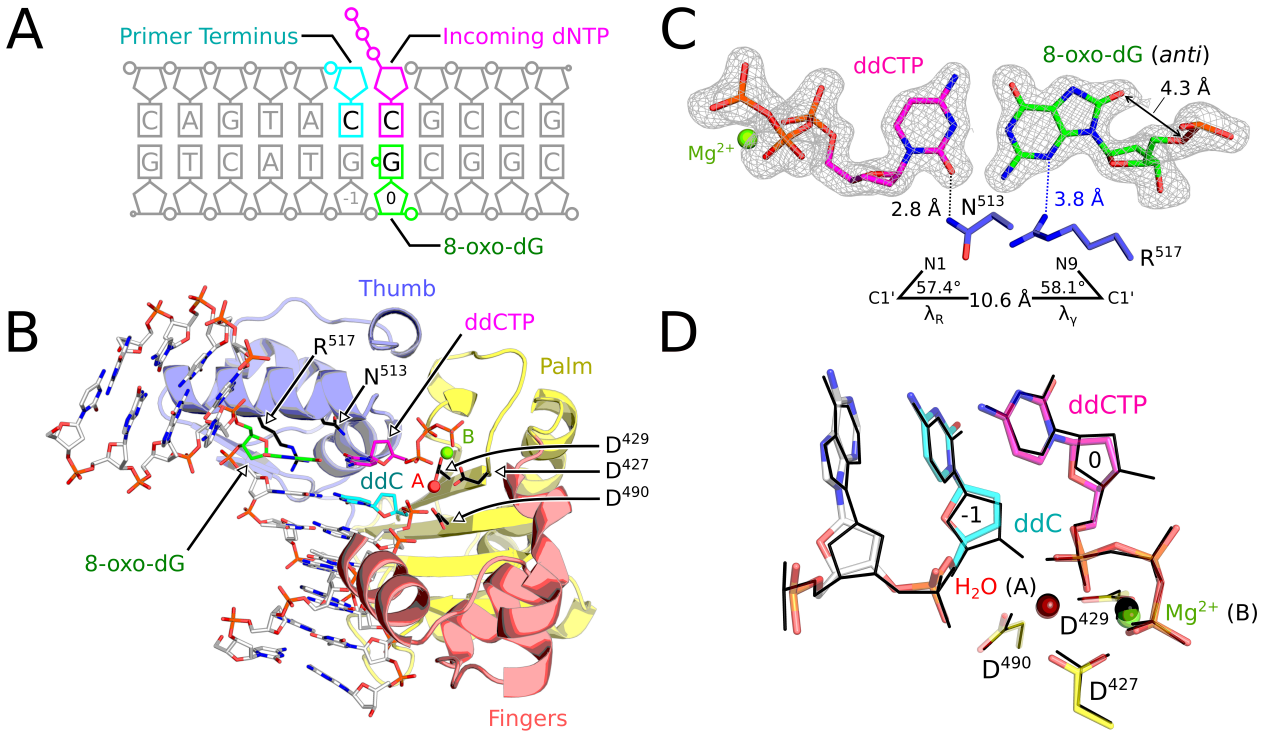

Figure 2-2. Pol λ accommodates an 8-oxo-dG:ddCTP base pair in its active site
(A) Substrates used for crystallization of the 8-oxo-dG:dATP insertion complex. The primer terminal base (ddC) is shown in cyan. The incoming dNTP (ddCTP) and corresponding templating 8-oxo-dG are shown in magenta and green, respectively. (B) Overview of the 8-oxo-dG:dATP insertion complex. The 39-kDa catalytic domain (8-kDa subdomain not shown for clarity) is colored by subdomain: fingers (salmon), palm (yellow) and thumb (purple). The polymerase is in complex with a 1-nt gapped 16-mer oligo (grey) containing a templating 8-oxo-dG (green). The primer terminal ddC and the incoming ddCTP are shown in cyan and magenta, respectively. Key residues that form the nascent base pair binding pocket (N^{513} and R^{517}) and are involved in catalysis (D^{427}, D^{429} and D^{490}) are shown in black. The catalytic metal A and the nucleotide binding metal B are shown in red and neon, respectively. (C) 8-oxo-dG (green) establishes a Watson-Crick pair with ddCTP (magenta). Binding of the 8-oxo-dG in the *anti*-conformation is only possible because the C8-carbonyl is far enough away not to clash with the 5′-phosphate. Asn^{513} and Arg^{517} (purple) interact with the minor groove of the nascent base pair. The base pair geometry (C1′ distance and λ angles) is indicated at the bottom of the figure. A simulated annealing Fo-Fc omit density map for the pair is also shown (contoured at 3σ). (D) Overlay of the primer terminus and active site with an undamaged reference structure (2PFO, black). The catalytic aspartic acids are shown in yellow, the primer terminus in cyan and the incoming dATP in magenta. A water molecule (red) and Mg^{2+} (neon) are occupying the metal A and metal B sites, respectively.

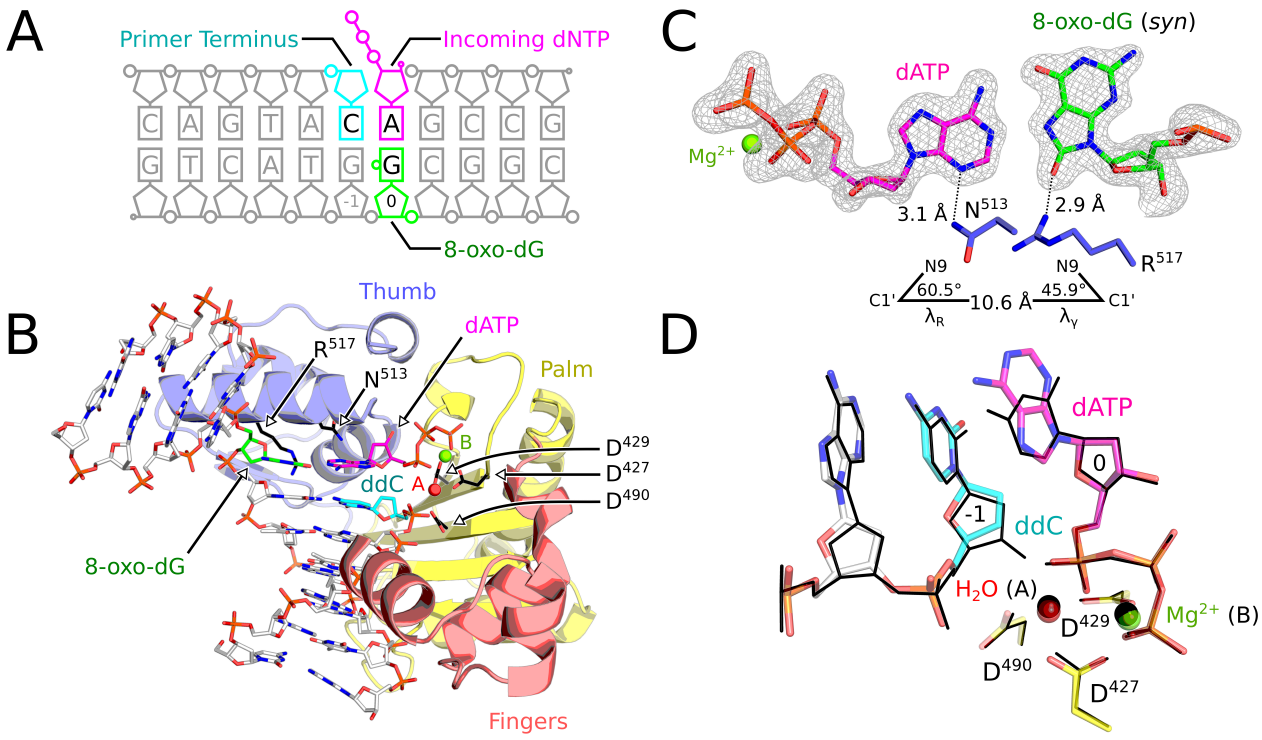

Figure 2-3. Pol λ fails to discriminate against dAMP incorporation opposite 8-oxo-dG
(A) Substrates used for crystallization of the 8-oxo-dG:dATP insertion complex. The primer terminal base (ddC) is shown in cyan. The incoming dNTP (dATP) and corresponding templating 8-oxo-dG are shown in magenta and green, respectively. (B) Overview of the 8-oxo-dG:dATP insertion complex. The 39-kDa catalytic domain (8-kDa subdomain not shown for clarity) is colored by subdomain: fingers (salmon), palm (yellow) and thumb (purple). The polymerase is in complex with a 1-nt gapped 16-mer oligo (grey) containing a templating 8-oxo-dG (green). The primer terminal ddC and the incoming dATP are shown in cyan and magenta, respectively. Key residues that form the nascent base pair binding pocket (N^{513} and R^{517}) and are involved in catalysis (D^{427}, D^{429} and D^{490}) are shown in black. The catalytic metal A and the nucleotide binding metal B are shown in red and neon, respectively. (C) 8-oxo-dG (green) establishes a Hoogsteen base pair with dATP (magenta). Asn^{513} and Arg^{517} (purple) interact with the minor groove of the nascent base pair. The base pair geometry (C1′ distance and λ angles) is indicated at the bottom of the figure. A simulated annealing Fo-Fc omit density map for the pair is also shown (contoured at 3σ). (D) Overlay of the primer terminus and active site with an undamaged reference structure (2PFO, black). The catalytic aspartic acids are shown in yellow, the primer terminus in cyan and the incoming dATP in magenta. A water molecule (red) and Mg^{2+} (neon) are occupying the metal A and B sites, respectively.

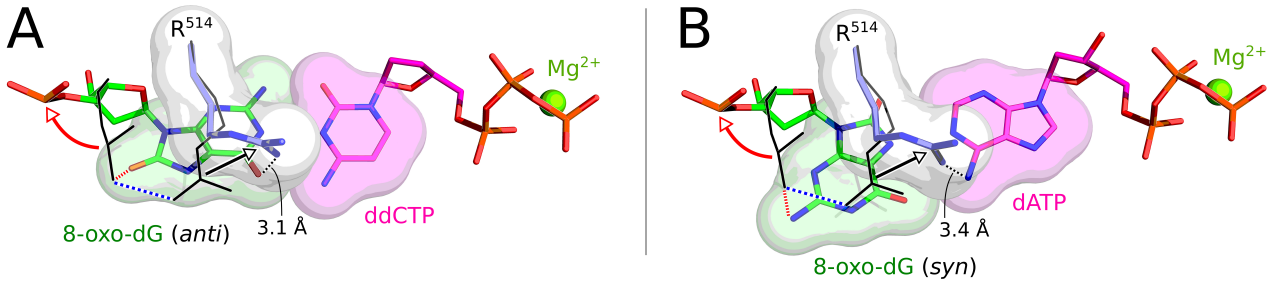

Figure 2-4. Structural rearrangements facilitate incorporation opposite 8-oxo-dG
(A and B) Overlay of the nascent base pair in the insertion structures with an undamaged reference structure (2PFO, black). Binding of 8-oxo-dG (green) in both the *anti*- (A) or *syn*- (B) conformation involves a repositioning of the 5′-phosphate (red arrow). Furthermore, the Arg^{514} side chain (purple) that normally stacks with the templating base and interacts with the 5′-phosphate (blue-dotted line), also repositions (black arrow). In both structures, Arg^{514} interacts with the C6-carbonyl of the templating 8-oxo-dG(*anti*) (A) or the C6-amino group of the incoming dATP (B). The incoming nucleotide is shown in magenta.

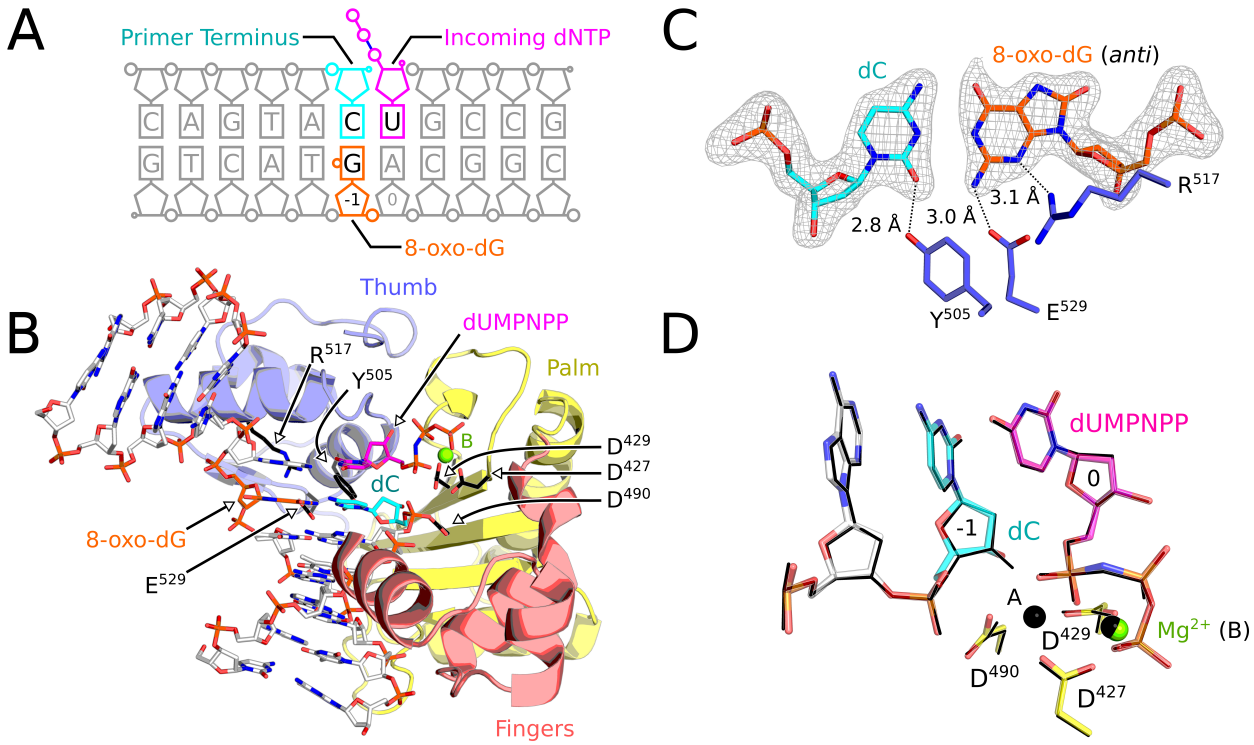

Figure 2-5. Pol λ can tolerate an 8-oxo-dG:dC base pair at the primer terminus
(A) Substrates used for crystallization of the 8-oxo-dG:dC extension complex. The incoming dNTP (dUMPNPP) is shown in magenta. The primer terminal base (dC) and corresponding templating base (8-oxo-dG) are shown in cyan and orange, respectively. (B) Overview of the 8-oxo-dG:dC extension complex. The 39-kDa catalytic domain (8-kDa subdomain not shown for clarity) is colored by subdomain: fingers (salmon), palm (yellow) and thumb (purple). The polymerase is in complex with a 1-nt gapped 16-mer oligo (grey) and an incoming dUMPNPP (magenta). The primer terminal dC and 8-oxo-dG are shown in cyan and magenta, respectively. Key residues that form the primer terminal base pair binding pocket (N^{513}, R^{517} and Glu^{529}) and are involved in catalysis (D^{427}, D^{429} and D^{490}) are shown in black. The nucleotide binding metal (B) is shown in neon. (C) 8-oxo-dG (orange) establishes a Watson-Crick base pair with dC (cyan) at the primer terminus. Tyr^{505}, Arg^{517}, and Glu^{529} (purple) interact with the minor groove of the base pair. The base pair geometry (C1′ distance and λ angles) is indicated at the bottom of the figure. A simulated annealing Fo-Fc omit density map for the pair is also shown (contoured at 3σ). (D) Overlay of the primer terminus and active site with an undamaged reference structure (2PFO, black). The catalytic aspartic acids are shown in yellow, incoming dUMPNPP in magenta, and primer terminal dC in cyan. Expectedly, Mg^{2+} (neon) is occupying the metal B site. However, the metal A is absent in the structure, resulting in a non-catalytic position of the 3′-OH. This is consistent with other structures containing an incoming non-hydrolyzable analog.

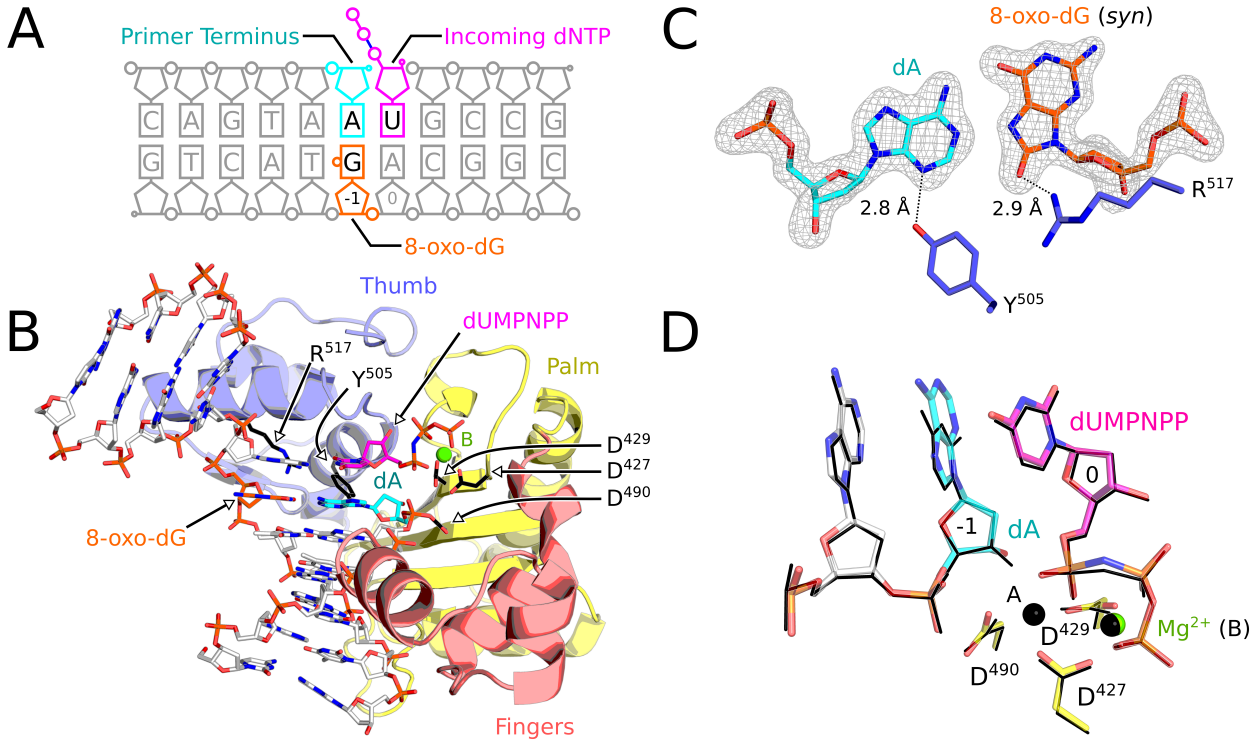

Figure 2-6. Pol λ also appears to tolerate an primer terminal 8-oxo-dG:dA mispair
(A) Substrates used for crystallization of the 8-oxo-dG:dA extension complex. The incoming dNTP (dUMPNPP) is shown in magenta. The primer terminal base (dA) and corresponding templating base (8-oxo-dG) are shown in cyan and orange, respectively. (B) Overview of the 8-oxo-dG:dC extension complex. The 39-kDa catalytic domain (8-kDa subdomain not shown for clarity) is colored by subdomain: fingers (salmon), palm (yellow) and thumb (purple). The polymerase is in complex with a 1-nt gapped 16-mer oligo (grey) and an incoming dUMPNPP (magenta). The primer terminal dA and 8-oxo-dG are shown in cyan and magenta, respectively. Key residues that form the primer terminal base pair binding pocket (N^{513} and R^{517}) and are involved in catalysis (D^{427}, D^{429} and D^{490}) are shown in black. The nucleotide binding metal (B) is shown in neon. (C) 8-oxo-dG (orange) establishes a Hoogsteen base pair with dA (cyan) at the primer terminus. Tyr^{505} and Arg^{517} (purple) interact with the minor groove of the base pair. The base pair geometry (C1′ distance and λ angles) is indicated at the bottom of the figure. A simulated annealing Fo-Fc omit density map for the pair is also shown (contoured at 3σ). (D) Overlay of the primer terminus and active site with an undamaged reference structure (2PFO, black). The catalytic aspartic acids are shown in yellow, incoming dUMPNPP in magenta, and primer terminal dA in cyan. Expectedly, Mg^{2+} (neon) is occupying the metal B site. However, the metal A is absent in the structure, resulting in a non-catalytic position of the 3′-OH. This is consistent with other structures containing an incoming non-hydrolyzable analog.

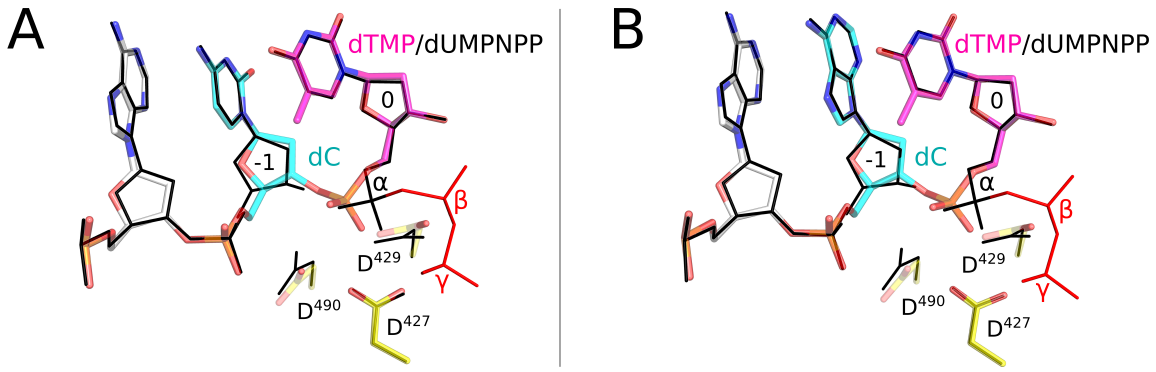

Figure 2-7. 8-oxo-dG at the primer terminus does not distort the Pol λ active site
(A and B) Overlay of the primer terminus and active site between the pre-catalytic and post-catalytic extension structures. The pre-catalytic structure is shown in black, and the β- and γ- phosphates that constitute the pyrophosphate-leaving group are highlighted in red. The post-catalytic structure is colored with the catalytic aspartic acids shown in yellow, the incoming dUMPNPP in magenta, and dC (A) or dA (B) at the primer terminus in cyan.

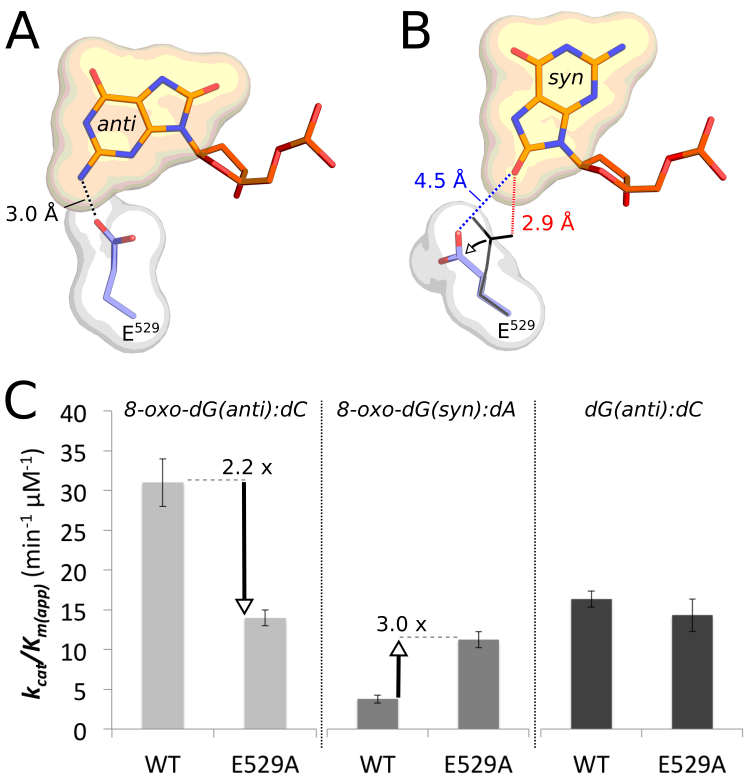

Figure 2-8. Pol λ discriminates against extension past an 8-oxo-dG(*syn*):dC mispair
(A) Glu[529] (purple) forms a hydrogen bond with the C2-amino group of the primer terminal templating 8-oxo-dG (orange) in the *anti*-conformation. (B) This interaction is abolished when 8-oxo-dG (orange) adopts the *syn*-conformation. An overlay with the 8-oxo-dG(*anti*)-containing structure reveals that Glu[529] (black) would likely clash (red-dotted line) with the C8-carbonyl of 8-oxo-dG(*syn*). Repositioning of Glu[529] (purple) places the side chain 4.5 Å away from the C8-carbonyl. (C) Comparison of catalytic efficiencies for extension past an 8-oxo-dG(*anti*):dC, 8-oxo-dG(*syn*):dA and dG:dC base pairs at the primer terminus using WT and E529A Pol λ.

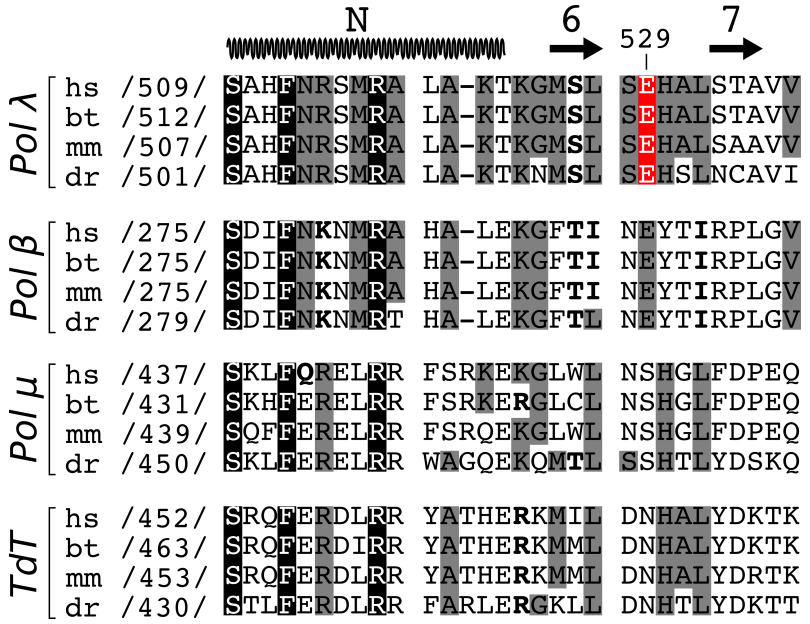

Figure 2-9. Amino acid sequence alignment of eukaryotic family X DNA polymerases
Secondary structure elements are indicated on top of the alignment. White bold letters boxed in black indicate conserved residues. Black letters boxed in grey show invariant residues in at least two of the four groups aligned. Similar residues are bolded. Glu^{529} is conserved among all higher eukaryotes (hs – Homo sapiens, bt – Bos taurus, mm – Mus musculus, dr – Danio rerio) in Pol λ (white bold letters boxed in red).

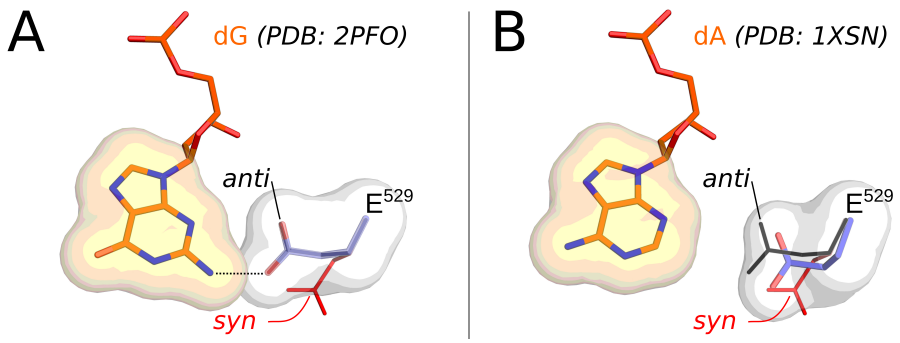

Figure 2-10. Glu^{529} forms a sequence specific interaction with guanines
(A) Undamaged structure containing a templating dG at the primer terminus (2PFO) was overlayed with a structure containing an 8-oxo-dG:dC base pair (black) or an 8-oxo-dG:dA mispair (red) at the primer terminus. (B) Undamaged structure containing a templating dA at the primer terminus (1XSN) was overlayed with a structure containing an 8-oxo-dG:dC base pair (black) or an 8-oxo-dG:dA mispair (red) at the primer terminus.

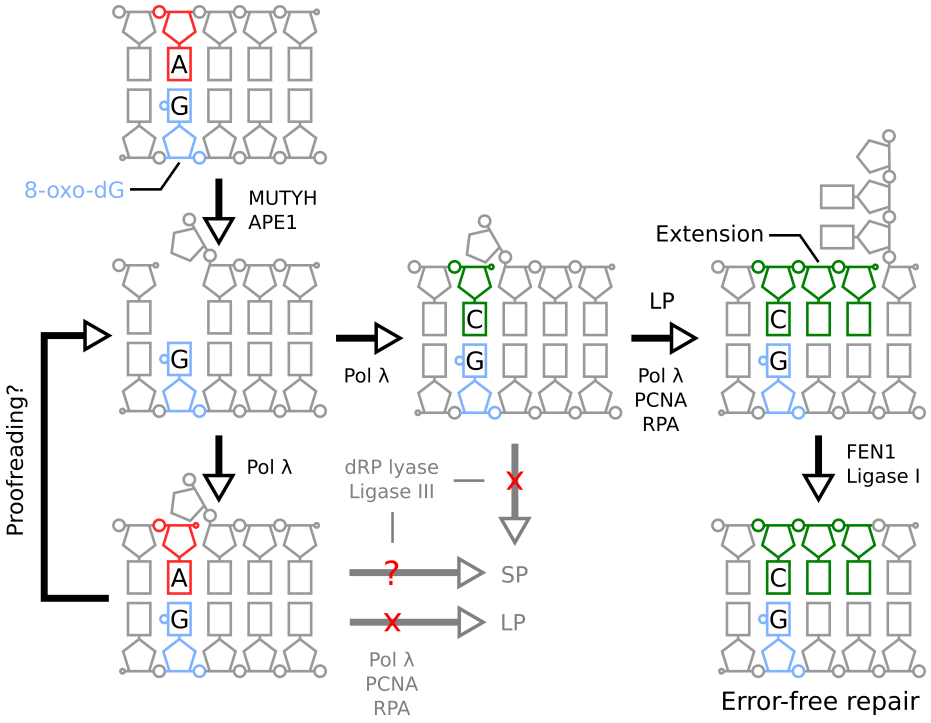

Figure 2-11. Proposed mechanism for Pol λ dependent MUTYH-initiated BER
MUTYH initiates the excision of the misincorporated adenine opposite 8-oxo-dG. The resulting 1-nt gap is subsequently filled by Pol λ in an error-free or error-prone manner. Completion of the canonical short-patch (SP) pathway is futile as DNA ligase III cannot seal an 8-oxo-dG:dC base pair at the primer terminus. Thus, Pol λ promotes the long-patch (LP) extension of past a correct base pair to complete error-free BER. Conversely, Pol λ is capable of stalling ligation (short-patch) or extension (long-patch) of an 8-oxo-dG:dA mispair, thus promoting excision by proofreading. The resulting intermediate can then proceed through the error-free long-patch pathway.

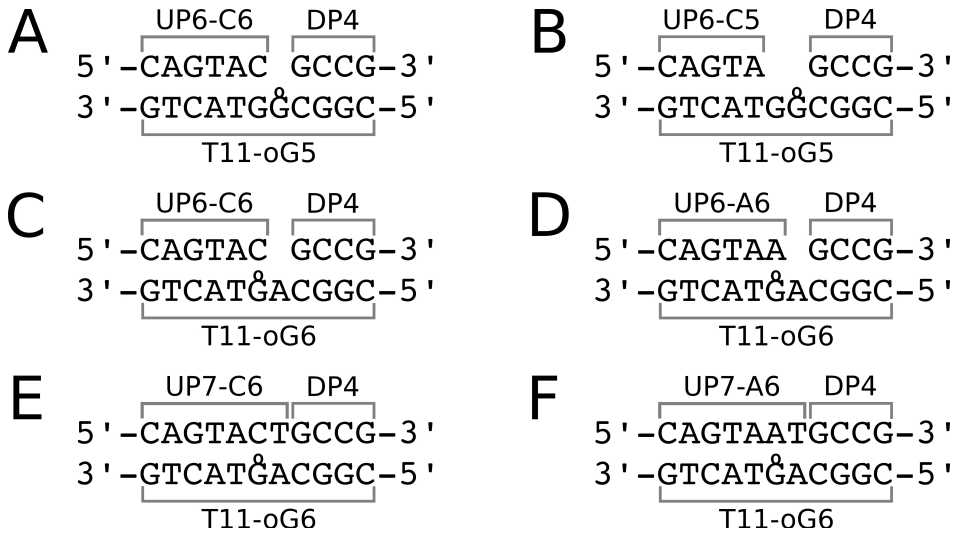

Figure 2-12. Oligonucleotides used in X-ray crystallography experiments
Synthetic oligonucleotides were hybridized and annealed as described in the Materials and Methods section. (A) Substrate used for crystallization of the DNA binding complex. The oligo contains a 1-nt gap and a templating 8-oxo-dG. (B) Substrate used for crystallization of both pre-catalytic insertion complexes. The oligo contains a 2-nt gap. ddCTP was subsequently added to generate a 1-nt gapped, dideoxy-terminated substrate containing a templating 8-oxo-dG. (C and D) Substrates used for the crystallization of the pre-catalytic extension complex. The oligos contain a 1-nt gap and either an 8-oxo-dG:dC (C) or dA (D) base pair at the primer terminus. (E and F) Substrates used for the crystallization of the post-catalytic extension complexes. The oligos contain a nicked primer and either an 8-oxo-dG:dC (E) or dA (F) base pair at the -1 position.

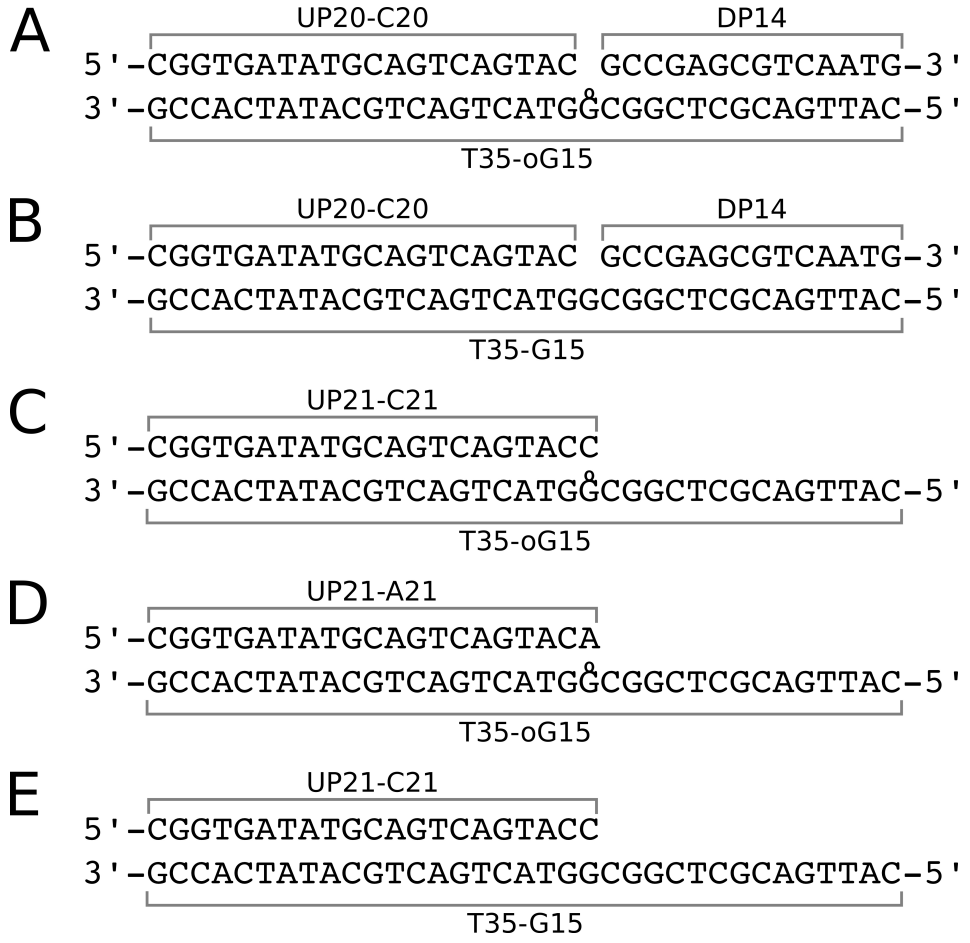

Figure 2-13. Oligonucleotides used in steady-state kinetic experiments
Synthetic oligonucleotides were hybridized as described in the Materials and Methods section. (A and B) Substrates used for WT/R514L Pol λ steady-state kinetic analysis. The oligos contain a 1-nt gap and either 8-oxo-dG (A) or dG (B) in the templating position. (C–E) Substrates used for WT/E529A Pol λ steady-state kinetic analysis. The oligos consist of an open duplex with either an 8-oxo-dG:dC (C), 8-oxo-dG:dA (D), or dG:dC (E) base pair at the primer terminus.

Table 2-1. Data collection and refinement statistics

Crystal	DNA-binding	8-oxo-dG(anti):ddCP insertion (pre-cat)	8-oxo-dG(syn):dATP insertion (pre-cat)	8-oxo-dG(anti):dC extension (pre-cat)	8-oxo-dG(syn):dA extension (pre-cat)	8-oxo-dG(anti):dC extension (post-cat)	8-oxo-dG(syn):dA extension (post-cat)
PDB ID	5IIO	5IIJ	5III	5IIN	5IIM	5IIK	5IIL
Data collection							
Space group	$P\,2_1\,2_1\,2$	$P\,2_1\,2_1\,2_1$	$P\,2_1\,2_1\,2_1$	$P\,2_1\,2_1\,2_1$	$P\,2_1\,2_1\,2_1$	$P\,2_1\,2_1\,2_1$	$P\,2_1\,2_1\,2_1$
Cell dimensions							
a, *b*, *c* (Å)	191.42 98.98 105.03	55.75 62.85 140.08	55.85 62.68 140.02	56.47 62.72 140.01	56.27 63.70 140.73	56.18 63.48 140.37	56.22 63.55 139.85
α, β, γ (˚)	90 90 90	90, 90, 90	90 90 90	90 90 90	90 90 90	90 90 90	90 90 90
Resolution (Å)	45.09 − 2.08 (2.084 − 2.077)	41.71 − 1.72 (1.730 − 1.724)	46.696 − 1.80 (1.805 − 1.799)	40.20 − 2.15 (2.160 − 2.153)	58.03 − 1.94 (1.947 − 1.941)	57.84 − 1.98 (1.989 − 1.982)	69.92 − 1.96 (1.962 − 1.955)
Wavelength (Å)	1.07501	0.97946	0.97946	0.97950	0.97950	1.00000	1.00000
R_{merge}	0.067 (0.745)	0.056 (0.851)	0.062 (0.860)	0.082 (0.780)	0.076 (0.766)	0.048 (0.333)	0.056 (0.562)
R_{meas}	0.073 (0.845)	0.061 (0.915)	0.066 (0.917)	0.089 (0.851)	0.084 (0.848)	0.052 (0.369)	0.061 (0.636)
R_{pim}	0.027 (0.391)	0.022 (0.336)	0.023 (0.316)	0.035 (0.329)	0.035 (0.357)	0.018 (0.155)	0.024 (0.290)
$CC_{1/2}$	0.999 (0.617)	1.000 (0.850)	0.999 (0.868)	0.999 (0.830)	0.994 (0.913)	0.999 (0.935)	0.999 (0.875)
I / σI	20.0 (2.1)	22.8 (2.1)	22.5 (2.7)	16.5 (3.1)	15.1 (2.4)	31.2 (4.7)	24.2 (2.3)
Completeness (%)	98.2 (81.3)	100 (100)	99.4 (100)	98.1 (100.0)	99.7 (99.7)	92.3 (52.4)	96.2 (90.9)
Multiplicity	6.9 (4.6)	7.2 (7.3)	8.1 (8.3)	6.1 (6.1)	5.8 (5.4)	7.8 (5.3)	6.3 (4.1)
Wilson B ($Å^2$)	36.4	25.0	25.1	34.6	28.5	24.7	29.8
Refinement							
Resolution (Å)	45.09 − 2.08	41.71 − 1.72	46.70 − 1.80	40.20 − 2.15	58.03 − 1.94	57.84 − 1.98	69.92 − 1.96
No. reflections	118,537	52,694	42,237	32,307	36,628	32,242	35,462
R_{work} / R_{free}	0.1913 / 0.2351	0.1969 / 0.2240	0.2007 / 0.2251	0.1872 / 0.2314	0.2044 / 0.2496	0.1916 / 0.2378	0.1791 / 0.2172
No. atoms							
Macromolecules	11,867	2,797	2,790	2,929	2,922	2,960	3,000
Ligands	6	48	51	30	30	15	15
Solvent	1,213	410	332	239	349	395	405
B-factors							
Macromolecules	44.0	32.9	34.4	37.0	28.1	26.4	29.6
Ligands	35.9	21.6	22.8	24.3	17.8	20.2	22.9
Solvent	43.6	36.3	38.3	36.3	32.1	30.2	34.4
R.M.S deviations							
Bond lengths (Å)	0.008	0.007	0.007	0.008	0.008	0.007	0.007
Bond angles (˚)	1.030	1.070	1.032	1.030	1.050	1.000	1.020
Ramachandran (favored/outliers; %)	98 / 0	97 / 0	97 / 0	97 / 0	98 / 0	98 / 0	97 / 0

Table 2-2. Steady-state kinetic parameters of insertion opposite 8-oxo-dG by Pol λ

Pol λ	Template	dNTP	K_M (μM)	k_{cat} (min^{-1})	k_{cat}/K_M (min^{-1} μM^{-1})
WT	dG	dCTP	0.8 ±0.2	30.0 ±4.1	42±5
	8-oxo-dG	dCTP	2.2±0.4	23.2±1.8	11±1
		dATP	1.5±0.3	62.6±1.9	42±5
R514L	dG	dCTP	2.5±0.3	43.7±6.6	18±2
	8-oxo-dG	dCTP	4.3±0.4	26.8±2.6	6.2±0.2
		dATP	4.7±0.1	58.9±4.2	13±1

*Each experiment was independently repeated. Reported results are mean ± s.d. from three independent experiments.

Table 2-3. Steady-state kinetic parameters of extension past 8-oxo-dG by Pol λ

Pol λ	Template:Primer	K_M (μM)	k_{cat} (min^{-1})	k_{cat}/K_M (min^{-1} μM^{-1})
WT	dG:dC	2.5 ±0.2	39.1 ±1.5	16±1
	8-oxo-dG:dC	3.3±0.4	101.2±3.5	31±3
	8-oxo-dG:dA	3.5±0.7	12.3±0.5	3.7±0.5
E529A	dG	3.3±0.5	43.9±1.3	14±2
	8-oxo-dG:dC	6.7±0.4	93.8±2.3	14±1
	8-oxo-dG:dA	4.9±0.3	51.9±1.9	11±1

*Each experiment was independently repeated. Reported results are mean ± s.d. from three independent experiments.

Chapter 3: Nucleotide-binding interactions modulate dNTP selectivity and facilitate 8-oxo-dGTP incorporation by DNA polymerase lambda

This chapter has been published as: Burak MJ, Guja KE, Garcia-Diaz M. Nucleotide-binding interactions modulate dNTP selectivity and facilitate 8-oxo-dGTP incorporation by DNA polymerase lambda. Nucleic Acids Res. 2015 Sep 18;43(16):8089-99.

Author contributions: MJB and MGD conceived the project. MJB performed experiments. MJB, KEG and MGD analyzed data. MJB, KEG, and MGD wrote the manuscript.

3.1 Abstract

8-oxo-7,8,-dihydro-2'-deoxyguanosine triphosphate (8-oxo-dGTP) is a major product of oxidative damage in the nucleotide pool. It is capable of mispairing with deoxyadenosine (dA), resulting in futile, mutagenic cycles of base excision repair. Therefore, it is critical that DNA polymerases discriminate against 8-oxo-dGTP at the insertion step. Because of its roles in oxidative DNA damage repair and non-homologous end joining, DNA polymerase lambda (Pol λ) may frequently encounter 8-oxo-dGTP. Here, we have studied the mechanisms of 8-oxo-dGMP incorporation and discrimination by Pol λ. We have solved high resolution crystal structures showing how Pol λ accommodates 8-oxo-dGTP in its active site. The structures indicate that when mispaired with dA, the oxidized nucleotide assumes the mutagenic *syn*-conformation, and is stabilized by multiple interactions. Steady-state kinetics reveal that two residues lining the dNTP binding pocket,

Ala^{510} and Asn^{513}, play differential roles in dNTP selectivity. Specifically, Ala^{510} and Asn^{513} facilitate incorporation of 8-oxo-dGMP opposite dA and dC, respectively. These residues also modulate the balance between purine and pyrimidine incorporation. Our results shed light on the mechanisms controlling 8-oxo-dGMP incorporation in Pol λ and on the importance of interactions with the incoming dNTP to determine selectivity in family X DNA polymerases.

3.2 Introduction

DNA is vulnerable to damage by reactive oxygen species (ROS). Of the four bases, guanine is the most susceptible to oxidative damage owing to its low redox potential (Neeley and Essigmann 2006). Moreover, guanine oxidation products have a high mutagenic potential (Kamiya, Miura et al. 1992, Moriya 1993, Kamiya, Murata-Kamiya et al. 1995, Kamiya, Murata-Kamiya et al. 1995, Le Page, Margot et al. 1995). 8-oxo-7,8-dihydro-2′-deoxyguanosine (8-oxo-dG) is a major oxidative product present in cells and can arise in either DNA or the free nucleotide pool (De Bont and van Larebeke 2004). Accordingly, oxidation of dGTP results in the formation of 8-oxo-7,8,-dihydro-2'-deoxyguanosine triphosphate (8-oxo-dGTP). Experimental measurements indicate that 8-oxo-dGTP may account for up to 10% of the total dGTP pool (Pursell, McDonald et al. 2008). In order to prevent the accumulation of 8-oxo-dGTP, cells encode a pyrophosphohydrolase, MutT/MTH1, which degrades the oxidized nucleotide (Maki and Sekiguchi 1992, Gad, Koolmeister et al. 2014, Huber, Salah et al. 2014). Despite expression of MutT/MTH1, nucleotide pools can accumulate enough 8-oxo-dGTP to promote mutagenesis and drive cancer progression (Colussi, Parlanti et al. 2002, Satou, Kawai et al. 2007). 8-oxo-dGTP is

capable of adopting either an *anti* or *syn* conformation and thus can base pair with either cytosine (dC) or adenine (dA) respectively (Kouchakdjian, Bodepudi et al. 1991, Oda, Uesugi et al. 1991, McAuley-Hecht, Leonard et al. 1994, Lipscomb, Peek et al. 1995). As a consequence of this, 8-oxo-dGTP is frequently misincorporated opposite dA *in vitro* by several DNA polymerases (Einolf, Schnetz-Boutaud et al. 1998, Miller, Prasad et al. 2000, Shimizu, Gruz et al. 2003, Hanes, Thal et al. 2006, Yamada, Nunoshiba et al. 2006, Brown, Duym et al. 2007, Shimizu, Gruz et al. 2007, Katafuchi, Sassa et al. 2010). Thus, *in vivo*, incorporation of 8-oxo-dGMP can lead to an A to C transversion mutation if left unrepaired (Maki and Sekiguchi 1992). Conversely, 8-oxo-dGTP incorporation opposite dC can also eventually result in G to T tranversion mutations after subsequent replication (Zaccolo, Williams et al. 1996).

All cells have specialized repair systems to deal with DNA modifications, and the base excision repair (BER) pathway is the main mechanism for purging the genome of oxidative lesions such as 8-oxo-dG (Svilar, Goellner et al. 2011). A specialized form of the BER pathway, initiated by the glycosylase MutY/MTYH, specifically recognizes and repairs 8-oxo-dG:dA mispairs by removing dA and replacing it with dC, enabling subsequent repair of the 8-oxo-dG lesion (Aburatani, Hippo et al. 1997, Williams and David 1998, Zharkov and Grollman 1998, Williams and David 1999). However, no repair mechanism exists to cope with misincorporated 8-oxo-dGMP. Significantly, 8-oxo-dGMP misincorporation would lead to mutagenic repair by the MutY/MTYH-dependent BER pathway, directing removal of dA and not 8-oxo-dGMP . Thus, 8-oxo-dGMP misincorporation would unavoidably lead to mutagenesis, resulting an A to C transversion (Zaccolo, Williams et al. 1996).

Therefore, preventing misincorporation of 8-oxo-dGMP outright is crucial to avoid mutagenesis. In addition to the hydrolytic activity of MutT/MUTH1, discrimination against 8-oxo-dGTP by DNA polymerases is an important factor in the prevention of mutagenesis. Therefore, understanding the mechanistic basis of this discrimination is of significant interest. With the exception of the recent characterization of the interaction between DNA polymerase beta (Pol β) and 8-oxo-dGTP (Batra, Beard et al. 2010, Freudenthal, Beard et al. 2014), there is a lack of structural information that might help explain how DNA polymerases avoid 8-oxo-dGTP-induced mutagenesis.

The family X DNA polymerase lambda (Pol λ) plays an important role in mediating cellular tolerance of guanine oxidation (Maga, Villani et al. 2007, Markkanen, Castrec et al. 2012, Markkanen, Dorn et al. 2013). A key element of the MutY/MTYH BER pathway is the ability to readily incorporate dCMP opposite a templating 8-oxodG. In the context of this repair reaction, Pol λ is uniquely capable of mediating faithful incorporation of dCMP to complete the repair (Brown, Duym et al. 2007). Pol λ also takes advantage of its unique catalytic properties to mediate additional roles in other DNA repair pathways related to oxidative damage, such as non-homologous end joining (NHEJ) (Fan and Wu 2004, Lee, Blanco et al. 2004, Nick McElhinny, Havener et al. 2005, Capp, Boudsocq et al. 2006, Akopiants, Zhou et al. 2009).

Considering that Pol λ operates under conditions where oxidative damage is prevalent, it is expected to frequently encounter 8-oxo-dGTP. Moreover, due to its function in NHEJ, Pol λ may be responsible for mediating 8-oxo-dGTP-driven mutagenesis. Curiously, despite its relatively error-free behavior when faced with a templating 8-oxodG, Pol λ readily misinserts 8-oxo-dGMP opposite dA (Brown, Duym et al. 2007). The contrast

between its behavior when incorporating 8-oxo-dGTP and opposite 8-oxo-dG indicates that the active site of Pol λ is asymmetrical, but the structural factors influencing 8-oxo-dGMP misincorporation by Pol λ are not well understood.

Here, we report high resolution pre- and post-catalytic crystal structures of Pol λ in complex with 8-oxo-dGTP and 8-oxo-dGMP, respectively. The structures demonstrate that the oxidized nucleotide can be accommodated in the Pol λ active site, where it is stabilized in the pro-mutagenic *syn*-conformation. Kinetic analysis demonstrates that two residues that partially conform the dNTP binding pocket influence 8-oxo-dGMP incorporation. Ala^{510} makes a Van der Waals interaction with the base of the incoming nucleotide, whereas Asn^{513} hydrogen-bonds with the C8-carbonyl. Our results indicate that Ala^{510} and Asn^{513} differentially impact 8-oxo-dGMP incorporation as well as the balance of purine/pyrimidine incorporation, confirming the importance of these residues in mediating nucleotide selectivity in family X DNA polymerases.

3.3 Results and Discussion

3.3.1 Pre-catalytic structure of Pol λ with an incoming 8-oxo-dGTP

In order to understand how 8-oxo-dGTP is misincorporated into DNA, we decided to solve a structure of Pol λ in complex with an incoming 8-oxo-dGTP in a pre- catalytic state. Thus, we crystallized Pol λ with a 1-nt gapped, dideoxy-terminated DNA substrate and an incoming 8-oxo-dGTP (Figure 3-1A). We obtained crystals that diffracted to a resolution of 1.95 Å. We were able to solve the structure using molecular replacement, and subsequent refinement converged to an Rwork and Rfree of 0.1999 and 0.2273 respectively (Table 3-1, PDB: 4XA5).

The electron density was of sufficient quality to build protein residues 252-575 and all DNA bases, including the incoming 8-oxo-dGTP. Inspection of the structure immediately reveals that, as expected, 8-oxo-dGTP is bound in the active site (Figure 3-1A). Mg^{2+} is present in the dNTP-binding metal (B) site. However, a water molecule is occupying the site of the catalytic metal (A), consistent with the absence of the 3′OH group from the nucleotide at the primer terminus (Figure 3-1A) (Garcia-Diaz, Bebenek et al. 2005).

The density for the 8-oxo-dGTP residue is of high quality, and the C8 carbonyl is clearly observed (Figure 3-1B). The structure indicates that the incoming 8-oxo-dGTP adopts a *syn*-conformation and forms a Hoogsteen base pair with the templating adenine base. Hydrogen-bonds are established between N6 of the adenine and O6 of the guanine (3.0 Å) and N1 of the adenine and N7 of the guanine (2.9 Å). An intramolecular hydrogen-bond between the N2 and a non-bridging oxygen on the α-phosphate of 8-oxo-dGTP may stabilize the *syn*-conformation. These interactions and the geometry of 8-oxo-dGTP in the active site of Pol λ are consistent with the conformation observed in existing structures of Pol β in complex with 8-oxo-dGTP (Batra, Beard et al. 2010, Freudenthal, Beard et al. 2014).

Interestingly, the geometry of the 8-oxo-dGTP:dA mispair differs from a canonical Watson-Crick base pair. The λ_R angle for 8-oxo-dGTP is 44.3° which is consistent with the *syn*-conformation of the base in other reported structures (Pol β – 44.2°) (Batra, Beard et al. 2010, Freudenthal, Beard et al. 2014). However, this differs from that of a dGMPCPP:dC base pair (54.2°) (Bebenek, Pedersen et al. 2011). The λ_Y angle for dA is 55.7° and is consistent with an ddTTP:dA base pair (1XSN) (Garcia-Diaz, Bebenek et al. 2005). This is in agreement with the idea that 8-oxo-dG adopts an alternate conformation in order to mispair with an adenine (Kouchakdjian, Bodepudi et al. 1991, McAuley-Hecht, Leonard et

al. 1994). Also, the C1'–C1' width of the mispair is 10.7 ± 0.015–0.091 Å (where 0.015 and 0.091 Å correspond to the minimum and maximum estimated errors respectively, Table 3-2) which is larger than for a dTTP:dA base pair (10.5 ± 0.021–0.094 Å, Table 3-2). Interestingly, this larger base pair width appears to be correlated with the presence of a mispair in the active site in Pol λ (dGMPCPP:dT, 10.8 Å) (Bebenek, Pedersen et al. 2011). However, despite these distortions, Pol λ can accommodate the 8-oxo-dGTP:dA mispair in the active site without any major conformational rearrangements, as evidenced by the small RMSD between our structure and a reference pre-catalytic complex containing a ddTTP:dA base pair in the active site (1XSN, RMSD of 0.320 Å over 261 Cα atoms) (Garcia-Diaz, Bebenek et al. 2005).

3.3.2 Post-catalytic structure of Pol λ with incorporated 8-oxo-dGMP

The absence of large-scale subdomain conformational motions during catalysis in Pol λ implies that completion of the nucleotidyl transfer reaction and advancement from pre-catalytic to the post-catalytic complex involves no significant conformational changes, other than stereochemical inversion of the α-phosphate (Garcia-Diaz, Bebenek et al. 2005). We therefore took advantage of this fact in order to determine whether our structure indeed represents a catalytically relevant conformation of 8-oxo-dGTP. We decided to crystallize a post-catalytic complex of Pol λ with a nicked DNA substrate containing an 8-oxo-dG moiety at the primer terminus (Figure 3-2A). The crystals of the post-catalytic complex diffracted to a resolution of 2.15 Å. The structure was solved by molecular replacement, and refinement converged to an R_{work} and R_{free} of 0.2144 and 0.2450 respectively (Table 3-1, PDB: 4X5V). The electron density

was of sufficient quality to build protein residues 251-575 and all DNA bases, including the incorporated 8-oxo-dGMP.

The post-catalytic structure contains both products of the phosphoryl transfer reaction (Garcia-Diaz, Bebenek et al. 2005). In the structure, 8-oxo-dGTP has been turned over, and the incorporated 8-oxo-dGMP maintains the *syn*-conformation. However, the pyrophosphate released by the reaction has diffused away from the active site and has been replaced by a citrate ion. Citrate is present in high concentration in the crystallization buffer and mimics the conformation of pyrophosphate in other post-catalytic structures (Garcia-Diaz, Bebenek et al. 2005). Additionally, the citrate is coordinating a Na^+ ion that is present in the metal B site (Figure 3-2A). The metal A is absent in the structure, consistent with the notion that it dissociates after nucleotide incorporation (Garcia-Diaz, Bebenek et al. 2005). Superimposition of the pre- and post-catalytic structures reveals that both complexes adopt similar conformations (RMSD of 0.238 Å over 236 Cα atoms). Furthermore, the geometry of all active site atoms is conserved (Figure 3-2B). This confirms that the conformations seen in our structures are catalytically relevant.

3.3.3 8-oxo-dGTP is stabilized by numerous interactions

Close inspection of the dNTP binding pocket reveals five residues that interact with 8-oxo-dGTP (Figure 3-3). Three residues form hydrogen-bonding interactions with non-bridging phosphate oxygen atoms in the incoming nucleotide. Arg^{386} forms a bidentate hydrogen-bond (3.0 and 3.2 Å) with the γ-phosphate while Ser^{417} and Arg^{420} each form a hydrogen-bond with the γ-phosphate (2.6 Å) and the β-phosphate (3.0 Å) respectively. Together, these three residues form the phosphate-binding pocket for the incoming

nucleotide. However, these interactions are unlikely to confer specificity, since they are established irrespective of the identity of the incoming nucleotide.

Ala^{510} provides a Van der Waals stacking interaction with the oxidized base (Figure 3-4A). This interaction is analogous to what is observed in a complex with undamaged substrates, and is thought to be responsible for the high dNTP binding affinity of Pol λ (Garcia-Diaz, Bebenek et al. 2002). It is however conceivable that the strength of the Ala^{510} interaction depends on the identity of the incoming dNTP. Consistent with this idea, Ala^{510} was shown to help discriminate against incorrect nucleotide binding (Brown, Pack et al. 2010). Thus, Pol λ may rely on Ala^{510} to probe for proper nascent base pair geometry of 8-oxo-dGTP.

In addition to Ala^{510}, another residue recognizes a unique structural characteristic of 8-oxo-dGTP. Asn^{513} forms a hydrogen-bonding interaction (3.1 Å) with the C8-carbonyl of 8-oxo-dGTP (Figure 3-4B). In the Pol λ active site, Asn^{513} establishes a sequence independent hydrogen-bond with the O2/N3 hydrogen-bond acceptors in the minor groove of the incoming nucleotide (Garcia-Diaz, Bebenek et al. 2004). These types of minor groove interactions are thought to be crucial to the ability of DNA polymerases to discriminate against non-Watson-Crick base pairs and thus promote fidelity of synthesis (Eom, Wang et al. 1996, Kiefer, Mao et al. 1998). Similar to what is observed with 8-oxo-dG in the active site of different polymerases (Krahn, Beard et al. 2003, Brieba, Eichman et al. 2004, Hsu, Ober et al. 2004, Vasquez-Del Carpio, Silverstein et al. 2009), 8-oxo-dGTP may hijack this fidelity checkpoint mechanism in order to stabilize *syn*-dependent misincorporation. The O8 of 8-oxo-dGTP (*syn*) in the DNA minor groove is in a position similar to that of O2 of dTTP for a canonical Watson-Crick base pair. This suggests that

Asn^{513} stabilizes the lesion in the *syn*-conformation and thus mediates misincorporation opposite dA. Asn^{513} is conserved in another family X DNA polymerase, human Pol β, where it plays a critical role in facilitating incorporation of 8-oxo-dGMP opposite template dA (Miller, Prasad et al. 2000, Batra, Beard et al. 2010, Freudenthal, Beard et al. 2014). Our structural data suggest that this residue could play a similar role in Pol λ .

3.3.4 Kinetic analysis of the relevance of Ala^{510} for 8-oxo-dGTP incorporation

As mentioned above, our structural results reveal that 8-oxo-dGTP is stabilized by two specific interactions. One of these, Ala^{510}, provides a Van der Waals stacking interaction with the base of 8-oxo-dGTP. Interestingly, Ala^{510} in Pol λ is replaced by an aspartic acid in Pol β (Asp^{276}), which is believed to restrict dNTP binding (Beard and Wilson 2000, Vande Berg, Beard et al. 2001). Thus, to further characterize the role of Ala^{510} on 8-oxo-dGTP misincorporation in Pol λ, we constructed an A510D active-site substitution and performed a steady-state kinetic analysis.

Previous data had determined the catalytic efficiency of incorporation of 8-oxo-dGMP opposite dA and dC (Brown, Duym et al. 2007). However, these studies lacked a comparison to dTMP incorporation. This is relevant, since 8-oxo-dGMP competes with dTTP for binding opposite a templating dA, and thus the relative incorporation efficiency of the two nucleotides ultimately determines the mutagenic potential of 8-oxo-dGTP *in vivo*. In order to avoid possible sequence-related effects, the core sequence of the P/T used was identical to that of the oligos used for crystallography (see Materials and Methods). Using

these substrates we determined the kinetic parameters [k_{cat} and $K_{m(app)}$] and catalytic efficiencies [$k_{cat}/K_{m(app)}$] for both WT and A510D Pol λ (Table 3-3).

A comparison of the catalytic efficiencies for WT Pol λ revealed a 150-fold difference between dGMP and 8-oxodGMP incorporation opposite dC. Conversely, incorporation of 8-oxo-dGMP was only 13-fold less efficient than dTMP opposite dA. The relatively small difference in catalytic efficiencies for 8-oxo-dGMP and dTMP incorporation opposite dA highlights the mutagenic potential of this lesion. Furthermore, comparison of the dA/dC selectivity for 8-oxo-dGTP also revealed that the pro-mutagenic *syn*-conformation is preferred in WT Pol λ (5:1).

Interestingly, the A510D substitution had a differential effect on all nucleotides tested. With respect to WT protein, dTTP and 8-oxodGTP incorporation opposite dA was reduced by 4.8-fold (Figure 3-4C) and 5.1-fold (Figure 3-4D) respectively. This suggests that the A510D substitution may affect 8-oxo-dGTP(*syn*) in a similar manner to dTTP. However, the same does not hold true for dGTP/8-oxo-dGTP opposite dC. Notably, the A510D substitution had the largest effect on the incorporation of 8-oxo-dGTP opposite dC (7.6-fold, Figure 3-4E) as opposed to dGTP (2.8-fold, Figure 3-4F). This suggests that Ala^{510} may preferentially stabilize the *anti*-conformation of 8-oxo-dGTP, promoting its incorporation opposite dC. Accordingly, Ala^{510} may enhance the ability of Pol λ to incorporation 8-oxo-dGMP opposite dC, which could ultimately increase the frequency of G to T tranversion mutations (Zaccolo, Williams et al. 1996).

3.3.5 Kinetic analysis of the relevance of Asn^{513} on 8-oxo-dGTP incorporation

In addition to Ala^{510}, Asn^{513} also makes a specific interaction with the oxidized base. To characterize the role of Asn^{513} on 8-oxo-dGTP misincorporation in Pol λ, we generated a N513A active-site substitution. Steady-state kinetic parameters [k_{cat} and $K_{m(app)}$] and catalytic efficiencies [$k_{cat}/K_{m(app)}$] for dTTP/8-oxo-dGTP incorporation opposite dA and dGTP/8-oxo-dGTP opposite dC were determined using N513A Pol λ (Table 3-3). Given the importance of Asn^{513} during normal polymerization, the N513A substitution expectedly affected the catalytic efficiency for all nucleotides tested. Interestingly, similar to what was observed with Ala^{510}, the effects were differential for all nucleotides tested. With respect to the WT protein, the catalytic efficiency for dTTP decreased by 5.8-fold (Figure 3-4C) in N513A Pol λ. However, the N513A substitution resulted in a much more drastic effect in the context of 8-oxo-dGMP incorporation opposite dA (25-fold, Figure 3-4D). Also, the catalytic efficiencies of dGMP and 8-oxo-dGMP incorporation opposite dC were reduced by 1.3 (Figure 3-4E) and 6.4-fold (Figure 3-4F) respectively. Taken together, these results suggest that Asn^{513} plays an important role in facilitating 8-oxo-dGMP incorporation opposite dA, implying that this residue selectively stabilizes the *syn*-conformation of 8-oxo-dGTP.

Our results suggest that dNTP binding by Pol λ is influenced by multiple amino acid residues. Moreover, both Ala^{510} and Asn^{513} appear to play critical roles for *anti*/*syn*-discrimination. To examine if these residues behave individually or cooperatively, we created a A510D/N513A double substitution (Table 3-3). As expected, the effects of both substitutions synergistically impacted all nucleotides tested (Figure 3-4C-F). Interestingly, the drop in catalytic efficiency was nearly identical for 8-oxo-dGMP incorporation opposite

dA and dC. This is consistent with the opposite effects of Ala^{510} and Asn^{513}, facilitating incorporation of the *anti*- and *syn*-conformations, respectively.

3.3.6 Structural features in Pol λ discourage 8-oxo-dGTP misincorporation

Although the 8-oxo-dGTP:dA mispair is tolerated in the active site of Pol λ, kinetic analysis indicates that the insertion efficiency is reduced relative to that of a Watson-Crick base pair (Table 3-3). In order to determine the structural features discouraging incorporation of 8-oxo-dGTP we crystallized Pol λ in complex with undamaged DNA in the exact same sequence context (Table 3-1, PDB: 4XUS). We rationalized that this would provide a more accurate basis for comparison to the 8-oxo-dGTP containing structure, since existing structural models either lacked a 3'-OH on the incoming nucleotide (1XSN) (Garcia-Diaz, Bebenek et al. 2005), or used a non-hydrolyzable dNTP analog to trap the ternary complex (2PFO) (Garcia-Diaz, Bebenek et al. 2007). The crystals diffracted with strong anisotropy, to a resolution limit of 2.4 Å in a* and c* reciprocal space directions, but only 2.9 Å along the b* direction. For this reason, an anisotropic correction was carried out using the Anisotropy Diffraction Server [PMID: 24203335]. The structure was solved with molecular replacement and the model was refined to convergence (R_{work}/R_{free}: 0.1874/0.2358). The electron density was of sufficient quality to build protein residues 252-575 and all DNA bases, including the incoming dTTP.

Comparing our precatalytic structure for 8-oxo-dGMP incorporation with this structure indicates that the overall fold of the polymerase is conserved (RMSD of 0.418

over 289 Cα atoms). However, closer inspection of the active site reveals some important differences. First, the 8-oxo-dGTP does not appear to stack as well as dTTP with the base at the primer terminus (Figure 3-5A). In an attempt to maximize this stacking interaction and accommodate 8-oxo-dGTP in the active site, the templating adenine shifts 0.3 Å away from the incoming nucleotide (Figure 3-5B). The direct consequence of this distortion places the templating base 0.4 Å away from the minor groove interacting residue, Arg^{517} (Figure 3-5B).

Arg^{517} plays an important role interrogating the nascent base pair conformation. This residue forms a hydrogen-bond with the templating base and adopts a base pair checking conformation in response to dNTP binding (Garcia-Diaz, Bebenek et al. 2005). This mechanism appears to be critical for fidelity of synthesis in family X polymerases. Consistently, substitution of Arg^{517} in Pol λ sharply decreases the fidelity of the polymerase as well as the catalytic efficiency of dNTP incorporation (Brown, Pack et al. 2010). Similarly, even subtle alterations of this residue in Pol β result in substantial reduction in the catalytic efficiency (Werneburg, Ahn et al. 1996). Thus, repositioning of the templating adenine away from Arg^{517} as observed in our structure would likely cause a loss of insertion efficiency. This provides a structural explanation for the decreased incorporation efficiency observed in our kinetic analysis (Table 3-3).

3.3.7 Ala^{510} and Asn^{513} influence the purine/pyrimidine balance in Pol λ

While Asn^{513} enhances 8-oxo-dGTP incorporation in Pol λ, this residue also had a differential effect on dTTP and dGTP incorporaton. Steady-state kinetic analysis demonstrated that the catalytic efficiency for dTTP incorporation by N513A Pol λ was 5.8-fold (Figure 3-4C) lower than WT, whereas the decrease observed in the case of dGTP

incorporation was just 1.3-fold (Figure 3-4E). Interestingly, the equivalent residue in the family X DNA polymerase from the heat-stable organism *T. thermophilus* (TthPolX) appears to also influence the balance of purine/pyrimidine incorporation(Garrido, Mejia et al. 2014). Asn^{513} appears to play a similar role in balancing the purine/pyrimidine bias in Pol λ.

Strikingly, Ala^{510} also appears to have a greater effect on pyrimidines than purines. A510D substitution results in a 4.8-fold (Figure 3-4C) decrease in catalytic efficiency for dTTP incorporation but only a 2.8-fold (Figure 3-4E) decrease for dGTP. In agreement with these results, the A510D/N513A double mutant displays a clear synergistic effect. The double substitution affects dTTP incorporation to a far greater extent (52-fold, Figure 3-4C) than dGTP (7.3-fold, Figure 3-4E), demonstrating that both residues contribute to balancing purine/pyrimidine incorporation in Pol λ. This indicates that residues in addition to Asn^{513} are important to achieve the correct purine/pyrimidine balance.

3.4 Conclusion

The free nucleotide pool is susceptible to oxidative damage (Fraga, Shigenaga et al. 1990). To cope with this oxidative burden, cells encode an enzyme (MutT/MTH1) to sanitize the nucleotide pools by degrading oxidized nucleotides such as 8-oxo-dGTP (Gad, Koolmeister et al. 2014, Huber, Salah et al. 2014). Despite the presence of this protein, residual 8-oxo-dGTP is still capable of promoting mutagenesis (Colussi, Parlanti et al. 2002, Satou, Kawai et al. 2007, Pursell, McDonald et al. 2008). As a result, DNA polymerases such as Pol λ may encounter and incorporate this oxidized nucleotide, ultimately leading to mutagenesis.

The structural and kinetic studies presented here reveal how 8-oxo-dGTP evades fidelity checkpoint mechanisms in Pol λ. Active site residues Ala^{510} and Asn^{513} establish critical interactions that help stabilize the incoming nucleotide during polymerization. Asn^{513} forms a minor groove interaction with the incoming nucleotide. While this interaction is used to ensure that a base pair with the proper geometry is formed in the active site of the polymerase (Garcia-Diaz, Bebenek et al. 2004, Garcia-Diaz, Bebenek et al. 2005), this mechanism is co-opted by 8-oxo-dGTP and appears to drive its mutagenic incorporation opposite dA. Asn^{513} is capable of forming a hydrogen-bond with the C8-carbonyl of 8-oxo-dGTP, thereby stabilizing the oxidized nucleotide in a *syn*-conformation. Consistently, substitution of asparagine to an alanine eliminates the stabilizing hydrogen-bond and results in a 25-fold reduction in the catalytic efficiency for 8-oxo-dGTP misincorporation opposite dA. Conversely, the N513A substitution has only a minor effect on dTTP incorporation opposite dA (5.8-fold). Thus, Asn^{513} appears to selectively facilitate 8-oxo-dGMP misincorporation.

Asn^{513} is also conserved in another family X DNA polymerase, Pol β (Asn^{279}). Accordingly, Asn^{279} also appears to play a role mediating 8-oxo-dGTP-induced mutagenesis. Strikingly, in comparison to Pol β (1000-fold), the effects of Asn^{513} on 8-oxo-dGMP misincorporation in Pol λ are far less pronounced (25-fold) (Miller, Prasad et al. 2000). This implies that minor groove interactions are less critical to stabilize 8-oxo-dGTP in a *syn*-conformation in the Pol λ active site. The lesser relative importance of Asn^{513} with respect to Asn^{279} is perhaps owed to the differential interactions established by Pol λ with the incoming nucleotide. Pol λ has a higher binding affinity for nucleotides than Pol β (Garcia-Diaz, Bebenek et al. 2002), which is thought to be largely the result of a Van der

Waals contact established between Ala^{510} and the incoming base. Conversely, the equivalent residue in Pol β, Asp^{276}, is believed to restrict dNTP binding (Beard and Wilson 2000, Vande Berg, Beard et al. 2001).

Our results demonstrate that Ala^{510} substitution differentially affects incorporation of the nucleotides tested. This implies that Ala^{510} establishes distinct interactions with each nucleotide and therefore is unequally responsible for their stability in the active site. While an A510D substitution had an nearly equivalent effect on both dTTP (4.8-fold) and 8-oxo-dGTP(*syn*) (5.1-fold), one consequence of this behavior is that substitution of Ala^{510} selectively impacts 8-oxo-dGTP misincorporation opposite dC. Substitution of Ala^{510} to aspartic acid results in a greater effect on 8-oxo-dGMP incorporation (7.6-fold) opposite dC than dGMP (2.8-fold). This may be due to an unfavorable electrostatic interaction between the side chain and the C8-carbonyl of the nucleotide. As a consequence, Ala^{510} selectively enhances the incorporation of 8-oxo-dGMP opposite dC. These results are consistent with the increased propensity of 8-oxo-dGTP incorporation opposite dA relative to dC by Pol λ (5:1) in comparison to Pol β (24:1) (Miller, Prasad et al. 2000, Brown, Duym et al. 2007). Furthermore, this implies that Pol λ may be more susceptible to G to T transversion mutations induced by 8-oxo-dGMP incorporation opposite dC than Pol β.

Curiously, the effects of Ala^{510} and Asn^{513} on normal nucleotide incorporation appear to have a more pronounced effect on dTMP than dGMP incorporation. The A510D substitution results in a greater effect for dTTP (4.8-fold) incorporation than dGTP (2.8-fold). Likewise, a N513A substitution has a more prominent effect on dTTP (5.8-fold) incorporation than dGTP (1.3-fold). Interestingly, the family X DNA polymerase from the heat-stable organism *T. thermophilus*, TthPolX, contains a serine in the equivalent position

of Asn^{513}. The lack of the asparagine in TthPolX restricts the error-prone insertion of 8-oxo-dGTP opposite dA by 10-fold (Garrido, Mejia et al. 2014). This is thought to be an adaptation to the higher levels of 8-oxo-dGTP in the dNTP pool expected at high temperatures. However, the absence of an asparagine residue at this position results in an imbalance in the efficiency of incorporation of purine and pyrimidine nucleotides (Garrido, Mejia et al. 2014), suggesting that acquiring an asparagine at this position is important for fidelity of incorporation when dealing with undamaged substrates. Accordingly, Asn^{513} appears to play a role in improving the purine/pyrimidine balance in Pol λ. Furthermore, our results demonstrate that Ala^{510} is also important for reducing the purine/pyrimindine bias. Owing to their larger surface area, purines have more stable base-stacking interactions than pyrimidines. Thus, direct interactions with the base appear to be relatively more important to stabilize the smaller pyrimidines. In that context, the energetics of the Ala^{510} interaction are likely to depend on the identity of the incoming nucleotide. At the same time, the hydrogen bond established by Asn^{513} appears to be critical to properly orient the incoming base. Thus, altering the Asn^{513} interaction in turn affects the Van der Waals contacts established by Ala^{510}. Accordingly, the effect of the double substitution on 8-oxo-dGMP/dTMP incorporation opposite dA is markedly different than the product of both individual single substitutions.

In all DNA polymerases, interactions with the incoming dNTP are essential for catalysis and selectivity. In the Pol λ active site, Ala^{510} and Asn^{513} cooperate to stabilize the incoming nucleotide. Our results highlight that dNTP binding involves multiple interactions and the relative importance of each interaction depends on the specific base being incorporated. Both Ala^{510} and Asn^{513} influence 8-oxo-dGMP incorporation as well as the

balance between purine/pyrimidine incorporation. Thus, the increased catalytic efficiency of incorporation of undamaged nucleotides and purine/pyrimidine balance conferred by these residues comes thus at the price of an increased mutagenic risk in the presence of a significant pool of 8-oxo-dGTP. The described structures and kinetic results provide a framework for understanding 8-oxo-dGTP incorporation by DNA polymerases, and specifically in the context of the Pol λ active site. These new structural insights into the catalytic cycle for 8-oxo-dGTP incorporation by Pol λ will contribute to our understanding of the mutagenic potential of oxidized nucleotide pools, and the mechanisms by which DNA polymerases cope with and discriminate against these mutagenic events.

3.5 Materials and Methods

3.5.1 Protein purification

The sequence corresponding to residues 242–575 of human Pol λ was previously cloned into the bacterial expression vector pET-22b (Garcia-Diaz, Bebenek et al. 2004). Site-directed mutagenesis was performed on the Pol λ expression vector to generate the A510D, N513A and A510D/N513A mutants. WT, A510D, N513A and A510D/N513A Pol λ were subsequently expressed in the *E. coli* strain BL21-CodonPlus(DE3)-RIL and purified as described (Garcia-Diaz, Bebenek et al. 2004).

3.5.2 Oligonucleotides for crystallography

Oligonucleotides used for the pre-catalytic ternary and post-catalytic nick complexes are shown in Figure 3-6A and 6B respectively. Oligos were synthesized by solid-state

synthesis methods using an automated DNA synthesizer. Oligos were subsequently purified by HPLC, ethanol precipitated and quantified by UV absorbance (A_{260}). P/T were annealed as previously described in 25 mM Tris–HCl pH 7.5 and 40 mM $MgCl_2$.

3.5.3 Crystallization

Pre-catalytic ternary complexes were formed using an upstream primer (UP5), downstream primer containing a 5'-phosphate group (DP4), and template (T8-A) (Figure 3-6A). UP5, DP4 and T8-A (1:1:1) were heated to 80°C for 10 min before slowly cooling to room temperature in 25 mM Tris–HCl pH 7.5 and 50 mM $MgCl_2$. The resulting primer/templates (P/T) were mixed with WT Pol λ. However, due to the low melting temperature of DP-4 (16 °C), a second annealing step in the presence of protein was used to ensure the proper formation of a 1-nt gapped substrate. Accordingly, the mixture was heated to 15°C for 5 min before slowly cooling to 4°C to ensure proper annealing of DP4. ddCTP and 8-oxo-dGTP/dTTP were sequentially added to the mixture in order to generate a pre-catalytic ternary complex. The resulting mixture (100 µl) contained 15 mM Tris–HCl pH 7.5, 75 mM NaCl, 10 mM $MgCl_2$, 1 mM DTT, P/T (0.5 mM), WT Pol λ (0.4 mM), 1 mM ddCTP and 3 mM 8-oxo-dGTP/dTTP. Crystals containing 8-oxo-dGTP were formed using the hanging drop method by mixing 2 µl of the protein/DNA solution containing DNA with 1 µl of the reservoir solution containing 0.1 M sodium cacodylate trihydrate pH 7.4 and 1.9 M sodium acetate trihydrate. The crystal was transferred to a solution containing 0.1 M sodium cacodylate trihydrate pH 7.4 and 1.9 M sodium acetate trihydrate and 25 % w/v glycerol and cryo-cooled in liquid nitrogen prior to data collection. dTTP-containing crystals were formed as previously stated in solution containing 0.1 M sodium acetate

trihydrate pH 4.6 and 2.0 M sodium formate. The crystal was transferred to a solution containing 0.1 M sodium acetate trihydrate pH 4.6 and 2.0 M sodium fomate and 25 % w/v glycerol, harvested with a Mitegen MicroMount and cryo-cooled in liquid nitrogen prior to data collection.

Post-catalytic nick complexes were formed using an upstream primer (UP6), DP4 and template T8-A (Figure 3-6B). Pre-hybridized UP6, DP4 and T8-A were mixed with WT Pol λ as previously described. 8-oxo-dGTP (4 mM) was subsequently added and the resulting mixture (100 µl) was equilibrated for 60 min on ice in order to generate a post-catalytic nick complex. Crystals containing 8-oxo-dGMP were grown using the hanging drop method by mixing 1 µl of the protein/DNA solution containing DNA with 1 µl of the reservoir solution containing 0.1 M sodium citrate pH 5.6 and 1 M ammonium phosphate. The crystal was transferred to a solution containing 0.1 M sodium citrate pH 5.6, 1.2 M ammonium phosphate and 30 % w/v glycerol, harvested with a Mitegen MicroMount and cryo-cooled in liquid nitrogen prior to data collection.

3.5.4 X-ray data collection and structure determination

Diffraction data were collected on beamline X25 of the National Synchrotron Light Source at Brookhaven National Laboratory for the dTTP pre-catalytic complex and the 8-oxo-dGTP post-catalytic complex, and on beamline 5.0.2 of the Advanced Light Source at Lawrence Berkeley National Laboratory for the 8-oxo-dGTP post-catalytic complex. All datasets were collected at 100 K using a wavelength of 1.0 Å. Diffraction data were processed using XDS (Kabsch 2010) and Aimless (Evans and Murshudov 2013) as implemented in the autoPROC pipeline (Vonrhein, Flensburg et al. 2011). Phases were

obtained by molecular replacement using Phaser (McCoy, Grosse-Kunstleve et al. 2007); search models for the pre- and post-catalytic complexes were created from 1XSN (Garcia-Diaz, Bebenek et al. 2005) and 1XSP (Garcia-Diaz, Bebenek et al. 2005), respectively. Model building was carried out in Coot (Emsley, Lohkamp et al. 2010), followed by refinement in Phenix (Zwart, Afonine et al. 2008), Refmac (Murshudov, Skubak et al. 2011), and BUSTER (Smart, Womack et al. 2012). Diffraction data for the dTTP pre-catalytic complex were strongly anisotropic, with resolution limits (defined by $CC_{1/2}$ and I / σI (Karplus and Diederichs 2012, Evans and Murshudov 2013) of 2.4 Å in a* and c* reciprocal space directions, but only 2.9 Å along the b* direction. For this reason, an ellipsoidal truncation was carried out using the Anisotropy Diffraction Server (Sawaya 2014). Briefly, data were truncated that fell outside an ellipse centered at the reciprocal lattice origin and having vertices at 1/2.4, 1/2.9, and 1/2.4 Å along a*, b*, and c* axes, respectively. Isotropy was approximated by applying a negative scale factor along b* (−16.8 $Å^2$) with no correction along a* or c*. These anisotropically scaled data then were used for refinement. In all three structures a small region of the protein surface, far removed from the active site (Loop 3) was disordered. The geometric quality of the refined models was assessed with MolProbity (Chen, Arendall et al. 2010) and the structure validation tools in the Phenix suite. Data collection and refinement statistics are shown in Table 3-1.

In order to facilitate more precise structural comparisons, a statistical analysis of atomic coordinate accuracy was carried out using SFCHECK (Vaguine, Richelle et al. 1999). Following the method of Cruickshank (Cruickshank 1949), the standard deviation of the atomic coordinates can be derived from the properties of the electron-density map:

$$\sigma(x) = \sigma(slope)/curvature$$

where $\sigma(slope)$ and *curvature* are the standard deviation of the slope and curvature of the electron density map at the atomic center. The curvature is approximated by:

$$curvature = 2\pi^2(\sum h^2 F_{obs})/a^2 V_{unit\_cell}$$

where *a* is the unit-cell length and *h* is the Miller index (Agarwal 1978, Murshudov, Vagin et al. 1997). The maximal expected coordinate error is calculated by expressing $\sigma(slope)$ as a function of the difference between F_{obs} and F_{calc}

$$\sigma(slope) = 2\pi\{\sum[h^2(F_{obs} - F_{calc})^2]\}^{1/2}/aV_{unit\_cell}$$

For any missing reflections, the program uses the average value of $\sigma(F)$ for the corresponding resolution shell instead of (F_{obs} – Fcalc). The expected minimal coordinate error is estimated using the experimental $\sigma(F)$ instead of the difference between the observed and calculated structure factors. In this case $\sigma(slope)$ is computed as

$$\sigma(slope) = 2\pi\{\sum[h^2\sigma(F)^2]\}^{1/2}/aV_{unit\_cell}$$

If there is no σ value for an observed structure factor, the program uses σ = $0.04F_{\text{obs}}$ as the default value, which is roughly the error magnitude usually encountered. The both minimal and maximal estimated errors were calculated to account for the fact that the local quality of the electron density will amost always vary across different regions of a given crystal structure. These values are listed in Table 3-2.

3.5.5 Oligonucleotides for steady-state primer extension assays

Oligonucleotides used for steady-state primer extension assays were obtained from Invitrogen and are shown in Figure 3-6C and 6D. Oligos were purified by HPLC and polyacrylamide gel-electrophoresis (PAGE), quantified by UV absorbance (A_{260}), and

heated to 80°C for 10 min before slowly cooling to room temperature overnight in 20 mM Tris–HCl pH 7.5 and 150 mM $MgCl_2$.

3.5.6 Steady-state primer extension assays

Steady-state experiments were performed with an upstream primer 5′ labeled with a Cy3 fluorophore (UP20), downstream primer containing a 5'-phosphate group (DP14), and a template (T35-A/T35-C) (Figure 3-6C and 6D). The core sequence of P/T used was the same as the crystallography experiments. Pre-hybridized UP20, DP14 and T35-A/T35-C (1:1.2:1.2) were mixed with either WT A510D, N513A or A510D/N513A Pol λ. The resulting mixture (18 μl) contained 50 mM Tris–HCl pH 8.5, 10 mM $MgCl_2$, 1 mM DTT, 4% glycerol, 0.1 mg/ml BSA, P/T (200 nM) and either WT (0.3–5.0 nM), A510D (0.3–5.0 nM), N513A (0.3–5.0 nM) or A510D/N513A (0.5–10.0 nM) Pol λ. The protein/DNA mixture was directly added to varying amounts of either dTTP (0–500 μM), dGTP (0-500 μM) or 8-oxo-dGTP (0–1000 μM) to start the polymerization reaction.

Reaction mixtures (20 μl) were quenched by the addition of 95% v/v formamide, 10 mM EDTA, 0.001% xylene cyanol, 0.001% bromophenol blue (10 μL). Extended primers were separated by denaturing (8 M urea) 18% v/v PAGE. The fluorescence intensity of the bands was quantified using a Typhoon FLA 9000 imager and ImageQuant software.

3.5.7 Kinetic analysis of primer extension assays

The observed rate of nucleotide incorporation (extended primer) was plotted as a function of nucleotide concentration. Steady-state kinetic parameters, $V_{\max}$ and K_M, were

determined by fitting the data to the Michaelis-Menten equation: $V=V_{max}[S]/(K_M+[S])$. k_{cat} was determined with the equation: $k_{cat} = V_{max}/[E]$.

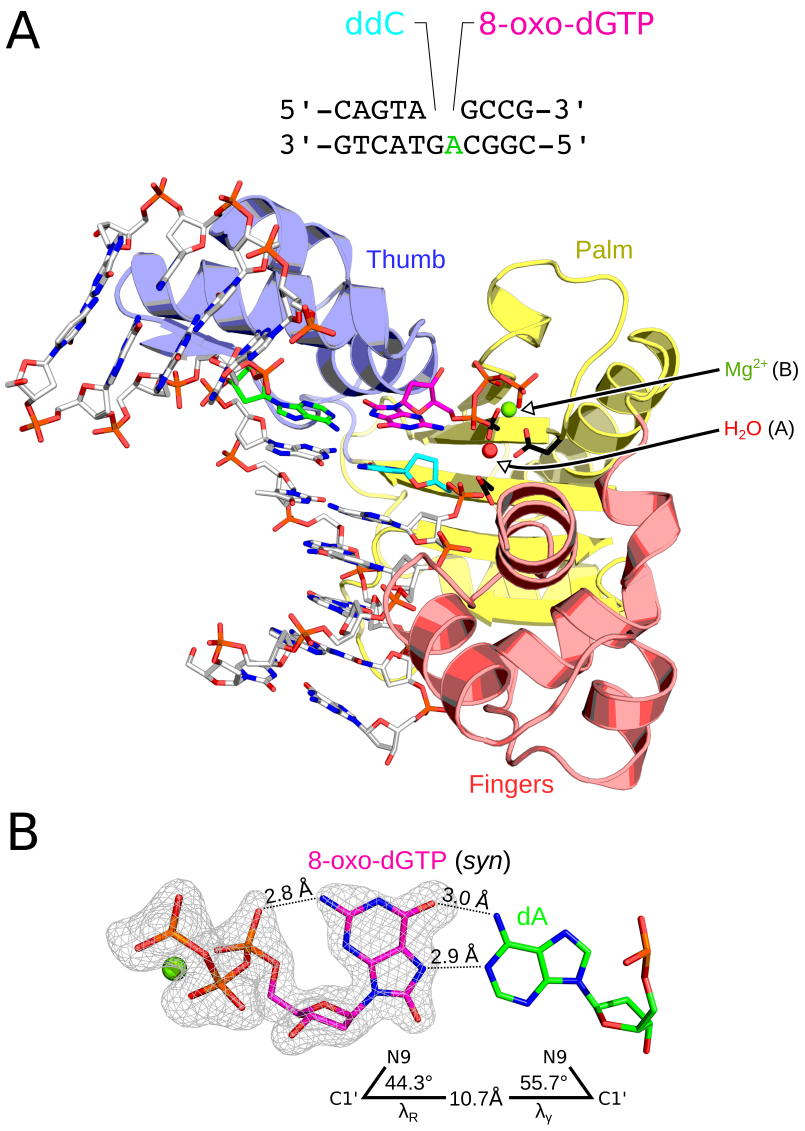

Figure 3-1. Pol λ pre-catalytic complex for 8-oxo-dGTP
(A) The 39-kDa catalytic domain (8-kDa subdomain not shown for clarity) is colored by subdomain: fingers (salmon), palm (yellow) and thumb (purple). The polymerase is in complex with 8-oxo-dGTP (magenta) and a 1-nt gapped 16-mer P/T (grey). The upstream primer is terminated with a dideoxynucleotide (ddC) (cyan). (B) 8-oxo-dGTP (magenta) establishes a Hoogsteen basepair with dA (green). Contoured at 3σ, the simulated annealing Fo-Fc omit density map (grey) for 8-oxo-dGTP is shown. The geometry (C1′ distance and λ angles) of the mismatched base pair is indicated at the bottom of the figure.

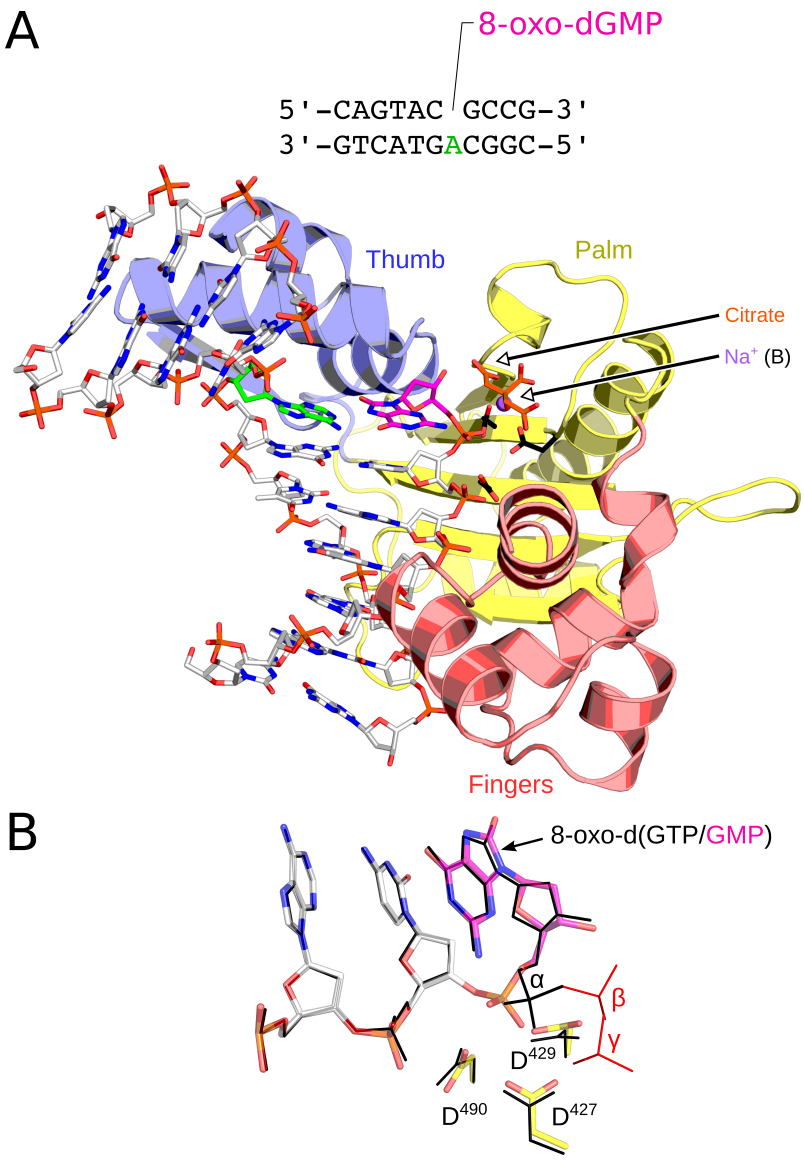

Figure 3-2. Pol λ post-catalytic complex for 8-oxo-dGMP incorporation
(A) The 39-kDa catalytic domain (8-kDa subdomain not shown for clarity) is colored by subdomain: fingers (salmon), palm (yellow) and thumb (purple). The polymerase is in complex with a nicked 16-mer P/T (grey) containing an 8-oxo-dGMP moiety at the primer terminus (magenta). (B) Overlay of the active sites between the pre- and post-catalytic 8-oxo-dGTP/8-oxo-dGMP complexes (RMSD of 0.278 Å over 678 Cα atoms). The β- and ϒ-phosphates that will constitute the pyrophosphate leaving group are highlighted in red.

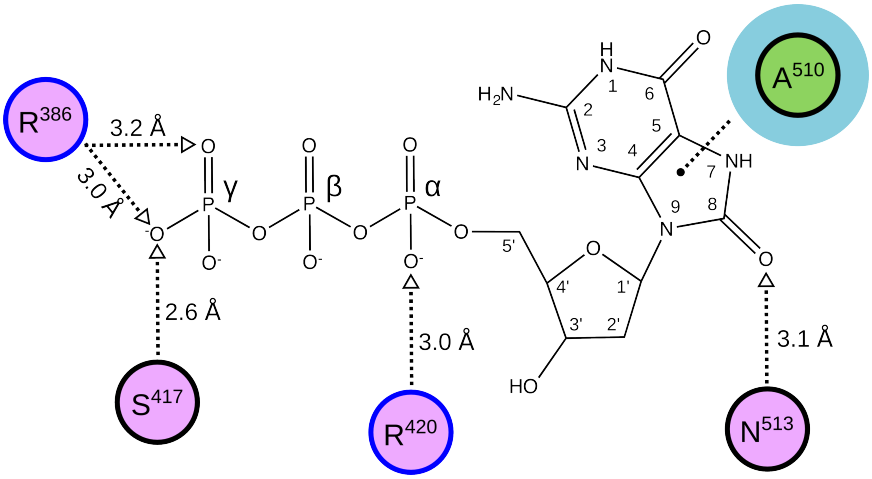

Figure 3-3. Schematic view of the interactions in the nascent base pair pocket
Residues that directly interact with 8-oxo-dGTP are shown. Hydrogen bonds and stacking interactions are indicated with an arrow and dot, respectively.

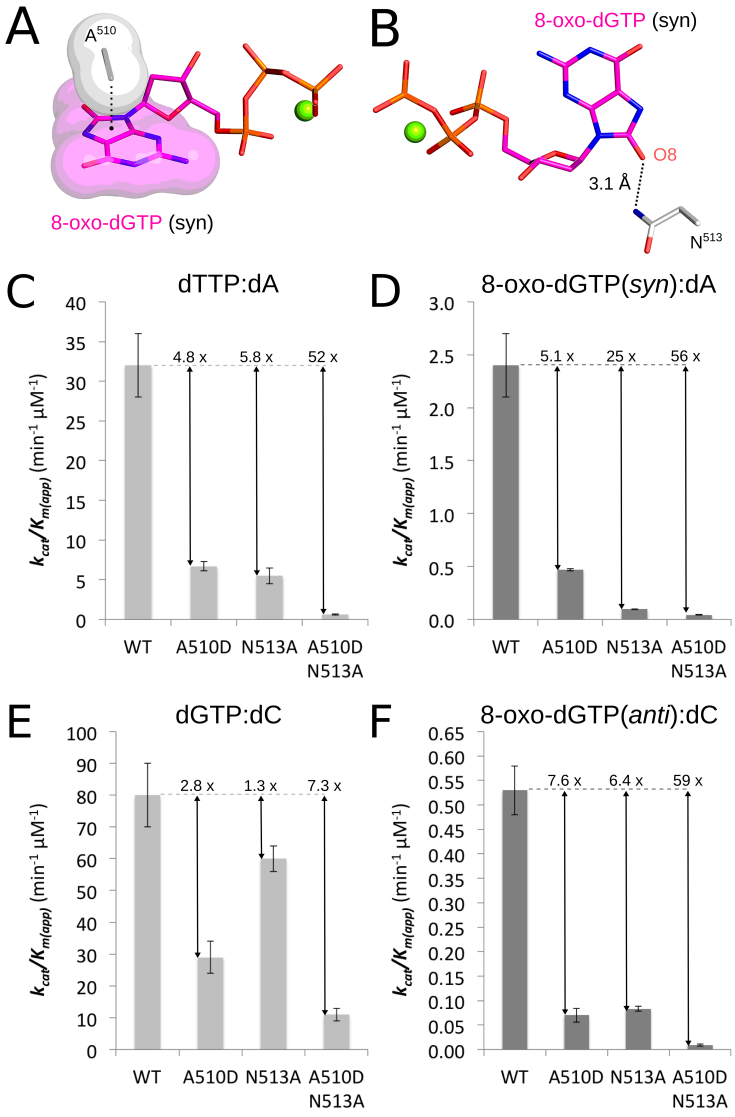

Figure 3-4. Structural features that promote 8-oxo-dGTP incorporation
(A) Ala^{510} provides a Van der Waals stacking interaction with the nucleotide of the incoming 8-oxo-dGTP (magenta). (B) Asn^{513} stabilizes 8-oxo-dGTP (magenta) in the *syn*-conformation. The amino group of the Asn^{513} side chain establishes a hydrogen-bond with the O8 of 8-oxo-dGTP. (C) Comparison of catalytic efficiencies for dTMP incorporation opposite dA using WT, A510D, N513A and A510D/N513A Pol λ. (D) Comparison of catalytic efficiencies for 8-oxo-dGMP(*syn*) incorporation opposite dA using WT, A510D, N513A and A510D/N513A Pol λ. (E) Comparison of catalytic efficiencies for dGMP incorporation opposite dC using WT, A510D, N513A and A510D/N513A Pol λ. (F) Comparison of catalytic efficiencies for 8-oxo-dGMP(*anti*) incorporation opposite dC using WT, A510D, N513A and A510D/N513A Pol λ.

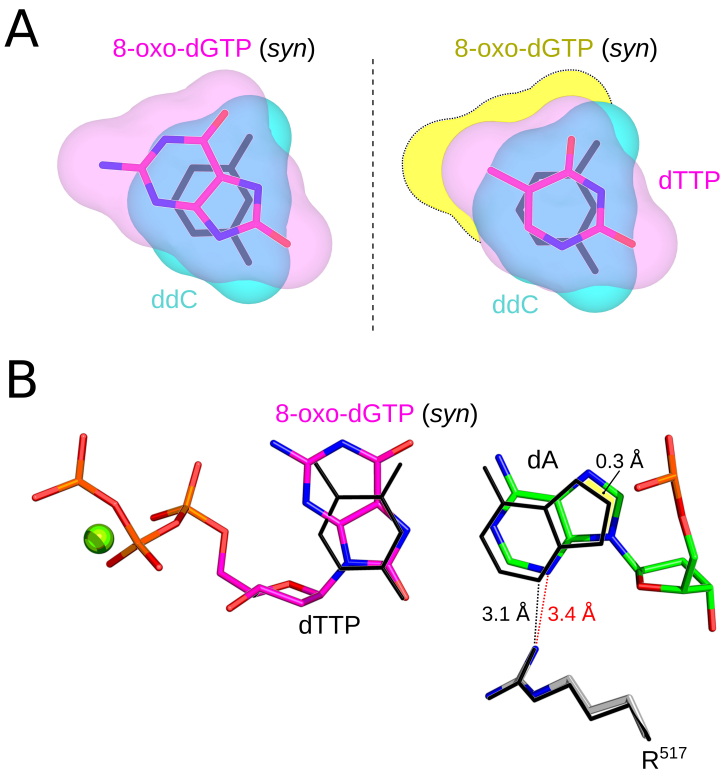

Figure 3-5. Structural features that discourage incorporation
(A) Comparison of dTTP and 8-oxo-dGTP stacking interactions in the pre-catalytic structures. The stacking interaction between 8-oxo-dGTP(*syn*) (magenta) and ddC (cyan) at the primer terminus of a complex is shown in the left panel. Comparison with dTTP (magenta) and the ddC (cyan) in the right panel demonstrates that 8-ox-dGTP stacks more poorly (yellow). (B) Overlay of the nascent base pair in the pre-catalytic 8-oxo-dGTP and dTTP complexes. 8-oxo-dGTP (magenta) appears to displace the templating dA away from its canonical position. The direct consequence of this is that dA shifts further away from Arg^{517}. The hydrogen-bonding distances for the pre-catalytic 8-oxo-dGTP and dTTP complexes are shown in black and red respectively.

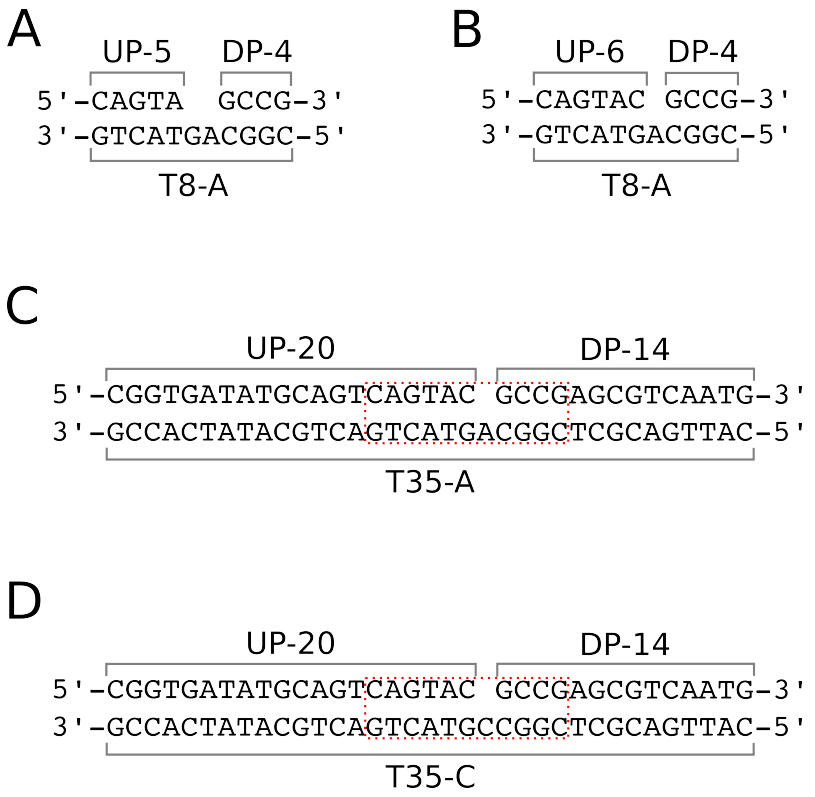

Figure 3-6. Oligonucleotides used in X-ray crystallography and kinetic experiments
Synthetic oligonucleotides were hybridized as described in the Materials and Methods section. (A) P/T duplex containing a 2-nt gap used for the crystallization of the pre-catalytic complex. ddCTP was subsequently added (Materials and Methods) to generate a 1-nt gapped, dideoxy-terminated substrate containing a templating dA. (B) P/T duplex containing a 1-nt gap and a templating dA used for the crystallization of the post-catalytic complex. (C) P/T duplex containing a 1-nt gap and a templating dA used for steady-state kinetic analysis. (D) P/T duplex containing a 1-nt gap and a templating dC used for steady-state kinetic analysis.

Table 3-1. Data collection and refinement statistics

Crystal	Pre-catalytic 8-oxo-dGTP ternary	Post-catalytic 8-oxo-dGTP nick complex	Pre-catalytic dTTP ternary	
Space group	*P* 2_1 2_1 2_1	*P* 2_1 2_1 2_1	*P* 2_1 2_1 2_1	
Cell dimensions				
a, *b*, *c* (Å)	55.97, 62.34, 141.61	56.01, 62.84, [illegible]	56.05, 63.28, 141.06	
α, β, γ (˚)	90, 90, 90	90, 90, 90	90, 90, 90	
Data collection†			*Before anisotropic correction*	*After anisotropic correction*
Resolution (Å)	46.79–1.90	46.98–2.15	41.96–2.63	41.96–2.40
Wavelength (Å)	1.0	1.0	1.0	1.0
Reflections				
Observed	320,727	243,189	110,946	126,671
Unique	40,080	27,980	15,638	17,565
R_{merge}	0.055 (0.898)	0.046 (0.825)	0.225 (0.869)	0.196 (0.717)
R_{meas}	0.058 (0.959)	0.049 (0.876)	0.258 (0.952)	0.211 (0.773)
R_{pim}	(0.021) (0.333)	(0.016) (0.292)	0.091 (0.357)	0.079 (0.283)
$CC_{1/2}$[a]	1.000 (0.771)	1.000 (0.932)	0.993 (0.875)	0.994 (0.826)
I / σI	22.3 (2.2)	26.4 (2.7)	12.9 (3.1)	13.4 (3.1)
Completeness (%)	100 (100)	100 (100)	100 (100)	86.4 (44.3)
Multiplicity	8.0 (8.2)	8.7 (8.7)	7.1 (6.9)	7.2 (7.3)
Wilson B	31.9	35.9	51.2	24.8
Refinement†				
Resolution (Å)	46.79–1.90	46.98–2.15	41.96–2.40	
No. reflections	40,015	27,913	17,565	
R_{work} / R_{free}	0.1999 / 0.2273	0.2144 / 0.2450	0.1874 / 0.2358	
CC*[a]	1.000 (0.948)	1.000 (0.967)	0.998 (0.951)	
No. atoms			3202	
Protein	2738	2801	2898	
8-oxo-dGMP	N/A	24	N/A	
8-oxo-dGTP	32	N/A	N/A	
dTTP	N/A	N/A	29	
Solvent	247	181	255	
B-factors				
Protein	42.6	44.8	30.1	
8-oxo-dGMP	N/A	28.7	N/A	
8-oxo-dGTP	28.6	N/A	N/A	
dTTP	N/A	N/A	16.9	
Solvent	41.8	44.1	24.8	
R.M.S. deviations				
Bond lengths (Å)	0.019	0.005	0.010	
Bond angles (˚)	0.890	0.970	0.97	
Ramachandran				
Favored (%)	95.5	97.8	97.2	
Outliers (%)	0	0	0	
PDB ID	4XA5	4X5V	4XUS	

[a] $CC_{1/2}$ and CC* are statistics for assessing the effective resolution limits and quality of diffraction data in the context of a refined model (Karplus and Diederichs 2012).
† Values in parenthesis are for the highest resolution shell.

Table 3-2. Statistical analysis of atomic coordinate accuracy

Structure	Minimal estimated error (Å)	Maximal estimated error (Å)
4XA5	0.015	0.091
4X5V	0.019	0.122
4XUS	0.048	0.130
1XSN	0.021	0.094

Table 3-3. Steady-state kinetic parameters of incorporation of 8-oxo-dGTP by Pol λ

Protein	Template	dNTP	K_M (μM)	k_{cat} (min^{-1})	k_{cat}/K_M (min^{-1} μM^{-1})
WT	A	dTTP	4.2±0.7	131±7	32±4
		8-oxo-dGTP	20±3	45.2±3.9	2.4±0.3
A510D		dTTP	35±4	234±10	6.7±0.6
		8-oxo-dGTP	120±8	56.8±2.8	0.47±0.01
N513A		dTTP	21±4	113±1	5.5±1.0
		8-oxo-dGTP	41±1.6	3.99±0.06	0.097±0.003
A510D N513A		dTTP	120±16	71.8±5.6	0.62±0.07
		8-oxo-dGTP	71±2	3.00±0.41	0.043±0.005
WT	C	dGTP	1.7±0.1	140±22	80±10
		8-oxo-dGTP	8.4±0.8	4.39±0.04	0.53±0.05
A510D		dGTP	2.8±0.5	80.0±6.8	29±5
		8-oxo-dGTP	24±6	1.53±0.05	0.070±0.014
N513A		dGTP	2.0±0.2	121±2	60±4
		8-oxo-dGTP	16±0.47	1.31±0.05	0.083±0.005
A510D N513A		dGTP	6.3±0.8	67.2±1.3	11±2
		8-oxo-dGTP	120±24	1.06±0.04	0.009±0.002

*Each experiment was independently repeated. Reported results are mean ± s.d. from three independent experiments.

References

Abbotts, J., D. N. SenGupta, B. Zmudzka, S. G. Widen, V. Notario and S. H. Wilson (1988). "Expression of human DNA polymerase beta in Escherichia coli and characterization of the recombinant enzyme." Biochemistry **27**(3): 901-909.

Aburatani, H., Y. Hippo, T. Ishida, R. Takashima, C. Matsuba, T. Kodama, M. Takao, A. Yasui, K. Yamamoto and M. Asano (1997). "Cloning and characterization of mammalian 8-hydroxyguanine-specific DNA glycosylase/apurinic, apyrimidinic lyase, a functional mutM homologue." Cancer Res **57**(11): 2151-2156.

Agarwal, R. (1978). "A new least-squares refinement technique based on the fast Fourier transform algorithm." Acta Crystallographica Section A **34**(5): 791-809.

Ahn, J., V. S. Kraynov, X. Zhong, B. G. Werneburg and M. D. Tsai (1998). "DNA polymerase beta: effects of gapped DNA substrates on dNTP specificity, fidelity, processivity and conformational changes." Biochem J **331 (Pt 1)**: 79-87.

Ahn, J., B. G. Werneburg and M. D. Tsai (1997). "DNA polymerase beta: structure-fidelity relationship from Pre-steady-state kinetic analyses of all possible correct and incorrect base pairs for wild type and R283A mutant." Biochemistry **36**(5): 1100-1107.

Akopiants, K., R. Z. Zhou, S. Mohapatra, K. Valerie, S. P. Lees-Miller, K. J. Lee, D. J. Chen, P. Revy, J. P. de Villartay and L. F. Povirk (2009). "Requirement for XLF/Cernunnos in alignment-based gap filling by DNA polymerases lambda and mu for nonhomologous end joining in human whole-cell extracts." Nucleic Acids Res **37**(12): 4055-4062.

Arai, K., K. Morishita, K. Shinmura, T. Kohno, S. R. Kim, T. Nohmi, M. Taniwaki, S. Ohwada and J. Yokota (1997). "Cloning of a human homolog of the yeast OGG1 gene that is involved in the repair of oxidative DNA damage." Oncogene **14**(23): 2857-2861.

Arai, T., V. P. Kelly, K. Komoro, O. Minowa, T. Noda and S. Nishimura (2003). "Cell proliferation in liver of Mmh/Ogg1-deficient mice enhances mutation frequency because of the presence of 8-hydroxyguanine in DNA." Cancer Res **63**(14): 4287-4292.

Arai, T., V. P. Kelly, O. Minowa, T. Noda and S. Nishimura (2002). "High accumulation of oxidative DNA damage, 8-hydroxyguanine, in Mmh/Ogg1 deficient mice by chronic oxidative stress." Carcinogenesis **23**(12): 2005-2010.

Au, K. G., M. Cabrera, J. H. Miller and P. Modrich (1988). "Escherichia coli mutY gene product is required for specific A-G----C.G mismatch correction." Proc Natl Acad Sci U S A **85**(23): 9163-9166.

Autexier, C. and N. F. Lue (2006). "The structure and function of telomerase reverse transcriptase." Annu Rev Biochem **75**: 493-517.

Barnes, D. E. and T. Lindahl (2004). "Repair and genetic consequences of endogenous DNA base damage in mammalian cells." Annu Rev Genet **38**: 445-476.

Batra, V. K., W. A. Beard, E. W. Hou, L. C. Pedersen, R. Prasad and S. H. Wilson (2010). "Mutagenic conformation of 8-oxo-7,8-dihydro-2'-dGTP in the confines of a DNA polymerase active site." Nat Struct Mol Biol **17**(7): 889-890.

Batra, V. K., D. D. Shock, W. A. Beard, C. E. McKenna and S. H. Wilson (2012). "Binary complex crystal structure of DNA polymerase beta reveals multiple conformations of the templating 8-oxoguanine lesion." Proc Natl Acad Sci U S A **109**(1): 113-118.

Beard, W. A., W. P. Osheroff, R. Prasad, M. R. Sawaya, M. Jaju, T. G. Wood, J. Kraut, T. A. Kunkel and S. H. Wilson (1996). "Enzyme-DNA interactions required for efficient nucleotide incorporation and discrimination in human DNA polymerase beta." J Biol Chem **271**(21): 12141-12144.
Beard, W. A., D. D. Shock, X. P. Yang, S. F. DeLauder and S. H. Wilson (2002). "Loss of DNA polymerase beta stacking interactions with templating purines, but not pyrimidines, alters catalytic efficiency and fidelity." J Biol Chem **277**(10): 8235-8242.
Beard, W. A. and S. H. Wilson (2000). "Structural design of a eukaryotic DNA repair polymerase: DNA polymerase beta." Mutat Res **460**(3-4): 231-244.
Beard, W. A. and S. H. Wilson (2014). "Structure and mechanism of DNA polymerase beta." Biochemistry **53**(17): 2768-2780.
Bebenek, K., M. Garcia-Diaz, L. Blanco and T. A. Kunkel (2003). "The frameshift infidelity of human DNA polymerase lambda. Implications for function." J Biol Chem **278**(36): 34685-34690.
Bebenek, K., L. C. Pedersen and T. A. Kunkel (2011). "Replication infidelity via a mismatch with Watson-Crick geometry." Proc Natl Acad Sci U S A **108**(5): 1862-1867.
Bebenek, K., L. C. Pedersen and T. A. Kunkel (2014). "Structure-function studies of DNA polymerase lambda." Biochemistry **53**(17): 2781-2792.
Beckman, K. B. and B. N. Ames (1997). "Oxidative decay of DNA." J Biol Chem **272**(32): 19633-19636.
Beese, L. S. and T. A. Steitz (1991). "Structural basis for the 3'-5' exonuclease activity of Escherichia coli DNA polymerase I: a two metal ion mechanism." EMBO J **10**(1): 25-33.
Bertocci, B., A. De Smet, E. Flatter, A. Dahan, J. C. Bories, C. Landreau, J. C. Weill and C. A. Reynaud (2002). "Cutting edge: DNA polymerases mu and lambda are dispensable for Ig gene hypermutation." J Immunol **168**(8): 3702-3706.
Bhattacharyya, N., H. C. Chen, S. Comhair, S. C. Erzurum and S. Banerjee (1999). "Variant forms of DNA polymerase beta in primary lung carcinomas." DNA Cell Biol **18**(7): 549-554.
Birben, E., U. M. Sahiner, C. Sackesen, S. Erzurum and O. Kalayci (2012). "Oxidative stress and antioxidant defense." World Allergy Organ J **5**(1): 9-19.
Bjoras, M., L. Luna, B. Johnsen, E. Hoff, T. Haug, T. Rognes and E. Seeberg (1997). "Opposite base-dependent reactions of a human base excision repair enzyme on DNA containing 7,8-dihydro-8-oxoguanine and abasic sites." EMBO J **16**(20): 6314-6322.
Boiteux, S., T. R. O'Connor and J. Laval (1987). "Formamidopyrimidine-DNA glycosylase of Escherichia coli: cloning and sequencing of the fpg structural gene and overproduction of the protein." EMBO J **6**(10): 3177-3183.
Boveris, A., E. Cadenas and A. O. Stoppani (1976). "Role of ubiquinone in the mitochondrial generation of hydrogen peroxide." Biochem J **156**(2): 435-444.
Braithwaite, E. K., P. S. Kedar, L. Lan, Y. Y. Polosina, K. Asagoshi, V. P. Poltoratsky, J. K. Horton, H. Miller, G. W. Teebor, A. Yasui and S. H. Wilson (2005). "DNA polymerase lambda protects mouse fibroblasts against oxidative DNA damage and is recruited to sites of DNA damage/repair." J Biol Chem **280**(36): 31641-31647.
Braithwaite, E. K., P. S. Kedar, D. J. Stumpo, B. Bertocci, J. H. Freedman, L. D. Samson and S. H. Wilson (2010). "DNA polymerases beta and lambda mediate overlapping and independent roles in base excision repair in mouse embryonic fibroblasts." PLoS One **5**(8): e12229.

Brieba, L. G., B. F. Eichman, R. J. Kokoska, S. Doublie, T. A. Kunkel and T. Ellenberger (2004). "Structural basis for the dual coding potential of 8-oxoguanosine by a high-fidelity DNA polymerase." EMBO J **23**(17): 3452-3461.
Brown, J. A., W. W. Duym, J. D. Fowler and Z. Suo (2007). "Single-turnover kinetic analysis of the mutagenic potential of 8-oxo-7,8-dihydro-2'-deoxyguanosine during gap-filling synthesis catalyzed by human DNA polymerases lambda and beta." J Mol Biol **367**(5): 1258-1269.
Brown, J. A., L. R. Pack, S. M. Sherrer, A. K. Kshetry, S. A. Newmister, J. D. Fowler, J. S. Taylor and Z. Suo (2010). "Identification of critical residues for the tight binding of both correct and incorrect nucleotides to human DNA polymerase lambda." J Mol Biol **403**(4): 505-515.
Bruner, S. D., D. P. Norman and G. L. Verdine (2000). "Structural basis for recognition and repair of the endogenous mutagen 8-oxoguanine in DNA." Nature **403**(6772): 859-866.
Bulychev, N. V., C. V. Varaprasad, G. Dorman, J. H. Miller, M. Eisenberg, A. P. Grollman and F. Johnson (1996). "Substrate specificity of Escherichia coli MutY protein." Biochemistry **35**(40): 13147-13156.
Cabrera, M., Y. Nghiem and J. H. Miller (1988). "mutM, a second mutator locus in Escherichia coli that generates G.C----T.A transversions." J Bacteriol **170**(11): 5405-5407.
Cadenas, E., A. Boveris, C. I. Ragan and A. O. Stoppani (1977). "Production of superoxide radicals and hydrogen peroxide by NADH-ubiquinone reductase and ubiquinol-cytochrome c reductase from beef-heart mitochondria." Arch Biochem Biophys **180**(2): 248-257.
Cai, J. P., T. Kakuma, T. Tsuzuki and M. Sekiguchi (1995). "cDNA and genomic sequences for rat 8-oxo-dGTPase that prevents occurrence of spontaneous mutations due to oxidation of guanine nucleotides." Carcinogenesis **16**(10): 2343-2350.
Capp, J. P., F. Boudsocq, P. Bertrand, A. Laroche-Clary, P. Pourquier, B. S. Lopez, C. Cazaux, J. S. Hoffmann and Y. Canitrot (2006). "The DNA polymerase lambda is required for the repair of non-compatible DNA double strand breaks by NHEJ in mammalian cells." Nucleic Acids Res **34**(10): 2998-3007.
Chagovetz, A. M., J. B. Sweasy and B. D. Preston (1997). "Increased activity and fidelity of DNA polymerase beta on single-nucleotide gapped DNA." J Biol Chem **272**(44): 27501-27504.
Chen, V. B., W. B. Arendall, 3rd, J. J. Headd, D. A. Keedy, R. M. Immormino, G. J. Kapral, L. W. Murray, J. S. Richardson and D. C. Richardson (2010). "MolProbity: all-atom structure validation for macromolecular crystallography." Acta Crystallogr D Biol Crystallogr **66**(Pt 1): 12-21.
Colussi, C., E. Parlanti, P. Degan, G. Aquilina, D. Barnes, P. Macpherson, P. Karran, M. Crescenzi, E. Dogliotti and M. Bignami (2002). "The mammalian mismatch repair pathway removes DNA 8-oxodGMP incorporated from the oxidized dNTP pool." Curr Biol **12**(11): 912-918.
Cooke, M. S., M. D. Evans, M. Dizdaroglu and J. Lunec (2003). "Oxidative DNA damage: mechanisms, mutation, and disease." FASEB J **17**(10): 1195-1214.
Crespan, E., G. Maga and U. Hubscher (2012). "A new proofreading mechanism for lesion bypass by DNA polymerase-lambda." EMBO Rep **13**(1): 68-74.

Cruickshank, D. (1949). "The accuracy of electron-density maps in X-ray analysis with special reference to dibenzyl." Acta Crystallographica **2**(2): 65-82.
David, S. S., V. L. O'Shea and S. Kundu (2007). "Base-excision repair of oxidative DNA damage." Nature **447**(7147): 941-950.
De Bont, R. and N. van Larebeke (2004). "Endogenous DNA damage in humans: a review of quantitative data." Mutagenesis **19**(3): 169-185.
DeMott, M. S., S. Zigman and R. A. Bambara (1998). "Replication protein A stimulates long patch DNA base excision repair." J Biol Chem **273**(42): 27492-27498.
Demple, B. and L. Harrison (1994). "Repair of oxidative damage to DNA: enzymology and biology." Annu Rev Biochem **63**: 915-948.
Demple, B., T. Herman and D. S. Chen (1991). "Cloning and expression of APE, the cDNA encoding the major human apurinic endonuclease: definition of a family of DNA repair enzymes." Proc Natl Acad Sci U S A **88**(24): 11450-11454.
Denver, D. R., S. L. Swenson and M. Lynch (2003). "An evolutionary analysis of the helix-hairpin-helix superfamily of DNA repair glycosylases." Mol Biol Evol **20**(10): 1603-1611.
DeWeese, T. L., J. M. Shipman, N. A. Larrier, N. M. Buckley, L. R. Kidd, J. D. Groopman, R. G. Cutler, H. te Riele and W. G. Nelson (1998). "Mouse embryonic stem cells carrying one or two defective Msh2 alleles respond abnormally to oxidative stress inflicted by low-level radiation." Proc Natl Acad Sci U S A **95**(20): 11915-11920.
Dianov, G., C. Bischoff, J. Piotrowski and V. A. Bohr (1998). "Repair pathways for processing of 8-oxoguanine in DNA by mammalian cell extracts." J Biol Chem **273**(50): 33811-33816.
Dianov, G. L. and U. Hubscher (2013). "Mammalian base excision repair: the forgotten archangel." Nucleic Acids Res **41**(6): 3483-3490.
Dionisi, O., T. Galeotti, T. Terranova and A. Azzi (1975). "Superoxide radicals and hydrogen peroxide formation in mitochondria from normal and neoplastic tissues." Biochim Biophys Acta **403**(2): 292-300.
Dobashi, Y., T. Shuin, H. Tsuruga, H. Uemura, S. Torigoe and Y. Kubota (1994). "DNA polymerase beta gene mutation in human prostate cancer." Cancer Res **54**(11): 2827-2829.
Dodson, M. L., M. L. Michaels and R. S. Lloyd (1994). "Unified catalytic mechanism for DNA glycosylases." J Biol Chem **269**(52): 32709-32712.
Dodson, M. L., R. D. Schrock, 3rd and R. S. Lloyd (1993). "Evidence for an imino intermediate in the T4 endonuclease V reaction." Biochemistry **32**(32): 8284-8290.
Doublie, S., M. R. Sawaya and T. Ellenberger (1999). "An open and closed case for all polymerases." Structure **7**(2): R31-35.
Doublie, S., S. Tabor, A. M. Long, C. C. Richardson and T. Ellenberger (1998). "Crystal structure of a bacteriophage T7 DNA replication complex at 2.2 A resolution." Nature **391**(6664): 251-258.
Einolf, H. J. and F. P. Guengerich (2001). "Fidelity of nucleotide insertion at 8-oxo-7,8-dihydroguanine by mammalian DNA polymerase delta. Steady-state and pre-steady-state kinetic analysis." J Biol Chem **276**(6): 3764-3771.
Einolf, H. J., N. Schnetz-Boutaud and F. P. Guengerich (1998). "Steady-state and pre-steady-state kinetic analysis of 8-oxo-7,8-dihydroguanosine triphosphate incorporation

and extension by replicative and repair DNA polymerases." Biochemistry **37**(38): 13300-13312.
Emsley, P., B. Lohkamp, W. G. Scott and K. Cowtan (2010). "Features and development of Coot." Acta Crystallogr D Biol Crystallogr **66**(Pt 4): 486-501.
Eom, S. H., J. Wang and T. A. Steitz (1996). "Structure of Taq polymerase with DNA at the polymerase active site." Nature **382**(6588): 278-281.
Esnouf, R., J. Ren, C. Ross, Y. Jones, D. Stammers and D. Stuart (1995). "Mechanism of inhibition of HIV-1 reverse transcriptase by non-nucleoside inhibitors." Nat Struct Biol **2**(4): 303-308.
Evans, P. R. and G. N. Murshudov (2013). "How good are my data and what is the resolution?" Acta Crystallogr D Biol Crystallogr **69**(Pt 7): 1204-1214.
Fan, W. and X. Wu (2004). "DNA polymerase lambda can elongate on DNA substrates mimicking non-homologous end joining and interact with XRCC4-ligase IV complex." Biochem Biophys Res Commun **323**(4): 1328-1333.
Forman, H. J. and J. A. Kennedy (1974). "Role of superoxide radical in mitochondrial dehydrogenase reactions." Biochem Biophys Res Commun **60**(3): 1044-1050.
Fortini, P., E. Parlanti, O. M. Sidorkina, J. Laval and E. Dogliotti (1999). "The type of DNA glycosylase determines the base excision repair pathway in mammalian cells." J Biol Chem **274**(21): 15230-15236.
Fraga, C. G., M. K. Shigenaga, J. W. Park, P. Degan and B. N. Ames (1990). "Oxidative damage to DNA during aging: 8-hydroxy-2'-deoxyguanosine in rat organ DNA and urine." Proc Natl Acad Sci U S A **87**(12): 4533-4537.
Freudenthal, B. D., W. A. Beard, L. Perera, D. D. Shock, T. Kim, T. Schlick and S. H. Wilson (2014). "Uncovering the polymerase-induced cytotoxicity of an oxidized nucleotide." Nature.
Freudenthal, B. D., W. A. Beard, L. Perera, D. D. Shock, T. Kim, T. Schlick and S. H. Wilson (2015). "Uncovering the polymerase-induced cytotoxicity of an oxidized nucleotide." Nature **517**(7536): 635-639.
Freudenthal, B. D., W. A. Beard and S. H. Wilson (2013). "DNA polymerase minor groove interactions modulate mutagenic bypass of a templating 8-oxoguanine lesion." Nucleic Acids Res **41**(3): 1848-1858.
Frosina, G., P. Fortini, O. Rossi, F. Carrozzino, G. Raspaglio, L. S. Cox, D. P. Lane, A. Abbondandolo and E. Dogliotti (1996). "Two pathways for base excision repair in mammalian cells." J Biol Chem **271**(16): 9573-9578.
Gad, H., T. Koolmeister, A. S. Jemth, S. Eshtad, S. A. Jacques, C. E. Strom, L. M. Svensson, N. Schultz, T. Lundback, B. O. Einarsdottir, A. Saleh, C. Gokturk, P. Baranczewski, R. Svensson, R. P. Berntsson, R. Gustafsson, K. Stromberg, K. Sanjiv, M. C. Jacques-Cordonnier, M. Desroses, A. L. Gustavsson, R. Olofsson, F. Johansson, E. J. Homan, O. Loseva, L. Brautigam, L. Johansson, A. Hoglund, A. Hagenkort, T. Pham, M. Altun, F. Z. Gaugaz, S. Vikingsson, B. Evers, M. Henriksson, K. S. Vallin, O. A. Wallner, L. G. Hammarstrom, E. Wiita, I. Almlof, C. Kalderen, H. Axelsson, T. Djureinovic, J. C. Puigvert, M. Haggblad, F. Jeppsson, U. Martens, C. Lundin, B. Lundgren, I. Granelli, A. J. Jensen, P. Artursson, J. A. Nilsson, P. Stenmark, M. Scobie, U. W. Berglund and T. Helleday (2014). "MTH1 inhibition eradicates cancer by preventing sanitation of the dNTP pool." Nature **508**(7495): 215-221.

Gan, G. N., J. P. Wittschieben, B. O. Wittschieben and R. D. Wood (2008). "DNA polymerase zeta (pol zeta) in higher eukaryotes." Cell Res **18**(1): 174-183.
Garcia-Diaz, M., K. Bebenek, J. M. Krahn, L. Blanco, T. A. Kunkel and L. C. Pedersen (2004). "A structural solution for the DNA polymerase lambda-dependent repair of DNA gaps with minimal homology." Mol Cell **13**(4): 561-572.
Garcia-Diaz, M., K. Bebenek, J. M. Krahn, T. A. Kunkel and L. C. Pedersen (2005). "A closed conformation for the Pol lambda catalytic cycle." Nat Struct Mol Biol **12**(1): 97-98.
Garcia-Diaz, M., K. Bebenek, J. M. Krahn, L. C. Pedersen and T. A. Kunkel (2007). "Role of the catalytic metal during polymerization by DNA polymerase lambda." DNA Repair (Amst) **6**(9): 1333-1340.
Garcia-Diaz, M., K. Bebenek, R. Sabariegos, O. Dominguez, J. Rodriguez, T. Kirchhoff, E. Garcia-Palomero, A. J. Picher, R. Juarez, J. F. Ruiz, T. A. Kunkel and L. Blanco (2002). "DNA polymerase lambda, a novel DNA repair enzyme in human cells." J Biol Chem **277**(15): 13184-13191.
Garcia-Diaz, M., O. Dominguez, L. A. Lopez-Fernandez, L. T. de Lera, M. L. Saniger, J. F. Ruiz, M. Parraga, M. J. Garcia-Ortiz, T. Kirchhoff, J. del Mazo, A. Bernad and L. Blanco (2000). "DNA polymerase lambda (Pol lambda), a novel eukaryotic DNA polymerase with a potential role in meiosis." J Mol Biol **301**(4): 851-867.
Garg, P. and P. M. Burgers (2005). "DNA polymerases that propagate the eukaryotic DNA replication fork." Crit Rev Biochem Mol Biol **40**(2): 115-128.
Garrido, P., E. Mejia, M. Garcia-Diaz, L. Blanco and A. J. Picher (2014). "The active site of TthPolX is adapted to prevent 8-oxo-dGTP misincorporation." Nucleic Acids Res **42**(1): 534-543.
Graziewicz, M. A., M. J. Longley and W. C. Copeland (2006). "DNA polymerase gamma in mitochondrial DNA replication and repair." Chem Rev **106**(2): 383-405.
Grigolava, I. V., M. Ksenzenko, A. A. Konstantinob, A. N. Tikhonov and T. M. Kerimov (1980). "[Tiron as a spin-trap for superoxide radicals produced by the respiratory chain of submitochondrial particles]." Biokhimiia **45**(1): 75-82.
Halliwell, B. (1978). "Superoxide-dependent formation of hydroxyl radicals in the presence of iron chelates: is it a mechanism for hydroxyl radical production in biochemical systems?" FEBS Lett **92**(2): 321-326.
Hamm, M. L., T. J. Gill, S. C. Nicolson and M. R. Summers (2007). "Substrate specificity of Fpg (MutM) and hOGG1, two repair glycosylases." J Am Chem Soc **129**(25): 7724-7725.
Hanes, J. W., D. M. Thal and K. A. Johnson (2006). "Incorporation and replication of 8-oxo-deoxyguanosine by the human mitochondrial DNA polymerase." J Biol Chem **281**(47): 36241-36248.
Haracska, L., L. Prakash and S. Prakash (2002). "Role of human DNA polymerase kappa as an extender in translesion synthesis." Proc Natl Acad Sci U S A **99**(25): 16000-16005.
Haracska, L., S. Prakash and L. Prakash (2003). "Yeast DNA polymerase zeta is an efficient extender of primer ends opposite from 7,8-dihydro-8-Oxoguanine and O6-methylguanine." Mol Cell Biol **23**(4): 1453-1459.
Hashimoto, K., Y. Tominaga, Y. Nakabeppu and M. Moriya (2004). "Futile short-patch DNA base excision repair of adenine:8-oxoguanine mispair." Nucleic Acids Res **32**(19): 5928-5934.

Helbock, H. J., K. B. Beckman, M. K. Shigenaga, P. B. Walter, A. A. Woodall, H. C. Yeo and B. N. Ames (1998). "DNA oxidation matters: the HPLC-electrochemical detection assay of 8-oxo-deoxyguanosine and 8-oxo-guanine." Proc Natl Acad Sci U S A **95**(1): 288-293.
Hinkle, P. C., R. A. Butow, E. Racker and B. Chance (1967). "Partial resolution of the enzymes catalyzing oxidative phosphorylation. XV. Reverse electron transfer in the flavin-cytochrome beta region of the respiratory chain of beef heart submitochondrial particles." J Biol Chem **242**(22): 5169-5173.
Hirano, S., Y. Tominaga, A. Ichinoe, Y. Ushijima, D. Tsuchimoto, Y. Honda-Ohnishi, T. Ohtsubo, K. Sakumi and Y. Nakabeppu (2003). "Mutator phenotype of MUTYH-null mouse embryonic stem cells." J Biol Chem **278**(40): 38121-38124.
Horton, J. K., A. Baker, B. J. Berg, R. W. Sobol and S. H. Wilson (2002). "Involvement of DNA polymerase beta in protection against the cytotoxicity of oxidative DNA damage." DNA Repair (Amst) **1**(4): 317-333.
Hsu, G. W., M. Ober, T. Carell and L. S. Beese (2004). "Error-prone replication of oxidatively damaged DNA by a high-fidelity DNA polymerase." Nature **431**(7005): 217-221.
Huang, H., R. Chopra, G. L. Verdine and S. C. Harrison (1998). "Structure of a covalently trapped catalytic complex of HIV-1 reverse transcriptase: implications for drug resistance." Science **282**(5394): 1669-1675.
Huber, K. V., E. Salah, B. Radic, M. Gridling, J. M. Elkins, A. Stukalov, A. S. Jemth, C. Gokturk, K. Sanjiv, K. Stromberg, T. Pham, U. W. Berglund, J. Colinge, K. L. Bennett, J. I. Loizou, T. Helleday, S. Knapp and G. Superti-Furga (2014). "Stereospecific targeting of MTH1 by (S)-crizotinib as an anticancer strategy." Nature **508**(7495): 222-227.
Jacobs, A. L. and P. Schar (2012). "DNA glycosylases: in DNA repair and beyond." Chromosoma **121**(1): 1-20.
Jessberger, R., V. Podust, U. Hubscher and P. Berg (1993). "A mammalian protein complex that repairs double-strand breaks and deletions by recombination." J Biol Chem **268**(20): 15070-15079.
Kabsch, W. (2010). "Xds." Acta Crystallogr D Biol Crystallogr **66**(Pt 2): 125-132.
Kakuma, T., J. Nishida, T. Tsuzuki and M. Sekiguchi (1995). "Mouse MTH1 protein with 8-oxo-7,8-dihydro-2'-deoxyguanosine 5'-triphosphatase activity that prevents transversion mutation. cDNA cloning and tissue distribution." J Biol Chem **270**(43): 25942-25948.
Kamiya, H., K. Miura, H. Ishikawa, H. Inoue, S. Nishimura and E. Ohtsuka (1992). "c-Ha-ras containing 8-hydroxyguanine at codon 12 induces point mutations at the modified and adjacent positions." Cancer Res **52**(12): 3483-3485.
Kamiya, H., N. Murata-Kamiya, M. Fujimuro, K. Kido, H. Inoue, S. Nishimura, C. Masutani, F. Hanaoka and E. Ohtsuka (1995). "Comparison of incorporation and extension of nucleotides in vitro opposite 8-hydroxyguanine (7,8-dihydro-8-oxoguanine) in hot spots of the c-Ha-ras gene." Jpn J Cancer Res **86**(3): 270-276.
Kamiya, H., N. Murata-Kamiya, S. Koizume, H. Inoue, S. Nishimura and E. Ohtsuka (1995). "8-Hydroxyguanine (7,8-dihydro-8-oxoguanine) in hot spots of the c-Ha-ras gene: effects of sequence contexts on mutation spectra." Carcinogenesis **16**(4): 883-889.
Karplus, P. A. and K. Diederichs (2012). "Linking crystallographic model and data quality." Science **336**(6084): 1030-1033.

Katafuchi, A., A. Sassa, N. Niimi, P. Gruz, H. Fujimoto, C. Masutani, F. Hanaoka, T. Ohta and T. Nohmi (2010). "Critical amino acids in human DNA polymerases eta and kappa involved in erroneous incorporation of oxidized nucleotides." Nucleic Acids Res **38**(3): 859-867.
Kiefer, J. R., C. Mao, J. C. Braman and L. S. Beese (1998). "Visualizing DNA replication in a catalytically active Bacillus DNA polymerase crystal." Nature **391**(6664): 304-307.
Kim, K., S. Biade and Y. Matsumoto (1998). "Involvement of flap endonuclease 1 in base excision DNA repair." J Biol Chem **273**(15): 8842-8848.
Klungland, A. and T. Lindahl (1997). "Second pathway for completion of human DNA base excision-repair: reconstitution with purified proteins and requirement for DNase IV (FEN1)." EMBO J **16**(11): 3341-3348.
Klungland, A., I. Rosewell, S. Hollenbach, E. Larsen, G. Daly, B. Epe, E. Seeberg, T. Lindahl and D. E. Barnes (1999). "Accumulation of premutagenic DNA lesions in mice defective in removal of oxidative base damage." Proc Natl Acad Sci U S A **96**(23): 13300-13305.
Korycka-Dahl, M. B. and T. Richardson (1978). "Activated oxygen species and oxidation of food constituents." CRC Crit Rev Food Sci Nutr **10**(3): 209-241.
Kouchakdjian, M., V. Bodepudi, S. Shibutani, M. Eisenberg, F. Johnson, A. P. Grollman and D. J. Patel (1991). "NMR structural studies of the ionizing radiation adduct 7-hydro-8-oxodeoxyguanosine (8-oxo-7H-dG) opposite deoxyadenosine in a DNA duplex. 8-Oxo-7H-dG(syn).dA(anti) alignment at lesion site." Biochemistry **30**(5): 1403-1412.
Krahn, J. M., W. A. Beard, H. Miller, A. P. Grollman and S. H. Wilson (2003). "Structure of DNA polymerase beta with the mutagenic DNA lesion 8-oxodeoxyguanine reveals structural insights into its coding potential." Structure **11**(1): 121-127.
Krokan, H. E., R. Standal and G. Slupphaug (1997). "DNA glycosylases in the base excision repair of DNA." Biochem J **325 (Pt 1)**: 1-16.
Kubota, Y., R. A. Nash, A. Klungland, P. Schar, D. E. Barnes and T. Lindahl (1996). "Reconstitution of DNA base excision-repair with purified human proteins: interaction between DNA polymerase beta and the XRCC1 protein." EMBO J **15**(23): 6662-6670.
Kumar, A., J. Abbotts, E. M. Karawya and S. H. Wilson (1990). "Identification and properties of the catalytic domain of mammalian DNA polymerase beta." Biochemistry **29**(31): 7156-7159.
Kunkel, T. A. (2004). "DNA replication fidelity." J Biol Chem **279**(17): 16895-16898.
Kunkel, T. A. and K. Bebenek (2000). "DNA replication fidelity." Annu Rev Biochem **69**: 497-529.
LaVerne, J. A. (1989). "The production of OH radicals in the radiolysis of water with 4He ions." Radiat Res **118**(2): 201-210.
Le Page, F., A. Margot, A. P. Grollman, A. Sarasin and A. Gentil (1995). "Mutagenicity of a unique 8-oxoguanine in a human Ha-ras sequence in mammalian cells." Carcinogenesis **16**(11): 2779-2784.
Lee, J. W., L. Blanco, T. Zhou, M. Garcia-Diaz, K. Bebenek, T. A. Kunkel, Z. Wang and L. F. Povirk (2004). "Implication of DNA polymerase lambda in alignment-based gap filling for nonhomologous DNA end joining in human nuclear extracts." J Biol Chem **279**(1): 805-811.

Lehman, I. R., M. J. Bessman, E. S. Simms and A. Kornberg (1958). "Enzymatic synthesis of deoxyribonucleic acid. I. Preparation of substrates and partial purification of an enzyme from Escherichia coli." J Biol Chem **233**(1): 163-170.
Li, Y., S. Korolev and G. Waksman (1998). "Crystal structures of open and closed forms of binary and ternary complexes of the large fragment of Thermus aquaticus DNA polymerase I: structural basis for nucleotide incorporation." EMBO J **17**(24): 7514-7525.
Lindahl, T. (1974). "An N-glycosidase from Escherichia coli that releases free uracil from DNA containing deaminated cytosine residues." Proc Natl Acad Sci U S A **71**(9): 3649-3653.
Lindahl, T. (1993). "Instability and decay of the primary structure of DNA." Nature **362**(6422): 709-715.
Lindahl, T. and R. D. Wood (1999). "Quality control by DNA repair." Science **286**(5446): 1897-1905.
Ling, H., F. Boudsocq, R. Woodgate and W. Yang (2001). "Crystal structure of a Y-family DNA polymerase in action: a mechanism for error-prone and lesion-bypass replication." Cell **107**(1): 91-102.
Lipscomb, L. A., M. E. Peek, M. L. Morningstar, S. M. Verghis, E. M. Miller, A. Rich, J. M. Essigmann and L. D. Williams (1995). "X-ray structure of a DNA decamer containing 7,8-dihydro-8-oxoguanine." Proc Natl Acad Sci U S A **92**(3): 719-723.
Liu, M. S., H. Y. Tsai, X. X. Liu, M. C. Ho, W. J. Wu and M. D. Tsai (2016). "Structural Mechanism for the Fidelity Modulation of DNA Polymerase lambda." J Am Chem Soc **138**(7): 2389-2398.
Loeb, L. A. and T. A. Kunkel (1982). "Fidelity of DNA synthesis." Annu Rev Biochem **51**: 429-457.
Longley, M. J., A. J. Pierce and P. Modrich (1997). "DNA polymerase delta is required for human mismatch repair in vitro." J Biol Chem **272**(16): 10917-10921.
Loschen, G., A. Azzi, C. Richter and L. Flohe (1974). "Superoxide radicals as precursors of mitochondrial hydrogen peroxide." FEBS Lett **42**(1): 68-72.
Lu, A. L., X. Li, Y. Gu, P. M. Wright and D. Y. Chang (2001). "Repair of oxidative DNA damage: mechanisms and functions." Cell Biochem Biophys **35**(2): 141-170.
Ma, Y., H. Lu, B. Tippin, M. F. Goodman, N. Shimazaki, O. Koiwai, C. L. Hsieh, K. Schwarz and M. R. Lieber (2004). "A biochemically defined system for mammalian nonhomologous DNA end joining." Mol Cell **16**(5): 701-713.
Maga, G., E. Crespan, U. Wimmer, B. van Loon, A. Amoroso, C. Mondello, C. Belgiovine, E. Ferrari, G. Locatelli, G. Villani and U. Hubscher (2008). "Replication protein A and proliferating cell nuclear antigen coordinate DNA polymerase selection in 8-oxo-guanine repair." Proc Natl Acad Sci U S A **105**(52): 20689-20694.
Maga, G., G. Villani, E. Crespan, U. Wimmer, E. Ferrari, B. Bertocci and U. Hubscher (2007). "8-oxo-guanine bypass by human DNA polymerases in the presence of auxiliary proteins." Nature **447**(7144): 606-608.
Mahajan, K. N., S. A. Nick McElhinny, B. S. Mitchell and D. A. Ramsden (2002). "Association of DNA polymerase mu (pol mu) with Ku and ligase IV: role for pol mu in end-joining double-strand break repair." Mol Cell Biol **22**(14): 5194-5202.
Maki, H. and M. Sekiguchi (1992). "MutT protein specifically hydrolyses a potent mutagenic substrate for DNA synthesis." Nature **355**(6357): 273-275.

Markkanen, E., B. Castrec, G. Villani and U. Hubscher (2012). "A switch between DNA polymerases delta and lambda promotes error-free bypass of 8-oxo-G lesions." Proceedings of the National Academy of Sciences of the United States of America **109**(50): 20401-20406.
Markkanen, E., B. Castrec, G. Villani and U. Hubscher (2012). "A switch between DNA polymerases delta and lambda promotes error-free bypass of 8-oxo-G lesions." Proc Natl Acad Sci U S A **109**(50): 20401-20406.
Markkanen, E., J. Dorn and U. Hubscher (2013). "MUTYH DNA glycosylase: the rationale for removing undamaged bases from the DNA." Front Genet **4**: 18.
Markkanen, E., B. van Loon, E. Ferrari, J. L. Parsons, G. L. Dianov and U. Hubscher (2012). "Regulation of oxidative DNA damage repair by DNA polymerase lambda and MutYH by cross-talk of phosphorylation and ubiquitination." Proc Natl Acad Sci U S A **109**(2): 437-442.
Matsumoto, Y. and K. Kim (1995). "Excision of deoxyribose phosphate residues by DNA polymerase beta during DNA repair." Science **269**(5224): 699-702.
Matsumoto, Y., K. Kim and D. F. Bogenhagen (1994). "Proliferating cell nuclear antigen-dependent abasic site repair in Xenopus laevis oocytes: an alternative pathway of base excision DNA repair." Mol Cell Biol **14**(9): 6187-6197.
McAuley-Hecht, K. E., G. A. Leonard, N. J. Gibson, J. B. Thomson, W. P. Watson, W. N. Hunter and T. Brown (1994). "Crystal structure of a DNA duplex containing 8-hydroxydeoxyguanine-adenine base pairs." Biochemistry **33**(34): 10266-10270.
Mcauleyhecht, K. E., G. A. Leonard, N. J. Gibson, J. B. Thomson, W. P. Watson, W. N. Hunter and T. Brown (1994). "Crystal-Structure of a DNA Duplex Containing 8-Hydroxydeoxyguanine-Adenine Base-Pairs." Biochemistry **33**(34): 10266-10270.
McCord, J. M. and E. D. Day, Jr. (1978). "Superoxide-dependent production of hydroxyl radical catalyzed by iron-EDTA complex." FEBS Lett **86**(1): 139-142.
McCoy, A. J., R. W. Grosse-Kunstleve, P. D. Adams, M. D. Winn, L. C. Storoni and R. J. Read (2007). "Phaser crystallographic software." J Appl Crystallogr **40**(Pt 4): 658-674.
Michaels, M. L., C. Cruz, A. P. Grollman and J. H. Miller (1992). "Evidence that MutY and MutM combine to prevent mutations by an oxidatively damaged form of guanine in DNA." Proc Natl Acad Sci U S A **89**(15): 7022-7025.
Michaels, M. L. and J. H. Miller (1992). "The GO system protects organisms from the mutagenic effect of the spontaneous lesion 8-hydroxyguanine (7,8-dihydro-8-oxoguanine)." J Bacteriol **174**(20): 6321-6325.
Michaels, M. L., L. Pham, C. Cruz and J. H. Miller (1991). "MutM, a protein that prevents G.C----T.A transversions, is formamidopyrimidine-DNA glycosylase." Nucleic Acids Res **19**(13): 3629-3632.
Miller, H., R. Prasad, S. H. Wilson, F. Johnson and A. P. Grollman (2000). "8-oxodGTP incorporation by DNA polymerase beta is modified by active-site residue Asn279." Biochemistry **39**(5): 1029-1033.
Minowa, O., T. Arai, M. Hirano, Y. Monden, S. Nakai, M. Fukuda, M. Itoh, H. Takano, Y. Hippou, H. Aburatani, K. Masumura, T. Nohmi, S. Nishimura and T. Noda (2000). "Mmh/Ogg1 gene inactivation results in accumulation of 8-hydroxyguanine in mice." Proc Natl Acad Sci U S A **97**(8): 4156-4161.

Miyamoto, H., Y. Miyagi, T. Ishikawa, Y. Ichikawa, M. Hosaka and Y. Kubota (1999). "DNA polymerase beta gene mutation in human breast cancer." Int J Cancer **83**(5): 708-709.
Mol, C. D., S. S. Parikh, C. D. Putnam, T. P. Lo and J. A. Tainer (1999). "DNA repair mechanisms for the recognition and removal of damaged DNA bases." Annu Rev Biophys Biomol Struct **28**: 101-128.
Morales, J. C. and E. T. Kool (1999). "Minor Groove Interactions between Polymerase and DNA: More Essential to Replication than Watson-Crick Hydrogen Bonds?" J Am Chem Soc **121**(10): 2323-2324.
Moriya, M. (1993). "Single-stranded shuttle phagemid for mutagenesis studies in mammalian cells: 8-oxoguanine in DNA induces targeted G.C-->T.A transversions in simian kidney cells." Proc Natl Acad Sci U S A **90**(3): 1122-1126.
Murphy, M. P. (2009). "How mitochondria produce reactive oxygen species." Biochem J **417**(1): 1-13.
Murshudov, G. N., P. Skubak, A. A. Lebedev, N. S. Pannu, R. A. Steiner, R. A. Nicholls, M. D. Winn, F. Long and A. A. Vagin (2011). "REFMAC5 for the refinement of macromolecular crystal structures." Acta Crystallogr D Biol Crystallogr **67**(Pt 4): 355-367.
Murshudov, G. N., A. A. Vagin and E. J. Dodson (1997). "Refinement of Macromolecular Structures by the Maximum-Likelihood Method." Acta Crystallographica Section D **53**(3): 240-255.
Nash, H. M., S. D. Bruner, O. D. Scharer, T. Kawate, T. A. Addona, E. Spooner, W. S. Lane and G. L. Verdine (1996). "Cloning of a yeast 8-oxoguanine DNA glycosylase reveals the existence of a base-excision DNA-repair protein superfamily." Curr Biol **6**(8): 968-980.
Neeley, W. L. and J. M. Essigmann (2006). "Mechanisms of formation, genotoxicity, and mutation of guanine oxidation products." Chem Res Toxicol **19**(4): 491-505.
Nghiem, Y., M. Cabrera, C. G. Cupples and J. H. Miller (1988). "The mutY gene: a mutator locus in Escherichia coli that generates G.C----T.A transversions." Proc Natl Acad Sci U S A **85**(8): 2709-2713.
Ni, T. T., G. T. Marsischky and R. D. Kolodner (1999). "MSH2 and MSH6 are required for removal of adenine misincorporated opposite 8-oxo-guanine in S. cerevisiae." Mol Cell **4**(3): 439-444.
Nick McElhinny, S. A., J. M. Havener, M. Garcia-Diaz, R. Juarez, K. Bebenek, B. L. Kee, L. Blanco, T. A. Kunkel and D. A. Ramsden (2005). "A gradient of template dependence defines distinct biological roles for family X polymerases in nonhomologous end joining." Mol Cell **19**(3): 357-366.
Ochs, K., R. W. Sobol, S. H. Wilson and B. Kaina (1999). "Cells deficient in DNA polymerase beta are hypersensitive to alkylating agent-induced apoptosis and chromosomal breakage." Cancer Res **59**(7): 1544-1551.
Oda, Y., S. Uesugi, M. Ikehara, S. Nishimura, Y. Kawase, H. Ishikawa, H. Inoue and E. Ohtsuka (1991). "Nmr-Studies of a DNA Containing 8-Hydroxydeoxyguanosine." Nucleic Acids Research **19**(7): 1407-1412.
Ollis, D. L., P. Brick, R. Hamlin, N. G. Xuong and T. A. Steitz (1985). "Structure of large fragment of Escherichia coli DNA polymerase I complexed with dTMP." Nature **313**(6005): 762-766.

Pande, P., K. Haraguchi, Y. L. Jiang, M. M. Greenberg and A. K. Basu (2015). "Unlike catalyzing error-free bypass of 8-oxodGuo, DNA polymerase lambda is responsible for a significant part of Fapy.dG-induced G --> T mutations in human cells." Biochemistry **54**(10): 1859-1862.
Parikh, S. S., C. D. Mol and J. A. Tainer (1997). "Base excision repair enzyme family portrait: integrating the structure and chemistry of an entire DNA repair pathway." Structure **5**(12): 1543-1550.
Pascucci, B., M. Stucki, Z. O. Jonsson, E. Dogliotti and U. Hubscher (1999). "Long patch base excision repair with purified human proteins. DNA ligase I as patch size mediator for DNA polymerases delta and epsilon." J Biol Chem **274**(47): 33696-33702.
Patra, A., L. D. Nagy, Q. Zhang, Y. Su, L. Muller, F. P. Guengerich and M. Egli (2014). "Kinetics, structure, and mechanism of 8-Oxo-7,8-dihydro-2'-deoxyguanosine bypass by human DNA polymerase eta." J Biol Chem **289**(24): 16867-16882.
Petruska, J., L. C. Sowers and M. F. Goodman (1986). "Comparison of nucleotide interactions in water, proteins, and vacuum: model for DNA polymerase fidelity." Proc Natl Acad Sci U S A **83**(6): 1559-1562.
Picher, A. J. and L. Blanco (2007). "Human DNA polymerase lambda is a proficient extender of primer ends paired to 7,8-dihydro-8-oxoguanine." DNA Repair (Amst) **6**(12): 1749-1756.
Pursell, Z. F., J. T. McDonald, C. K. Mathews and T. A. Kunkel (2008). "Trace amounts of 8-oxo-dGTP in mitochondrial dNTP pools reduce DNA polymerase gamma replication fidelity." Nucleic Acids Res **36**(7): 2174-2181.
Ramadan, K., I. Shevelev and U. Hubscher (2004). "The DNA-polymerase-X family: controllers of DNA quality?" Nat Rev Mol Cell Biol **5**(12): 1038-1043.
Ray, P. D., B. W. Huang and Y. Tsuji (2012). "Reactive oxygen species (ROS) homeostasis and redox regulation in cellular signaling." Cell Signal **24**(5): 981-990.
Robson, C. N., A. M. Milne, D. J. Pappin and I. D. Hickson (1991). "Isolation of cDNA clones encoding an enzyme from bovine cells that repairs oxidative DNA damage in vitro: homology with bacterial repair enzymes." Nucleic Acids Res **19**(5): 1087-1092.
Russo, M. T., G. De Luca, P. Degan, E. Parlanti, E. Dogliotti, D. E. Barnes, T. Lindahl, H. Yang, J. H. Miller and M. Bignami (2004). "Accumulation of the oxidative base lesion 8-hydroxyguanine in DNA of tumor-prone mice defective in both the Myh and Ogg1 DNA glycosylases." Cancer Res **64**(13): 4411-4414.
Sale, J. E., A. R. Lehmann and R. Woodgate (2012). "Y-family DNA polymerases and their role in tolerance of cellular DNA damage." Nat Rev Mol Cell Biol **13**(3): 141-152.
Satou, K., K. Kawai, H. Kasai, H. Harashima and H. Kamiya (2007). "Mutagenic effects of 8-hydroxy-dGTP in live mammalian cells." Free Radic Biol Med **42**(10): 1552-1560.
Sawaya, M. R. (2014). "Methods to refine macromolecular structures in cases of severe diffraction anisotropy." Methods Mol Biol **1091**: 205-214.
Sawaya, M. R., R. Prasad, S. H. Wilson, J. Kraut and H. Pelletier (1997). "Crystal structures of human DNA polymerase beta complexed with gapped and nicked DNA: evidence for an induced fit mechanism." Biochemistry **36**(37): 11205-11215.
Seeman, N. C., J. M. Rosenberg and A. Rich (1976). "Sequence-specific recognition of double helical nucleic acids by proteins." Proc Natl Acad Sci U S A **73**(3): 804-808.

SenGupta, D. N., B. Z. Zmudzka, P. Kumar, F. Cobianchi, J. Skowronski and S. H. Wilson (1986). "Sequence of human DNA polymerase beta mRNA obtained through cDNA cloning." Biochem Biophys Res Commun **136**(1): 341-347.
Shibutani, S., M. Takeshita and A. P. Grollman (1991). "Insertion of specific bases during DNA synthesis past the oxidation-damaged base 8-oxodG." Nature **349**(6308): 431-434.
Shimizu, M., P. Gruz, H. Kamiya, S. R. Kim, F. M. Pisani, C. Masutani, Y. Kanke, H. Harashima, F. Hanaoka and T. Nohmi (2003). "Erroneous incorporation of oxidized DNA precursors by Y-family DNA polymerases." EMBO Rep **4**(3): 269-273.
Shimizu, M., P. Gruz, H. Kamiya, C. Masutani, Y. Xu, Y. Usui, H. Sugiyama, H. Harashima, F. Hanaoka and T. Nohmi (2007). "Efficient and erroneous incorporation of oxidized DNA precursors by human DNA polymerase eta." Biochemistry **46**(18): 5515-5522.
Singhal, R. K., R. Prasad and S. H. Wilson (1995). "DNA polymerase beta conducts the gap-filling step in uracil-initiated base excision repair in a bovine testis nuclear extract." J Biol Chem **270**(2): 949-957.
Singhal, R. K. and S. H. Wilson (1993). "Short gap-filling synthesis by DNA polymerase beta is processive." J Biol Chem **268**(21): 15906-15911.
Slupska, M. M., C. Baikalov, W. M. Luther, J. H. Chiang, Y. F. Wei and J. H. Miller (1996). "Cloning and sequencing a human homolog (hMYH) of the Escherichia coli mutY gene whose function is required for the repair of oxidative DNA damage." J Bacteriol **178**(13): 3885-3892.
Smart, O. S., T. O. Womack, C. Flensburg, P. Keller, W. Paciorek, A. Sharff, C. Vonrhein and G. Bricogne (2012). "Exploiting structure similarity in refinement: automated NCS and target-structure restraints in BUSTER." Acta Crystallogr D Biol Crystallogr **68**(Pt 4): 368-380.
Sobol, R. W., J. K. Horton, R. Kuhn, H. Gu, R. K. Singhal, R. Prasad, K. Rajewsky and S. H. Wilson (1996). "Requirement of mammalian DNA polymerase-beta in base-excision repair." Nature **379**(6561): 183-186.
Sobol, R. W., M. Kartalou, K. H. Almeida, D. F. Joyce, B. P. Engelward, J. K. Horton, R. Prasad, L. D. Samson and S. H. Wilson (2003). "Base excision repair intermediates induce p53-independent cytotoxic and genotoxic responses." J Biol Chem **278**(41): 39951-39959.
Sobol, R. W., R. Prasad, A. Evenski, A. Baker, X. P. Yang, J. K. Horton and S. H. Wilson (2000). "The lyase activity of the DNA repair protein beta-polymerase protects from DNA-damage-induced cytotoxicity." Nature **405**(6788): 807-810.
Sobol, R. W. and S. H. Wilson (2001). "Mammalian DNA beta-polymerase in base excision repair of alkylation damage." Prog Nucleic Acid Res Mol Biol **68**: 57-74.
Starcevic, D., S. Dalal and J. B. Sweasy (2004). "Is there a link between DNA polymerase beta and cancer?" Cell Cycle **3**(8): 998-1001.
Steitz, T. A. (1999). "DNA polymerases: structural diversity and common mechanisms." J Biol Chem **274**(25): 17395-17398.
Steitz, T. A. and J. A. Steitz (1993). "A general two-metal-ion mechanism for catalytic RNA." Proc Natl Acad Sci U S A **90**(14): 6498-6502.

Sugo, N., Y. Aratani, Y. Nagashima, Y. Kubota and H. Koyama (2000). "Neonatal lethality with abnormal neurogenesis in mice deficient in DNA polymerase beta." EMBO J **19**(6): 1397-1404.
Suh, D., D. M. Wilson, 3rd and L. F. Povirk (1997). "3'-phosphodiesterase activity of human apurinic/apyrimidinic endonuclease at DNA double-strand break ends." Nucleic Acids Res **25**(12): 2495-2500.
Sun, B., K. A. Latham, M. L. Dodson and R. S. Lloyd (1995). "Studies on the catalytic mechanism of five DNA glycosylases. Probing for enzyme-DNA imino intermediates." J Biol Chem **270**(33): 19501-19508.
Svilar, D., E. M. Goellner, K. H. Almeida and R. W. Sobol (2011). "Base excision repair and lesion-dependent subpathways for repair of oxidative DNA damage." Antioxid Redox Signal **14**(12): 2491-2507.
Tano, K., J. Nakamura, K. Asagoshi, H. Arakawa, E. Sonoda, E. K. Braithwaite, R. Prasad, J. M. Buerstedde, S. Takeda, M. Watanabe and S. H. Wilson (2007). "Interplay between DNA polymerases beta and lambda in repair of oxidation DNA damage in chicken DT40 cells." DNA Repair (Amst) **6**(6): 869-875.
Tchou, J. and A. P. Grollman (1995). "The catalytic mechanism of Fpg protein. Evidence for a Schiff base intermediate and amino terminus localization of the catalytic site." J Biol Chem **270**(19): 11671-11677.
Tchou, J., H. Kasai, S. Shibutani, M. H. Chung, J. Laval, A. P. Grollman and S. Nishimura (1991). "8-oxoguanine (8-hydroxyguanine) DNA glycosylase and its substrate specificity." Proc Natl Acad Sci U S A **88**(11): 4690-4694.
Terrados, G., J. P. Capp, Y. Canitrot, M. Garcia-Diaz, K. Bebenek, T. Kirchhoff, A. Villanueva, F. Boudsocq, V. Bergoglio, C. Cazaux, T. A. Kunkel, J. S. Hoffmann and L. Blanco (2009). "Characterization of a natural mutator variant of human DNA polymerase lambda which promotes chromosomal instability by compromising NHEJ." PLoS One **4**(10): e7290.
Thomas, D., A. D. Scot, R. Barbey, M. Padula and S. Boiteux (1997). "Inactivation of OGG1 increases the incidence of G . C-->T . A transversions in Saccharomyces cerevisiae: evidence for endogenous oxidative damage to DNA in eukaryotic cells." Mol Gen Genet **254**(2): 171-178.
Tsuzuki, T., A. Egashira, H. Igarashi, T. Iwakuma, Y. Nakatsuru, Y. Tominaga, H. Kawate, K. Nakao, K. Nakamura, F. Ide, S. Kura, Y. Nakabeppu, M. Katsuki, T. Ishikawa and M. Sekiguchi (2001). "Spontaneous tumorigenesis in mice defective in the MTH1 gene encoding 8-oxo-dGTPase." Proc Natl Acad Sci U S A **98**(20): 11456-11461.
Turrens, J. F. and A. Boveris (1980). "Generation of superoxide anion by the NADH dehydrogenase of bovine heart mitochondria." Biochem J **191**(2): 421-427.
Vaguine, A. A., J. Richelle and S. J. Wodak (1999). "SFCHECK: a unified set of procedures for evaluating the quality of macromolecular structure-factor data and their agreement with the atomic model." Acta Crystallogr D Biol Crystallogr **55**(Pt 1): 191-205.
van der Kemp, P. A., D. Thomas, R. Barbey, R. de Oliveira and S. Boiteux (1996). "Cloning and expression in Escherichia coli of the OGG1 gene of Saccharomyces cerevisiae, which codes for a DNA glycosylase that excises 7,8-dihydro-8-oxoguanine and 2,6-diamino-4-hydroxy-5-N-methylformamidopyrimidine." Proc Natl Acad Sci U S A **93**(11): 5197-5202.

van Gent, D. C. and M. van der Burg (2007). "Non-homologous end-joining, a sticky affair." Oncogene **26**(56): 7731-7740.
van Loon, B. and U. Hubscher (2009). "An 8-oxo-guanine repair pathway coordinated by MUTYH glycosylase and DNA polymerase lambda." Proc Natl Acad Sci U S A **106**(43): 18201-18206.
van Loon, B., E. Markkanen and U. Hubscher (2010). "Oxygen as a friend and enemy: How to combat the mutational potential of 8-oxo-guanine." DNA Repair (Amst) **9**(6): 604-616.
Vande Berg, B. J., W. A. Beard and S. H. Wilson (2001). "DNA structure and aspartate 276 influence nucleotide binding to human DNA polymerase beta. Implication for the identity of the rate-limiting conformational change." J Biol Chem **276**(5): 3408-3416.
Vasquez-Del Carpio, R., T. D. Silverstein, S. Lone, M. K. Swan, J. R. Choudhury, R. E. Johnson, S. Prakash, L. Prakash and A. K. Aggarwal (2009). "Structure of human DNA polymerase kappa inserting dATP opposite an 8-OxoG DNA lesion." PLoS One **4**(6): e5766.
Vermeulen, C., B. Bertocci, A. C. Begg and C. Vens (2007). "Ionizing radiation sensitivity of DNA polymerase lambda-deficient cells." Radiat Res **168**(6): 683-688.
Vonrhein, C., C. Flensburg, P. Keller, A. Sharff, O. Smart, W. Paciorek, T. Womack and G. Bricogne (2011). "Data processing and analysis with the autoPROC toolbox." Acta Crystallogr D Biol Crystallogr **67**(Pt 4): 293-302.
Vyas, R., A. J. Reed, E. J. Tokarsky and Z. Suo (2015). "Viewing Human DNA Polymerase beta Faithfully and Unfaithfully Bypass an Oxidative Lesion by Time-Dependent Crystallography." J Am Chem Soc **137**(15): 5225-5230.
Wang, J., A. K. Sattar, C. C. Wang, J. D. Karam, W. H. Konigsberg and T. A. Steitz (1997). "Crystal structure of a pol alpha family replication DNA polymerase from bacteriophage RB69." Cell **89**(7): 1087-1099.
Wang, L., U. Patel, L. Ghosh and S. Banerjee (1992). "DNA polymerase beta mutations in human colorectal cancer." Cancer Res **52**(17): 4824-4827.
Wei, Y. F., P. Robins, K. Carter, K. Caldecott, D. J. Pappin, G. L. Yu, R. P. Wang, B. K. Shell, R. A. Nash, P. Schar and et al. (1995). "Molecular cloning and expression of human cDNAs encoding a novel DNA ligase IV and DNA ligase III, an enzyme active in DNA repair and recombination." Mol Cell Biol **15**(6): 3206-3216.
Werneburg, B. G., J. Ahn, X. Zhong, R. J. Hondal, V. S. Kraynov and M. D. Tsai (1996). "DNA polymerase beta: pre-steady-state kinetic analysis and roles of arginine-283 in catalysis and fidelity." Biochemistry **35**(22): 7041-7050.
Williams, S. D. and S. S. David (1998). "Evidence that MutY is a monofunctional glycosylase capable of forming a covalent Schiff base intermediate with substrate DNA." Nucleic Acids Res **26**(22): 5123-5133.
Williams, S. D. and S. S. David (1999). "Formation of a Schiff base intermediate is not required for the adenine glycosylase activity of Escherichia coli MutY." Biochemistry **38**(47): 15417-15424.
Wong, D., M. S. DeMott and B. Demple (2003). "Modulation of the 3'-->5'-exonuclease activity of human apurinic endonuclease (Ape1) by its 5'-incised Abasic DNA product." J Biol Chem **278**(38): 36242-36249.

Wong, I., S. S. Patel and K. A. Johnson (1991). "An induced-fit kinetic mechanism for DNA replication fidelity: direct measurement by single-turnover kinetics." Biochemistry **30**(2): 526-537.
Wood, R. D. (1996). "DNA repair in eukaryotes." Annu Rev Biochem **65**: 135-167.
Xie, Y., H. Yang, C. Cunanan, K. Okamoto, D. Shibata, J. Pan, D. E. Barnes, T. Lindahl, M. McIlhatton, R. Fishel and J. H. Miller (2004). "Deficiencies in mouse Myh and Ogg1 result in tumor predisposition and G to T mutations in codon 12 of the K-ras oncogene in lung tumors." Cancer Res **64**(9): 3096-3102.
Yamada, M., T. Nunoshiba, M. Shimizu, P. Gruz, H. Kamiya, H. Harashima and T. Nohmi (2006). "Involvement of Y-family DNA polymerases in mutagenesis caused by oxidized nucleotides in Escherichia coli." J Bacteriol **188**(13): 4992-4995.
Yousefzadeh, M. J. and R. D. Wood (2013). "DNA polymerase POLQ and cellular defense against DNA damage." DNA Repair (Amst) **12**(1): 1-9.
Zaccolo, M., D. M. Williams, D. M. Brown and E. Gherardi (1996). "An approach to random mutagenesis of DNA using mixtures of triphosphate derivatives of nucleoside analogues." J Mol Biol **255**(4): 589-603.
Zhang, Y., F. Yuan, X. Wu, O. Rechkoblit, J. S. Taylor, N. E. Geacintov and Z. Wang (2000). "Error-prone lesion bypass by human DNA polymerase eta." Nucleic Acids Res **28**(23): 4717-4724.
Zhao, J. and M. E. Winkler (2000). "Reduction of GC --> TA transversion mutation by overexpression of MutS in Escherichia coli K-12." J Bacteriol **182**(17): 5025-5028.
Zharkov, D. O. and A. P. Grollman (1998). "MutY DNA glycosylase: base release and intermediate complex formation." Biochemistry **37**(36): 12384-12394.
Zwart, P. H., P. V. Afonine, R. W. Grosse-Kunstleve, L. W. Hung, T. R. Ioerger, A. J. McCoy, E. McKee, N. W. Moriarty, R. J. Read, J. C. Sacchettini, N. K. Sauter, L. C. Storoni, T. C. Terwilliger and P. D. Adams (2008). "Automated structure solution with the PHENIX suite." Methods Mol Biol **426**: 419-435.